Instituto Universitario de Investigación
en Ingeniería de Aragón
Universidad Zaragoza

Ph.D. Thesis

Non-Invasive Assessment of Autonomic Nervous System through Cardiovascular Signals Variability Analysis in Non-Stationary Environments

Evaluación no Invasiva del Sistema Nervioso Autónomo mediante Análisis de la Variabilidad de Señales Cardiovasculares en Entornos no Estacionarios

David Hernando Jumilla

SUPERVISORS:
Raquel Bailón Luesma
Pablo Laguna Lasaosa

Ph.D. in Biomedical Engineering

Zaragoza, June, 2017

Non-Invasive Assessment of Autonomic Nervous System through Cardiovascular Signals Variability Analysis in Non-Stationary Environments

David Hernando Jumilla, 2017
Non-Invasive Assessment of Autonomic Nervous System through Cardiovascular Signals Variability Analysis in Non-Stationary Environments

Date of current version: Thursday 25th May, 2017

This thesis was supported by Diputación General de Aragón (DGA), Spain, through a fellowship with Ref: *B195/12*, by a research contract from University of Zaragoza and a research contract from Centro de Iinvestigación Biomédica en Red - Bioingeniería, Biomateriales y Nanomedicina (CIBER-BBN). The research visits were both supported by CIBER-BBN. The research presented in this thesis was also supported by the following projects: *TEC2010-21703-C03-02*, *UZ2014-TEC-01*, *TIN2014-53567-R* and *DPI2016-75458-R*. In addition, it was supported by Aragón Gobernment (Spain) and European Social Fund through Grupo Consolidado Biomedical Signal Interpretation and Computational Simulation (BSICoS), Ref: *T96*, by Grupo de Tecnologías de la Comunicación, Ref: *T30*, and by CIBER-BBN through Instituto de Salud Carlos III. The computation of some parts of this thesis was performed at the High Performance Computing platform of the NANBIOSIS ICTS, CIBER-BBN and Aragón Institute of Engineering Research (I3A), Zaragoza, Spain.

This thesis was printed thanks to the financial support of BSICoS Group at University of Zaragoza.

Abstract

Autonomic nervous system (ANS) is in charge of the maintenance of homeostasis of the body and regulates different functions such as heart rate, blood pressure, gastrointestinal responses, and thermoregulation. It is interesting to have a regular ANS evaluation in different applications, some examples include understanding the response of ANS to stress to early detect or diagnose cardiovascular, metabolic or mental diseases.

Heart rate variability (HRV) analysis is one of the most popular non-invasive methods of ANS evaluation and is easily obtained from the electrocardiogram (ECG) signal. HRV reflects purposely generated responses to internal and external stimuli, being ANS the primary regulator of cardiac chronotropy. Aditionally, other cardiovascular variability signals (such as blood pressure variability) and respiration can also provide added value to the assessment of ANS state.

Most of the tools developed to analyze HRV have been designed in a stationary environment. When this premise is not valid, there is a necessity to develop robust methodologies adapted to each scenario to make sure that measurements allow us to correctly interpret changes in ANS activity. The objective of this thesis is to extract information about ANS state from cardiovascular signals, mainly HRV, and respiratory information in non-stationary environments.

A robust methodological framework suitable for HRV analysis during exercise is presented which addresses many limitations in HRV analysis during exercise. To have a better QRS detection in the noisy ECG, an evolutionary algorithm is applied to optimize some of the parameters of the detector. The HRV signal is computed based on the time-varying threshold integral pulse frequency modulation (TVIPFM) model, which takes into account the high variations in the mean heart rate expected during exercise. To deal with the non-stationary nature of the signal, a time-frequency analysis is used which allows to extract instantaneous power parameters. Since the respiratory frequency varies during exercise, usually reaching high frequencies, the high frequency (HF) band is needed to be redefined. Moreover, spectral components related to cardiolocomotor coupling (CC) are identified in the HRV spectrum, and a correction is applied whenever this component overlaps with the HF component.

This framework is then applied to three different exercise tests in order to study the response of ANS to the stress of exercise in healthy subjects: one maximal test on a treadmill, and two submaximal tests on a treadmill and on a cyclo ergometer. Different intervals are determined in each test: one related to the resting phase, one for the recovery phase, and the rest, during exercise, based on a similar metabolic

demand based on the level of oxygen consumption. Normalized powers related to low frequency (LF) and HF are analyzed in these intervals: in the first exercise interval, during low intensities of exercise, LF increases as a response of an activation of the sympathetic nervous system, while there is a decrease in HF following the inhibition of the parasympathetic activity. During high intensities of exercise, however, HF increases while LF decreases since now HF power does not only reflect autonomic response, but also the increasing mechanical effect of breathing. CC power, related to the cardiolocomotor coupling, increases with the intensity of exercise, reaching up to 30% of the total power in the last exercise intervals, being higher in the treadmill tests.

Additionally, a heart rate monitor is validated in terms of HRV measurements. RR series were adquired simultaneously from the ECG and a Polar device during dynamic exercise of low, medium and high intensity. Reliability and agreement coefficients show that both methods are interchangeable when measuring instantaneous mean heart rate and LF power, regardless of the level of exercise (reliability and agreement > 0.9). However, instantaneous HF power measurements present reliability and agreement coefficients lower than 0.7 in the last intervals of the exercise phase. In spite of this low agreement and reliability, when computing the HRV parameters as the mean value in the analyzed intervals and addressing the CC spectral components, no significant differences were found between the ECG and Polar measurements. Both parameters describe the same ANS response to the exercise stress. As a result, the use of HRV measurements from the Polar device is appropriate regardless of the intensity of exercise.

HRV analysis is also applied to exercise test with the aim of determining the diagnostic performance of HRV measurements during exercise in the detection of CAD. These patients present a high number of abnormalities in the RR series, mainly due to arrhythmic events, therefore a special care is needed in the selection of the interval to analyze. Moreover, due to the effect of medications and differences in exercise duration between CAD and low-likelihood CAD groups (CAD vs LLC), it is seen that mean HR and respiratory frequency cannot be reliably used to diagnose CAD. HF power, when guided by respiration, achieves the highest AUC, above 0.7 both in rest and in recovery. When measuring in intervals with a similar metabolic demand, based on the increment in the mean HR, a significant difference can be observed in the last interval of exercise between LLC and CAD patients, with lower normalized LF power and higher HF power (both normalized and absolute power) in CAD patients, suggesting that HRV parameters can diagnose CAD before finishing the exercise test. Due to the lack of cadence frequency information, the CC component cannot be corrected, and the use of an extended band for HF power will surely measure additional spectral components. This emphasizes the necessity of a standard methodology for HRV analysis during exercise.

A different application where HRV is analyzed is in hemodialysis patients. The hypothesis behind this study is that intradialytic hypotension (IDH) prone patients present an impairment in autonomic regulation of the cardiovascular system. Different parameters are proposed to differenciate between IDH prone and resistant patients. Not only parameters from HRV are used, but also additional information from blood

pressure variability (BPV), baroreflex sensitivity (BRS) and respiration by means of ECG derived respiratory (EDR) signals to improve the IDH state diagnosis. A very low frequency (VLF) was found in HRV, BPV and EDR series, and it is characterized under the hypothesis that it is caused by the hemodinamic inestability of IDH patients. A MVDR method is applied to extract spectral parameters since, in general, it presents a better frequency resolution than other spectral estimators. All these parameters are analyzed individually, where respiratory frequency shows no apparent correlation with the IDH status of the patient. VLF modulation appears more often in prone patients and may be related with an altered ANS. Additionally, some of the parameters related to HRV (normalized LF and ratio), BPV (HF) and BRS (LF) are indeed able to discriminate between both groups.

The rest of the parameters from HRV, BPV and BRS are used to design a classifier that, using information of the first 30 minutes of the treatment, is able to classify IDH prone and resistant patients with the aim of having an early identification of IDH prone patients. The classifier is trained using a leave-one-patient-out method (due to the small size of the database), where all sessions belonging to the same patient are left out of the training, and the process is repeated for each patient. The process of features selection both selects and removes features until the best set is found. With the inclusion of information of the diabetes state of the patients, the overall performance of the classifier improves, reaching values of sensitivity and accuracy of Se=97.5% and Acc=92.1%. Since the majority of parameters are related to HRV, mainly the ratio of LF/HF powers and the normalized LF power, a new classifier which uses only HRV parameters is proposed, having the advantage of not needing to record blood pressure. This new classifier achieves Se=95% and Acc=90.2%.

Last application is the proposal of HRV parameters as markers of ANS integrity in critically ill patients in an exploratory study. Critically ill patients present alterations in ANS which can persist even after hospital discharge, in particular, it has been observed an increasing number of cases of neurocognitive impairments. A neurocognitive rehabilitation has been suggested for these patients to improve cognitive deficits, and HRV parameters are proposed for analyzing the response to this rehabilitation and its effectiveness to improve the ANS integrity. The main limitations in these patients are that they take a great number of medication which alter ANS activity, some of them are mechanically ventilated, other suffer from delirum (which is unclear if it is caused by an autonomic dysfunction), and in general they form a highly heterogeneous group of patients. Respiratory information is included in the HRV analysis, and to address the highly irregular breathing pattern of some patients, the spectral band related to HF component has been accordingly adapted for each patient. Comparing with baseline values, 7 patients showed an increase in the HF power after the session, suggesting an increase of parasympathetic activity, while 5 of them presented a decrease in the normalized LF power, suggesting a decrease of the sympathetic activity. These results need to be interpreted with special care due to the patients characteristics, who already have altered the ANS either by the underlying diseases or medications. A larger database with more controlled factors is being recorded at the moment with the aim to continue exploring the capability of HRV measurements to assess ANS integrity in these patients.

Keywords: Autonomic Nervous System; Heart Rate Variability; Cardiovascular Signals Variability; Respiration; Non-invasive Monitoring; Non-stationary Spectral Analysis; Stress Testing; Heart Rate Monitor; Coronary Artery Disease Diagnosis; Hemodialysis; Signal Processing

Resumen y Conclusiones

El sistema nervioso autónomo (SNA) está al cargo de mantener la homeostasis del cuerpo y regula diferentes funciones como el ritmo cardiaco, presión sanguínea, respuestas gastrointestinales y termorregulación. Es interesante tener una evaluación regular del SNA en diferentes aplicaciones, como por ejemplo en el entendimiento de la respuesta del SNA al estrés para detectar de manera temprana o diagnosticar enfermedades cardiovasculares, metabólicas o mentales.

El análisis de la variabilidad del ritmo cardiaco (HRV) es uno de los métodos no invasivos más populares para evaluar el SNA y se puede obtener fácilmente a partir del electrocardiograma (ECG). La HRV refleja respuestas a estímulos internos y externos, siendo el SNA el regulador primario de la cronotropía cardiaca. Además, la variabilidad de otras señales cardiovasculares (como la variabilidad de la presión sanguinea) y la respiración pueden aportar valor añadido a la evaluación del SNA.

La mayoría de las herramientas desarrolladas para analizar la HRV han sido diseñadas para entornos estacionarios. Cuando esta premisa no es válida, es necesario desarrollar metodologías robustas adaptadas a cada escenario que asegure que las medidas tomadas permitan interpretar correctamente cambios en la actividad del SNA. El objetivo de esta tesis es extraer información sobre el estado del SNA a partir de señales cardiovasculares, en especial la HRV, y de la información respiratoria en entornos no estacionarios.

Se presenta una metodología robusta adecuada al análisis de la HRV durante ejercicio que aborda muchas de las limitaciones del análisis de la HRV en ejercicio. Para mejorar la detección de los QRS en ECG ruidosos, se propone un algoritmo evolutivo para optimizar los parámetros del detector. La señal de HRV se obtiene a partir del modelo TVIPFM, que tiene en cuenta las variaciones en el ritmo cardiaco medio durante el ejercicio. Para tratar con la naturaleza no estacionaria de la señal, se usa un análisis frecuencial de tiempo-frecuencia para extraer parámetros de potencia instantánea. Debido a que la frecuencia respiratoria cambia durante el ejercicio, normalmente alcanzando altas frecuencias, se hace necesario redefinir la banda de alta frecuencia (HF). Además, componentes espectrales relacionados con el acoplo cardiolocomotor (CC) son identificados en el espectro de potencia de la HRV, y se aplica una corrección cuando esta componente solapa con la componente de HF.

Esta metodología se aplica a tres pruebas de esfuerzo para estudiar la respuesta del SNA al estrés del ejercicio en sujetos sanos: una prueba máxima en tapiz rodante, una prueba submáxima en tapiz rodante y otra prueba submáxima en bicicleta estática.

Se definen diferentes intervalos en cada test: uno relacionado con la fase de reposo, uno al principio de la fase de recuperación, y el resto, durante el ejercicio, basados en una demanda metabólica similar basada en el consumo de oxígeno. Se analizan las potencias normalizadas relacionadas con la baja frecuencia (LF) y HF en estos intervalos: en el primer intervalo del ejercicio, durante intensidades bajas del ejercicio, la LF aumenta como respuesta a una activación del sistema simpático nervioso, mientras que la HF disminuye a causa de la inhibición de la actividad parasimpática. Durante intensidades altas de ejercicio, la HF aumenta mientras que la LF disminuye, ya que ahora la HF no solo refleja la respuesta autónoma, sino también el efecto mecánico de la respiración. La potencia del acoplo cardiolocomotor, CC, aumenta con la intensidad del ejercicio, alcanzando hasta un 30% de la potencia total en los últimos intervalos de ejercicio, siendo mayor en las pruebas de tapiz rodante.

También se pretende validar un monitor de ritmo cardiaco en función de las medidas de HRV. Las series de RR son obtenidas de manera simultánea a partir del ECG y un equipo Polar comercial durante ejercicio dinámico de baja, media y alta intensidad. Coeficientes de confianza y conformidad muestran que ambos métodos son intercambiables cuando se mide el ritmo medio cardiaco y la potencia LF instantáneos, con independencia de la intensidad del ejercicio (coeficientes > 0.9). Sin embargo, las medidas de potencia HF instantánea muestran coeficientes por debajo de 0.7 en los últimos intervalos de ejercicio. A pesar de estos coeficientes de confianza y conformidad bajos, cuando se obtienen los parámetros de HRV como valores medios en los intervalos de análisis y se corrigen las componentes espectrales de CC, no se encuentran diferencias significativas entre las medidas del ECG y del Polar. Ambos parámetros describen la misma respuesta del SNA ante el estrés del ejercicio. Por tanto, el uso de las medidas de HRV a partir del Polar es apropiado sin importar la intensidad del ejercicio.

El análisis de la HRV se aplica también a una prueba de esfuerzo con el objetivo de determinar la capacidad de diagnóstico de las medidas de HRV en ejercicio para la detección de enfermedades de las arterias coronarias (CAD). Estos pacientes presentan un alto número de anomalías en la serie de RR, principalmente debido a eventos arrítmicos, y por tanto es necesario un cuidado especial a la hora de seleccionar los intervalos a analizar. Además, debido a los efectos de la medicación y a la diferencia en la duración de la prueba de esfuerzo entre los pacientes de CAD y el grupo de baja probabilidad (LLC), tanto el ritmo cardiaco medio como la frecuencia respiratoria no son fiables para diagnosticar CAD. La potencia de HF, cuando es guiada por la respiración, alcanza el mayor AUC, por encima del 0.7 tanto en reposo como en recuperación. Cuando se mide en intervalos con una demanda metabólica similar, basado en el incremento en el ritmo cardiaco medio, se puede apreciar una diferencia significativa en el último intervalo de ejercicio entre los grupos CAD y LLC, con menor potencia LF normalizada y mayor potencia HF (normalizada y en valor absoluto) en los pacientes de CAD, lo que sugiere que los parámetros de HRV pueden diagnosticar CAD antes de acabar la prueba de esfuerzo. Debido a la falta de monitorización de la frecuencia de pedaleo, la componente CC no puede corregirse, y el uso de una banda extendida de HF medirá componentes no deseadas. Esto hace resaltar la necesidad de una metodología estándar para el análisis de la HRV durante ejercicio.

Otra aplicación donde se analiza la HRV es en hemodiálisis. La hipótesis de este estudio es que los pacientes propensos a sufrir hipotensión presentan una alteración en la regulación autonómica del sistema cardiovascular. Se proponen diferentes parámetros para diferenciar a los pacientes propensos de los resistentes a sufrir hipotensión. A los parámetros de HRV se les añade información adicional a partir de la variabilidad de la presión sanguínea (BPV), sensibilidad barorrefleja (BRS) y respiración por medio de señales respiratorias derivadas del ECG (EDR) para mejorar la diferenciación. Se encontró además una modulación de muy baja frecuencia (VLF) en las series de HRV, BPV y EDR, y se propone caracterizarla con la hipótesis de que su causa es la inestabilidad hemodinámica de los pacientes. Se aplica el método MVDR para extraer los parámetros espectrales ya que, en general, presenta mejor resolución espectral que otros estimadores espectrales. Todos estos parámetros se analizan individualmente. La frecuencia respiratoria no presenta correlación aparente con el estatus del paciente. La modulación de VLF aparece de manera más frecuente en pacientes propensos y podría estar relacionado con una alteración en el SNA. Algunos parámetros de HRV (LF normalizada y ratio), BPV (HF) y BRS (LF) son también capaces de discriminar entre los dos grupos.

El resto de parámetros de HRV, BPV y BRS se usan para diseñar un clasificador que, usando información de los primeros 30 minutos del tratamiento, sea capaz de clasificar pacientes propensos y resistentes a sufrir hipotensión con el objetivo de tener una identificación temprana de los pacientes propensos. El clasificador se entrena usando un método de leave-one-out (debido al limitado tamaño de la base de datos), donde todos los registros pertenecientes a un mismo paciente se dejan fuera del entrenamiento, y el proceso se repite para cada paciente. El proceso de selección de características selecciona y elimina características hasta que encuentra el set óptimo. Añadiendo información del estado de diabetes de los pacientes, el rendimiento global del clasificador mejora, obteniendo valores de sensibilidad y precisión de Se=97.5% y Acc=92.1%. Ya que la mayoría de los parámetros están relacionados con la HRV, principalmente el ratio LF/HF y la potencia LF normalizada, se propone usar un nuevo clasificador que solo use parámetros de HRV, con la ventaja de no tener que registrar la presión sanguínea. Este nuevo clasificador consigue Se=95% y Acc=90.2%.

La última aplicación es la propuesta de los parámetros de HRV como marcadores de la integridad del SNA en pacientes críticos en la UCI como un estudio exploratorio. Los pacientes críticos presentan alteraciones en el SNA que pueden perdurar incluso después del alta, y en particular se ha observado que cada vez hay más casos de problemas neurocognitivos. Se ha sugerido una rehabilitación cognitiva para este tipo de pacientes para mejorar el déficit cognitivo, y se proponen los parámetros de HRV para analizar la respuesta a esta rehabilitación y su efectividad para mejorar la integridad del SNA. Las principales limitaciones en estos pacientes son que toman un gran número de medicación que altera la actividad del SNA, que algunos pacientes están mecánicamente ventilados, otros sufren delirio (que no está claro si está causado por una deficiencia autonómica), y en general forman un grupo muy heterogéneo de pacientes. Al análisis de la HRV se le añade la información respiratoria, y para tratar con el patrón tan irregular de la respiración en algunos pacientes, la banda espectral relacionada con la componente HF se adapta en consecuencia para cada paciente.

Comparando con los valores de base, 7 pacientes mostraron un incremento en la potencia de HF después de la sesión, sugiriendo un aumento en la actividad parasimpática, mientras que 5 pacientes mostraron un descenso en la potencia de LF normalizada, lo que sugiere un descenso en la actividad simpática. Estos resultados deben interpretarse con especial cuidado debido a las características de los pacientes, que ya tienen alterado el SNA por las enfermedades o la medicación. Se está registrando una mayor base de datos en este momento con la intención de seguir explorando la capacidad de los parámetros de HRV como marcadores de la integridad del SNA en pacientes críticos.

Palabras clave: Sistema Nervioso Autónomo; Variabilidad de Ritmo Cardiaco; Variabilidad de Señales Cardiovasculares; Respiración; Monitorización No Invasiva; Análisis Espectral No Estacionario; Prueba de Esfuerzo; Monitor de Ritmo Cardiaco; Diagnóstico de Enfermedades de las Arterias Coronarias; Hemodiálisis; Procesado de Señal

Acknowledgements

This thesis is the result of years of work, and I have met a lot of people who have helped me in one way or another. First of all, I would like to thank my supervisors, Raquel Bailón and Pablo Laguna, for all the support and assistance through all these years. Raquel, you have always been the first one to cheer me up when things were not the way we expected, and you have taught me a lot about the research world. Pablo, with your contagious curiosity, you have taught me to always ask "why?". Both of you have greatly helped me to reach this point of my life.

I would also like to extend my thankfulness to the group BSICoS: Eduardo, Juan Pablo, Esther, Jesús, Sampedro, Carlos, Violeta... all of you have contributed to this work in one way or another. Special mention to the best lab mate I could ever have, Julia, I met you a lot of years ago and you have been a real support through all these years and we have a lot of memories together, I simply can't imagine all these years without your company. Also special mention to Jesús, our talks about everything and nothing at the same time are really precious to me, you have helped me both professionally and personally so many times, I don't think I can ever thank you enough. And of course, thanks to the rest of the JADAJ team (because we also deserve a name!) too, Alba and Alex. Alba, it's great having you here from time to time, even though your stays are always too short. Alex, thanks for your willingness to help me whenever I needed. I will always remember all of you, wherever you are.

Following with the rest of BSICoS group, a special mention to the HRV team. Juan, thanks for all the coffees together, our never ending debates about HRV units, and our talks full of nonsense. Spyros, thanks for teaching me Greek in your free time and our travels by tram together. And Javier Milagro, for your great company in the coffees. And thanks to Arantxa, for all the administrative work (one task per day) and for your contagious joy and optimism, it is almost like you are always in our lab... no, really, your voice is literally inside our lab.

I would also like to thank all the researchers I have had the pleasure to collaborate with. I have met a lot of great people in my two research stays and I have a lot of memories from those days. Thanks to Michele and Frida, for reading this thesis in such a short amount of time.

También quiero agradecer a toda la gente que ha vivido esta etapa de mi vida a mi lado fuera del ámbito de la universidad. A Jorge, por aguantar todos los malos momentos. A Almudena, porque siempre estás disponible para charlar. A Bea y a Jorge, por sacar siempre un hueco y por nuestras cenas en el Matarraña. A Loreto,

que cada vez que nos vemos parece que nunca pasa el tiempo. Y a los Revientatours, que prácticamente me han visto crecer.

Y no quiero acabar esta sección sin darles las gracias a dos personas esenciales en mi vida: mis padres, que han hecho tantísino por mi y me han apoyado en cada decisión que he tomado. Gracias.

Contents

List of Figures

List of Tables

List of Acronyms

A agreement . . . 56
ANS autonomic nervous system . . . 1
AV atrioventricular . . . 6
BP blood pressure . . . 8
BPV blood pressure variability . . . 3
BRS baroreflex sensitivity . . . 2
CAD coronary artery disease . . . 16
CC cardiolocomotor coupling . . . xvi
CCC concordance correlation coefficient . . . 56
CF cadence frequency . . . 36
CR cognitive rehabilitation . . . 112
EA evolutionary algorithm . . . 24
EDR ECG-derived respiration . . . 10
ECG electrocardiogram . . . 2
HF high frequency . . . 13
HRV heart rate variability . . . 2
HR heart rate . . . 2
ICC intraclass correlation coefficient . . . 56
ICU intensive care unit . . . 111
IDH intradialytic hypotension . . . 2
IPFM integral pulse frequency modulation . . . 12
LF low frequency . . . 13
LLC low likelihood of CAD . . . 67
LOA limits of agreement . . . 55
MI miocardial infraction . . . 14
MV mechanically ventiled . . . 114

Chapter 1

Introduction

1.1 Motivation

The autonomic nervous system (ANS) is in charge of the maintenance of homeostasis of the body. This system is also known as the involuntary nervous system, since it functions without conscious control. Because it innervates cardiac muscle, smooth muscle, and various endocrine and exocrine glands, this nervous system influences the activity of most tissues and organ systems in the body [1]. The regulation of heart rate, blood pressure, gastrointestinal responses, focusing of the eyes, and thermoregulation are just a few of the many homeostatic functions regulated by the ANS [1]. Impaired autonomic regulation has been observed in cardiovascular, metabolic and mental diseases. Regular ANS evaluation might be helpful to early detect malfunctioning, monitor diseases, develop personal treatments or even anticipate relapses.

There are different methods to measure ANS activity [2]. Many invasive measurements focus on measuring neurotransmitter levels, like circulating catecholamines and other substances in plasma, which are modulated by the ANS and can provide information about ANS activity [3]. Other measurements, like the noradrenaline spillover rate, allow concrete information in specific target organs [4]. Radioisotope techniques

have also been used to measure cardiac innervation [4]. On the other hand, non-invasive measurements of ANS activity are more appealing. Since ANS modulates different systems of the body, such as heart rate, blood pressure, respiration, or even sweat secretion, studying changes in these variables also provides information of ANS activity.

One of the most popular non-invasive methods of ANS evaluation is heart rate variability (HRV) analysis and is easily obtained from the electrocardiogram (ECG) signal. HRV reflects purposely generated responses to internal and external stimuli, being ANS the primary regulator of cardiac chronotropy [5]. Even at rest, the beat time occurences are not constant. By recognizing patterns in these variations, information about the activity of ANS can be extracted. Aditionally, other cardiovacular variability signals (such as blood pressure variability) and respiration can also provide added value to the assessment of ANS state, since they are either regulated by it, or trigger its response.

Most of the tools developed to analyze and interpret HRV have been designed in a stationary environment [6]. When this premise is not valid, the algorithms need to be adapted and interpretation of HRV parameters requires special care. A clear example is HRV analysis during exercise. Sports physiologists are interested in HRV to understand autonomic changes due to exercise training and the cardiovascular response to the stress of exercise, as well as a marker of overreaching and overtraining [7, 8]. For physicians, HRV analysis during exercise may allow to detect ANS alterations which may not be visible at rest, or that are more evident in those conditions, such as ischemia events [9]. Wearable heart rate (HR) monitors have increased even more the interest of analyzing HR during exercise, although the validity of HRV measurements derived from these devices during exercise still needs to be validated.

Not only the common methodology is not appropriate in these conditions, but also its interpretation is still challenging and a matter of debate. During high intensity exercise, new components appear when analyzing HRV which reflect cardiolocomotor coupling and increase with workload [10]. It is important to understand the mechanisms underlying these components to correctly interpret HRV measurements. Additionally, respiration plays a crucial role in HRV analysis during exercise. The lack of a standard methodological framework may lead to contradictory results when interpreting HRV parameters [11].

Another application where analysis of HRV as a measure of ANS is challenging is in patients undergoing hemodialysis. During this treatment, hypotension events are likely to happen. Patients prone to suffer intradialytic hypotension experiment a decrease in blood pressure which ultimately leads to the premature termination of the treatment. ANS alterations have been suggested as one of the main underlying causes of these hypotension events [12, 13]. In fact, HRV parameters have previously shown significant differences between prone and resistant patients [13–15]. However, they may not be powerful enough to alone predict intradialytic hypotension (IDH) with a clinically acceptable accuracy [16]. To better assess ANS state, the addition of other signals has been proposed. One example is blood pressure signal, which can be used to assess baroreflex functioning. The baroreflex sensitivity (BRS) measures how

the baroreflex response modulates heart rate in response to changes in blood pressure, which is thought to play an important role during these events. BRS parameters have shown contradictory results in their capability to discriminate prone and resistant patients [17, 18], although these differences may be due to different methodological approaches. Respiratory information has never been studied in these patients, but several works have demonstrated that it has a direct relation with HRV and blood pressure variability (BPV) [19–21]. Combining information from HRV, BPV, BRS and respiration may improve the early identification of prone patients to properly adapt the treatment and minimize the risks of hipotension events.

Lastly, interest on HRV analysis is increasing in intensive care units. Growing evidence suggests that critical illness often results in significant long-term morbidities and develop neurocognitive impairments in a magnitude similar to mild-moderate dementia [22] that can persist for years after hospital discharge. As an explorative study, HRV measurements are proposed as markers of ANS integrity, and are used to test the effectiveness of early cognitive rehabilitation in critically ill patients.

The objective of this thesis is to extract information about ANS state from cardiovascular signals and respiratory information in different environments. This work addresses the necessity to develop robust methodologies adapted to three different scenarios to make sure that measurements allow us to correctly interpret changes in ANS activity. The first scenario is HRV analysis during high intensity levels of exercise: a methodological framework will be presented which addresses the noisy and non-stationary nature of the signals and changes in the mean heart rate and respiratory frequency. It will be applied to study ANS response of athletes to running and cycling stress testings. Then, the clinical value of exercise HRV assessed using the proposed methodology will be studied in coronary artery disease diagnosis. The second scenario is hemodialysis: HRV, BPV, BRS and respiration will be studied with the aim to identify hypotension prone and resistant patients. The third scenario is the proposal of HRV measurements as markers of ANS integrity in a proof of concept regarding an early cognitive rehabilitation in critically ill patients.

1.2 Autonomic nervous system

The efferent nervous activity of the ANS is largely regulated by autonomic reflexes. Subconscious sensory signals from a visceral organ are transmitted to homeostatic control centers, in particular those located in the hypothalamus and brain stem, and then subconscious reflex responses are returned directly back to the visceral organ to control its activities [1, 23]. The efferent autonomic signals are transmitted through two major subdivisions called the *sympathetic nervous system* and the *parasympathetic nervous system* [23].

Both systems are tonically active, i. e., they provide some degree of nervous input to a given tissue at all times. It is the frequency of discharge of neurons what modulates the activity. As a result, tissue activity may be either enhanced or inhibited [1]. Sympathetic tone is related to the *fight-or-flight* response, it activates increasing heart

rate and respiratory rate (among other changes) to confront any threats. On the other hand, in a relaxing environment the parasympathetic tone (also called vagal tone) is more predominant and is related to the *rest and digest* state. Many tissues and organs are innervated by both systems. Since sympathetic and parasympathetic systems typically have opposing effects, if one system increases its activity while the other decreases it, the result is a rapid and precise control of a tissue's function. Other tissues, however, are only innervated by one system. Figure 1.1 shows both systems and the tissues and organs related to each of them.

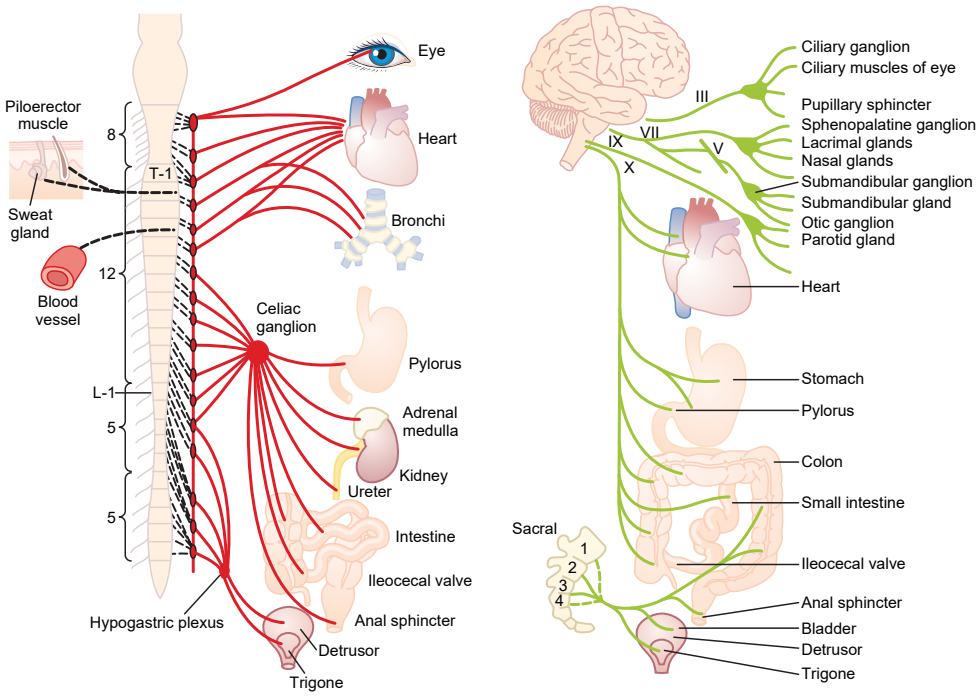

Figure 1.1: Sympathetic nervous system (left) and parasympathetic nervous system (right), from [23].

The two most common neurotransmitters released by neurons of the ANS are acetylcholine and norepinephrine. Those fibers that secrete acetylcholine are said to be cholinergic. Those that secrete norepinephrine are said to be adrenergic [23]. The sympathetic nerves are different from skeletal motor nerves in the sense that each pathway innervated tissue is composed of two neurons, a preganglionic neuron and a postganglionic neuron, in contrast to only a single neuron in the skeletal motor pathway. All preganglionic neurons are cholinergic in both systems. However, almost all of the postganglionic neurons of the parasympathetic system are cholinergic, while most of the postganglionic sympathetic neurons are adrenergic. Therefore, with a few exceptions, the terminal nerve endings of the parasympathetic system secrete acetylcholine and the sympathetic nerve endings secrete norepinephrine. When measuring neuro-

transmitters, acetylcholine is called a parasympathetic transmitter and norepinephrine is called a sympathetic transmitter.

The *sympathetic nervous system* innervates the sinoatrial (SA) node and alter the natural pace of the electric impulse origination, increasing the heart rate. The myocardium is innervated and the muscle contractility increases by a sympathetic activation, thus achieving a higher stroke volume. Additionally, sympathetic innervation causes vasoconstricition on blood vessels. Therefore, there is an increase in blood pressure caused by increased cardiac output and vascular resistance. Sympathetic stimulation also contracts the meridional fibers of the iris that dilate the pupil. The sweat glands secrete large quantities of sweat when the sympathetic nerves are stimulated; however this is an exception of sympathetic nerve ending which secretes acetylcholine and furthermore, they are stimulated primarily by centers in the hypothalamus that are usually considered to be parasympathetic centers.

The *parasympathetic nervous system* makes the HR decrease. The blood pressure is decreased due to a lower cardiac output, although parasympathetic activity has almost no effect on blood vessels. Parasympathetic stimulation contracts the circular muscle of the iris to constrict the pupil and is in charge of the focusing of the lens. Effect of this system can also be seen in the bronchial tubes constriction, in stomach movements and secretions and the increase in saliva production, among others. About 75% of all parasympathetic nerve fibers are in the vagus nerves, therefore parasympathetic tone is also known as vagal tone.

Focusing on the heart, both systems are altering the natural heart rate at the same time. At rest, parasympathetic tone is more predominant, lowering the HR. As a reference, an innervated heart has a HR of about 120 beats per minute [24]. On the other hand, while doing physical activities, the sympathetic tone is the one that dominates. The two different modulations in HR can be observed as rhythms at different frequencies in the variability of HR, allowing the interpretation of ANS activity by analyzing HRV.

1.3 Biological signals

1.3.1 Electrocardiogram

The ECG signal describes the electrical activity of the heart and provides, in a non-invasive way, information about the cardiac muscle activity. It is recorded using electrodes placed on the body surface. Cardiac cells can be excited and, as a result, an action potential is produced. During the action potential the electrical membrane potential of the cell rapidly rises and then falls back to its original state. At the same time, this action potential excites the surrounding cells. The sum of the contribution of all action potentials of the cardiac cells as the electric impulse propagates through the heart generates a series of waves on the ECG. These waves have different morphology and temporal duration, which gives information about the state of the heart, and abnormal changes in these waves can be used to diagnose cardiac deseases.

A normal beat is generated in the sinoatrial (SA) node, located in the upper part of the right atrium. The electric impulse is propagated to the rest of the right atrium and left atrium and arrives to the atrioventricular (AV) node. During this phase, the contraction of the atria makes the blood go into the ventricles. From the AV node, the impulse is delayed by slower conduction tissues in that area so that blood can completely fill the ventricles, before starting to propagate to the ventricular cells. When ventricles are contracted, the heart pumps out the blood. The ECG signal gathers all this spatio-temporal information in the different waves, see Figure 1.2. The union of the Q, R and S waves is called the QRS complex, which is usually used to establish the beat time occurence. The distance between two consecutive beats is usually measured as the distance between two consecutive R waves, hence called RR interval.

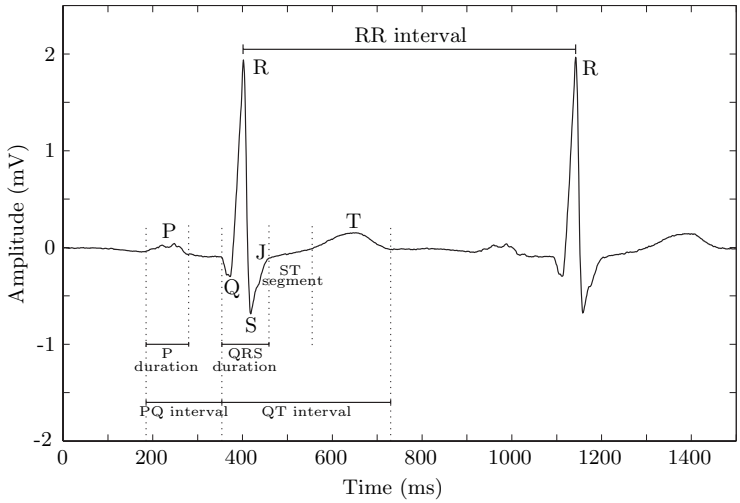

Figure 1.2: ECG signal with the most important waves and intervals, from [25].

The ECG usually is measured using several electrodes over the skin. Differences on voltage between two electrodes are represented as a *bipolar lead*, although voltage variation in a single electrode can also be used as a *unipolar lead*. The standard 12-lead ECG is the most widely used lead system in clinical routine, which combines three different lead configurations: the bipolar limb leads *I*, *II* and *III*; the augmented unipolar limb leads *aVR*, *aVL* and *aVF*; and the unipolar precordial leads *V1*, ..., *V6*, see Figure 1.3. Additionally, the three orthogonal leads have been proposed as an alternative representation and each lead (X, Y and Z) represents the spatial axis: right-left axis, head-to-feet axis and front-back axis, respectively. This configuration is specially useful to track the loop that describes the dominant direction of the electrical axis and is referred to as vectorcardiogram (VCG) [25], see Figure 1.4.

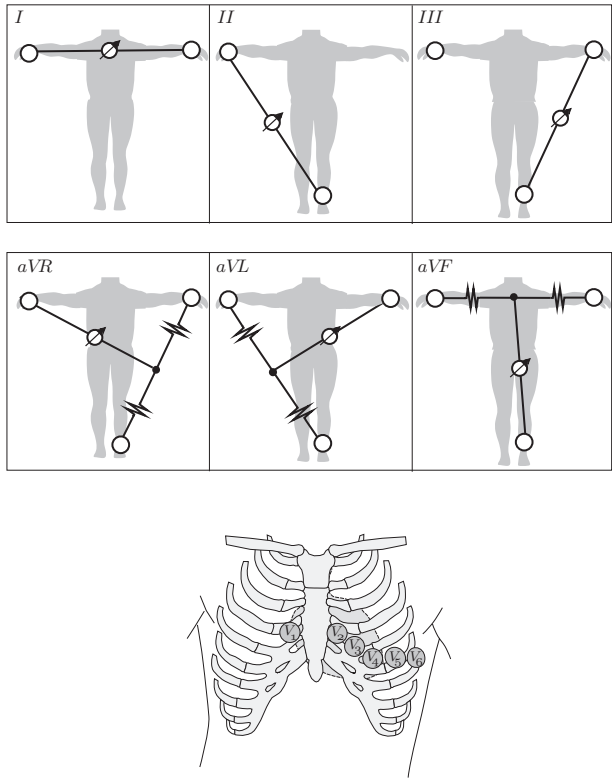

Figure 1.3: Electrode positions for the bipolar limb leads (*I*, *II* and *III*), the augmented unipolar leads (*aVR*, *aVL* and *aVF*) and the unipolar precordial leads (*V1*, ..., *V6*), from [25].

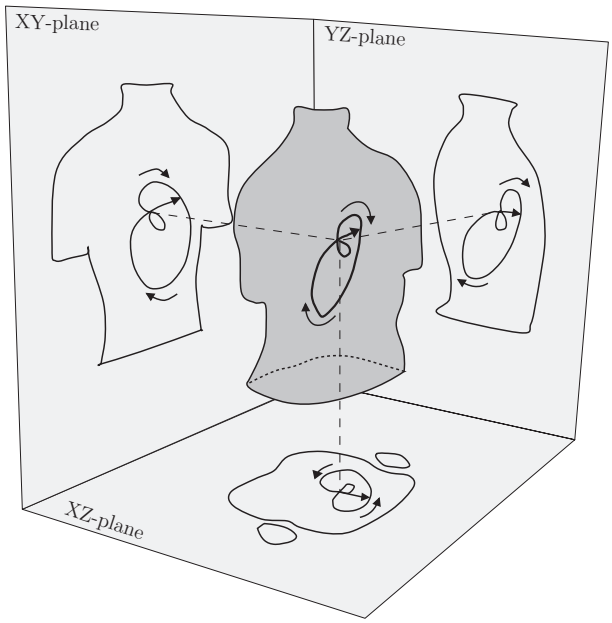

Figure 1.4: A VCG loop and its projection onto the three orthogonal planes, from [25].

1.3.2 Blood pressure

The blood pressure (BP) is defined as the pressure exerted by circulating blood upon the walls of blood vessels (arteries, arterioles, veins and capillaries), although it generally means arterial pressure. Together with respiratory frequency, heart rate and thermoregulation, it is the most common measured parameter in clinical routine.

It is closely related to the cardiac cycle. Following the ventricular systole, i. e., the contraction of the ventricles, the heart pumps out the blood to the arteries and the BP reaches its maximum value. This peak of the pressure wave is known as systolic pressure. Meanwhile, during the diastole or relaxation of the ventricles, the pressure wave reaches its minimum value, known as diastolic pressure. An example of the BP signal can be seen in Figure 1.5.

The typical blood pressure values for an adult, healthy, rested person are approximately 120 mmHg for systolic and 80 mmHg for diastolic pressure. A general classification can be seen in Table 1.1.

However, systolic and diastolic pressure levels are not constant and they experiment beat-to-beat natural variations, and there are large variations among different patients. A continuous monitoring of BP signal can be obtained with especific devices, such as cuff-finger BP monitors, to provide added value to HRV analysis in the ANS assessment.

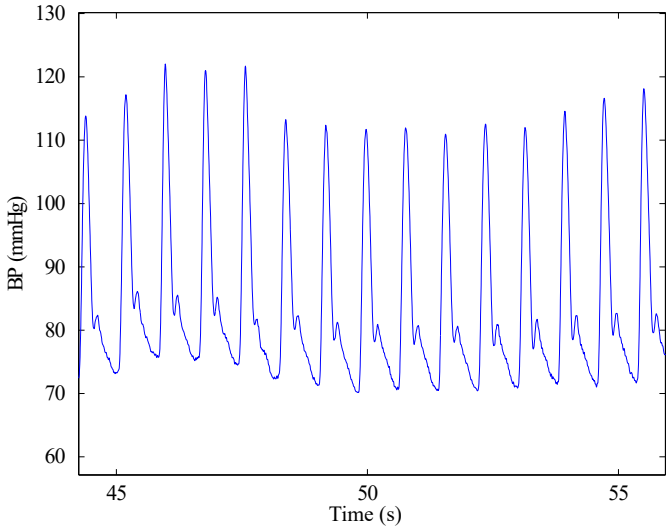

Figure 1.5: Blood pressure signal recorded by Finometer system.

CATEGORY	Systolic pressure (mmHg)	Diastolic pressure (mmHg)
Hypotension	< 90	< 60
Optimal	90 - 119	60 - 79
Normal	120 - 129	80 - 84
Normal high	130 - 139	85 - 89
Hypertension grade 1	140 - 159	90 - 99
Hypertension grade 2	160 - 179	100 - 109
Hypertension grade 3	$\geqslant 180$	$\geqslant 120$

Table 1.1: Classification of blood pressure for adult people.

1.3.3 Respiratory signal

The process of breathing is an automatic and effortless inspiratory expansion and expiratory contraction of the chest cage. During inspiration the person takes in oxygen, while during expiration the carbon dioxide is released. Normal breathing has a relatively constant rate and inspiratory volume that together constitute normal respiratory rhythm [26]. The respiratory center can alter the breathing timing or intensity to adapt to the body's need, leading to changes in the rate and tidal volume.

Autonomic nervous system dysfunction has been related to impairment on breathing during sleep [27]. Obstructive sleep apnea is the most common, which is associated with an elevated sympathetic tone [28]. Altered autonomic control has also been found in patients with asthma [29,30] and periodic breathing patterns occurs typically in patients with congestive heart failure [31].

Respiration has an effect with cardiovascular regulation in different ways [19–21]. Respiration affects both HR and BP, which in turn are mutually related [21]. The respiratory sinus arrhythmia (RSA) is a well known effect of respiration in HR, where a faster HR appears in inspiration and a slower HR can be seen in expiration. One possible explanation is that during respiration, changes in intrathoracic pressure rhythmically alter venous return to the heart, thereby impacting cardiac output and subsequently changing arterial blood pressure [5]. These variations in BP produce inverse variations in HR via the baroreflex. In turn, changes in HR cause changes in blood pressure through direct mechanical effects. However, the mechanisms responsible for the coordination between the autonomic control of circulation and respiration are still unclear, and there is still a debate wether the origin of RSA is direct central nervous modulation, reflex phenomena, mechanical influence of respiration or a mixture of them [32–35].

The magnitude of RSA is thought to reflect the degree of respiratory modulation of vagal outflow [5], since it is attenuated with progressive suppression of cardiac vagal activity and abolished by complete vagal blockage with atropine. Despite physiological studies questioning respiratory sinus arrhythmia as a valid and reliable cardiac parasympathetic index [36,37], numerous clinicians and experimentalists routinely estimate vagus nerve activity over the heart with measurements of RSA.

Additionally, chest movements and changes in the thorax impedance distribution due to filling and emptying of the lungs cause a rotation of the electrical axis of the heart which affects beat morphology [38]. This information can be used to extract respiratory information from the ECG obtaining the so called ECG-derived respiration (EDR) [38]. The advantage of these methodologies is that repiratory information can be extracted without the need of other devices which can interfere with natural breathing or are unconfortable for the subject. Two different EDR methodologies have been used in this thesis: one that exploits the respiration-induced beat morphology variations on the QRS slopes of the ECG [39], and one that exploits variations in the direction of the heart's electrical axis [40].

1.4 Heart rate variability

The origin of the heart rate variability lies in the electrical impulses which are generated in the SA node. The heart rate varies beat-to-beat with small variations around the mean, and these variations are controlled by the ANS. Generally speaking, sympathetic system is the responsible of increasing the heart rate while the parasympathetic system decreases it. The interaction between both systems is the origin of the HRV.

Cardiac cells can autoexcite themselves with a frequency that is dependant on the slope of diastolic depolarization [41]. While they have an inherent discharge rate, ANS can alter this rate, thus accelerating or delaying the beat generation rate. Figure 1.6 shows how the slope of the action potential of a cell in the SA node varies depending of ANS influence.

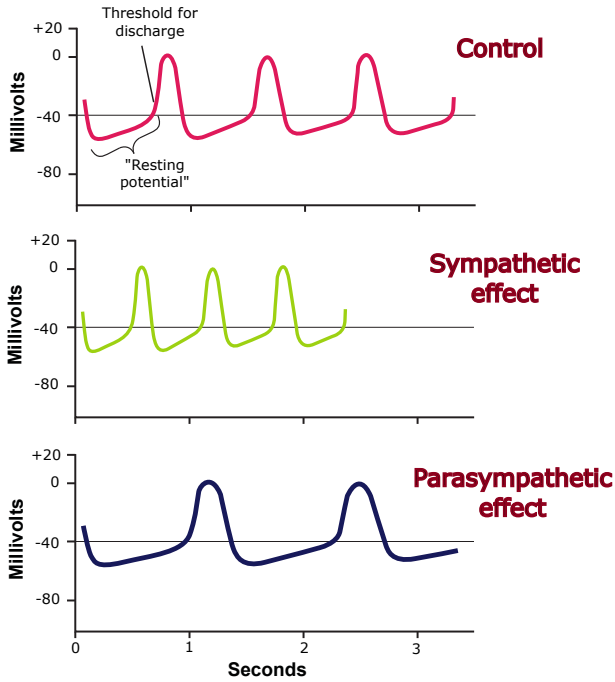

Figure 1.6: Effect of ANS activity on the SA node cells. From [23] (modified).

Representation of HRV

There is not a unique representation of the heart rhythm [25]. The simplest one is the *interval tachogram*, whis is a series of RR intervals, and has been extensively

used to measure temporal parameters of HRV. Another series is the *inverse interval tachogram*, which gives information about the frequency, or rate, i.e, the inverse of the RR intervals. An extension of these series leads to the *interval function* and the *inverse interval function*, which are the unevenly sampled, continuous-time versions of the tachograms. Evenly sampled versions can be also obtained by interpolating the interval functions. Some examples can be found in Figure 1.7.

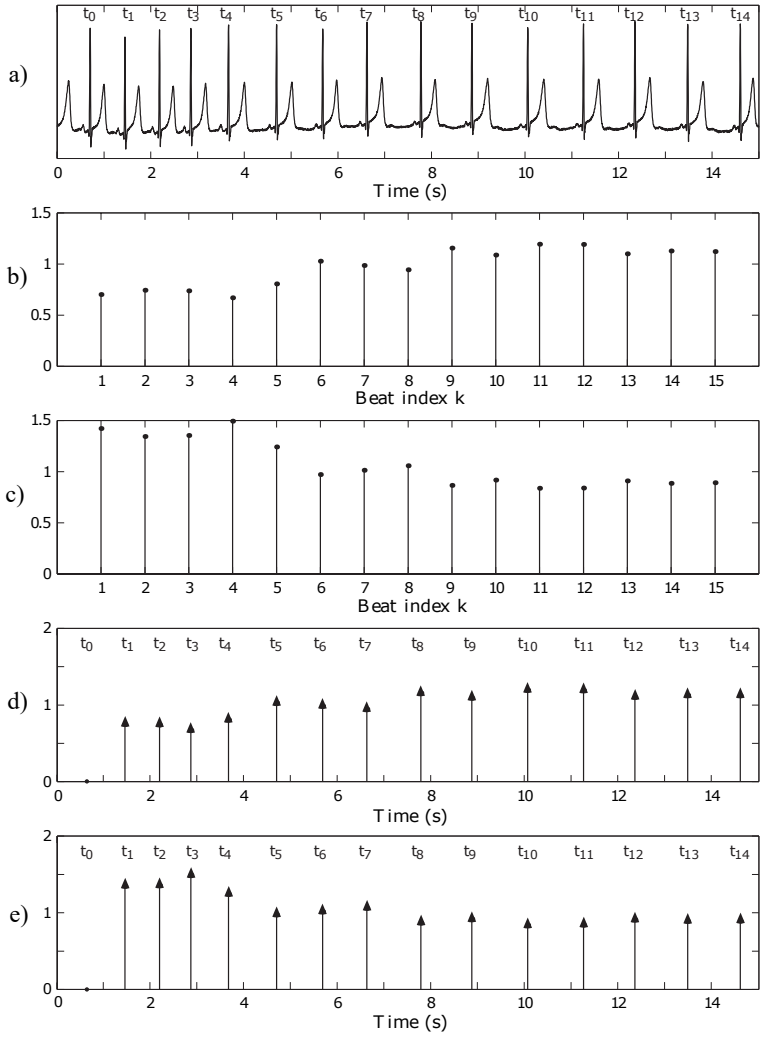

Figure 1.7: a) Example of an ECG signal with the beat occurrence times. b) Interval tachogram. c) Inverse interval tachogram. d) Interval function. e) Inverse interval function. From [25]

The heart timing signal is another representation which is based on the integral pulse frequency modulation (IPFM) model. The hypothesis under this model is that the sympathetic and parasympathetic systems activity can be represented as a mod-

ulating signal with zero mean, which is added to a DC level (equal to 1), and is integrated up to a threshold, defined by the mean cardiac period. At that time, a beat is produced and the integrator is reset, starting the process again [42]. The modulating signal carries the ANS activity information and represents slope changes in the SA node cells "resting potential", induced by ANS, as explained in Section 1.2. The heart timing signal has been proposed as an unevenly sampled signal defined as the deviation of the event time from the expected occurrence time, and is aimed explicitly at estimating the modulating signal.

In situations where the mean heart period is not constant, IPFM model with a constant threshold is not appropriate, and several works have pointed out the necessity of taking into account the time varying mean heart rate [43–45]. In this thesis, we focus on estimating this modulating signal, based on a modification of the IPFM model called time-varying threshold IPFM (TVIPFM) [46].

HRV parameters

The most used HRV parameters at rest are explained in [6,47,48]. Basically, they can be divided in three groups: temporal, frequency and non-linear parameters.

- *Time-domain parameters* are based on statistical or geometric measurements of the normal-to-normal interval series (NN). Information about HRV are extracted from the standard deviation (SDNN), the root mean square of differences of successive intervals (rMSSD), among others [6].

- *Frequency-domain parameters* use information of the power spectrum density estimation of the HRV signal. Three major components appear in the HRV spectrum: a very low frequency (VLF) component whose oscillatory frequency is between 0 to 0.04 Hz, a low frequency (LF) component with frequencies ranging from 0.04 to 0.15 Hz, and a high frequency (HF) component with frequencies from 0.15 to 0.4 Hz. The LF component is considered to be a measure of the sympathetic branch activity, at least when its power is expressed in normalized units with regard to the total power in HRV, taking VLF component apart [49, 50]. The HF component is considered a measure of the parasympathetic activity, mainly due to the RSA [50]. A quantitative measure of the interaction between the two systems, that is, the sympathovagal balance, can be measured as the ratio of the LF power to the HF power [49,50].

- *Non linear parameters* use theory of nonlinear dynamics to describe the process which generates the HRV signal. Some of these parameters are the correlation dimension (CD), largest Lyapunov exponent (LLE), SD1/SD2 of Poincare plot, approximate entropy (ApEn), Hurst exponent, among others [47,48].

Note that these methodologies may need to be adapted in non-stationary environments. In this thesis, we will focus on frequency-domain parameters, since they can better separate the effect of sympathetic and parasympathetic modulations.

Clinical relevance of HRV

HRV is used in the clinic as a noninvasive way to assess ANS state in patients with different diseases. It is known that HRV is depressed in patients with congestive heart failure [51]. In patients with miocardial infraction (MI), a predominance of sympathetic activity and reduction in parasympathetic cardiac control has been found [52], but the general reduced HRV may only be partially caused by ischemia [53]. A significant reduction in HRV has also been found in patients with left ventricular hypertrophy [54], which is associated with increased cardiovascular mortality and sudden cardiac death [55]. Other fields where HRV has been studied are patients with renal failure [56] and with disorders of the central and peripheral nervous system [57, 58], among others. Still, HRV measurements may show contradictory results in other applications, which may be due to differences in the methodology or in the inability of HRV to reflect underlying ANS alterations.

When interpreting HRV parameters, other information should be taken into account. For example, the significant gender-related difference of HRV has been shown to decrease with increasing age [59]. There are also differences, in the same patient and with the same conditions, in measurements taken in different times of the day [60]. Drugs, alcohol and smoking also affect ANS [61–63].

1.5 Blood pressure variability and baroreflex sensitivity

The blood pressure waveform changes continuously over time in response to the needs of the different vascular districts, the effects of external perturbations, and the autonomic and humoral regulation of circulation. The beat-to-beat dynamics of the BP can be analyzed in the systolic and diastolic blood pressure, and even a surrogate of heart rate can be obtained with the blood pulse rate [64].

Respiration affects BP in each breathing cycle: arterial BP falls on inspiration, and rises on expiration. This variations are located in the HF band, synchronous with the respiratory rate. LF component is thought to be related to central oscillators modulating the sympathetic efferences on the heart and vasculature [65] or to a resonance in the baroreflex loop [65].

The baroreflex system is in charge of the blood pressure homeostasis. When there are changes in the blood pressure, the baroreflex modulates the heart rate, peripheral vascular tone, and other cardiovascular variables to return the BP to its initial value [64]. The state of the baroreflex system is usually assessed by evaluating the sensitivity of the baroreflex control over the heart (BRS). Thus, BRS parameters measure changes in HR due to changes in BP.

Similar to HRV, BRS can be measured in several ways. The sequence technique is a time domain method which consist of analyzing systolic blood pressure (SBP) and RR interval series beat-by-beat to find similar changes [66]. Other time domain methods

are the x-BRS approach, which is based on the cross-correlation between SBP and RR in very short segments [67], or the identification of baroreflex events, which are not constrained to be of constant length [68]. Regarding the frequency domain techniques, the alpha coefficient is measured as the root square of the ratio between the spectral power of RR and SBP in a given frequency band. The transfer function is also used, evaluated as the ratio between the cross-spectrum and the SBP spectrum [69]. Other approaches use model-based techniques (ARMA, ARXAR) [70, 71].

1.6 Objectives and structure of the thesis

The main objective of this thesis is to assess ANS activity by means of the analysis of cardiovascular signals variability in non-stationary environments, namely stress testings (Chapters 2 to 4), hemodialysis (Chapter 5) and critically ill patients (Chapter 6). The content of the thesis is organized as follows:

- **Chapter 1. Introduction**: In the present chapter, we introduce the concept of ANS and different biological signals from which we can obtain information of ANS activity. We focus on heart rate variability, which will be the main tool throughout the thesis to assess the integrity of ANS.
- **Chapter 2. Methodological framework for heart rate variability analysis during exercise: application to running and cycling stress testing**: This chapter focuses on the uses and limitations of HRV analysis during exercise, namely the noisy and non-stationary nature of HRV during exercise, changes in mean HR and high and varying respiratory rate. It also characterizes a spectral component realted to CC which appears in the HRV spectrum, and deals with its overlapping with other spectral components. This framework is applied to running and cycling stress testing. During low intensities of exercise, mean heart rate and oxygen consumption rapidly increases, together with an increase in normalized LF power and a decrease in normalized HF power. During moderate-to-high exercise intensities, an increase in normalized HF power is observed despite the parasympathetic withdrawal, mainly due to the mechanical effect of breathing. Power related to CC components is stronger while running, being higher if this cadence is fixed. The research described in this chapter generated the following publications:
  - **D. Hernando**, R. Bailón, R. Almeida, A. Hernández (2014). QRS Detection Optimization in Stress Test Recordings using Evolutionary Algorithms. *XLI International Conference on Computing in Cardiology*. Cambridge, USA, pp. 737-740.
  - A. Hernando, **D. Hernando**, N. Garatachea, J.A. Casajús, R. Bailón (2015). Attenuation of the Influence of Cardiolocomotor Coupling in Heart Rate Variability Interpretation During Exercise Test. *37nd Annual International Conference of the IEEE EMBS*. Milan, Italy, pp. 1508-1511.

  - **D. Hernando**, A. Hernando, J.A. Casajús, P. Laguna, N. Garatachea, R. Bailón. Methodological Framework for Heart Rate Variability Analysis During Exercise: Application to Running and Cycling Stress Testing. Submitted to *Medical & Biological Engineering & Computing*. Accepted with minor revisions.

- **Chapter 3. Validation of heart rate monitor Polar RS800 for heart rate variability analysis during exercise**: This chapter compares the RR series obtained directly from the ECG and from a HR monitor during dynamic exercise of low, medium and high intensity. Reliability and agreement coefficients show that both methods are interchangeable when measuring mean heart rate and LF power, regardless of the level of exercise (reliability and agreement $>$ 0.9). However, the performance of the HF power measurements from the Polar device decreases as the level of the exercise increases, with reliability and agreement coefficients lower than 0.7. In spite of these results, when computing HRV parametrs as the mean value in the analyzed intervals and addressing the CC spectral components, no significant differences were found between the ECG and Polar measurements. Both parameters describe the same ANS response to the exercise stress. The research described in this chapter generated the following publications:

  - **D. Hernando**, N. Garatachea, R. Almeida, J. A. Casajús, R. Bailón (2017). Validation of heart rate monitor Polar RS800 for heart rate variability analysis during exercise. *Journal of Strength and Conditioning Research*. DOI: 10.1519/JSC.0000000000001662.
  - **D. Hernando**, N. Garatachea, J. A. Casajús, R. Bailón. Comparison of HRV assessment during exercise from Polar RS800 and ECG. Submitted to *Computing in Cardiology 2017 conference*.

- **Chapter 4. Coronary artery disease diagnosis by means of heart rate variability analysis using respiratory information**: In this chapter, HRV analysis is applied to exercise test with the aim of determining the diagnostic performance of HRV measurements during exercise in the detection of coronary artery disease (CAD). Due to the effect of medications and differences in exercise duration in this database, mean HR cannot be reliably used to diagnose CAD. HF power, when guided by respiration, achieves the highest AUC, above 0.7 both in rest and in recovery. The research described in this chapter generated the following publication:

  - **D. Hernando**, M. Kähönen, J. Lázaro, R. Lehtinen, T. Nieminen, K. Nikus, T. Lehtimäki, R. Bailón, J. Viik. Coronary artery disease diagnosis by means of heart rate variability analysis using respiratory information. Submitted to *EMBEC 2017 conference*.

- **Chapter 5. Identification of hypotension prone patients during hemodialysis based on the analysis of heart rate variability, blood pressure variability and baroreflex sensitivity**: This chapter focus on the hypothesis that

IDH prone patients would present an impairment in autonomic regulation of the cardiovascular system. Several parameters are extracted from HRV, BPV and ECG-derived respiration, including parameters to describe a VLF modulation found in HRV, BPV and ECG-derived respiration. The VLF modulation, which could be related to the hemodynamic stability of the patients, is characterized in both groups. Some differences were found in the coherence values and the duration, with longer duration in patients with ANS altered, but the modulation appeared in very short periods of time and in a very irregular pattern. Some of the parameters related to HRV (normalized LF and ratio), BPV (HF) and BRS (LF) were found to be able to discriminate between both groups using information of the first 30 minutes of the treatment. No differences were found in respiratory rate. A classifier is also proposed in this chapter to differenciate IDH prone and resistant patients. The best indices for the classification were selected, and a linear classifier was evaluated. A leave–one–patient–out technique was applied due to the small size of the database. A division into diabetic and non diabetic subgroups proved to improve the results, leading to a global classifier with Acc = 92.1%. The research described in this chapter generated the following publications:

- **D. Hernando**, R. Bailón, P. Laguna, L. Sörnmo (2011). Heart Rate Variability Analysis during Hemodialysis and its Relation with Hypotension. *XXXVIII International Conference on Computing in Cardiology*. Hangzhou, China, pp. 189-192.
- **D. Hernando**, A. Alcaine, P. Laguna, E. Pueyo and R. Bailón (2013). Very low frequency modulation in QRS slopes and its relation with respiration and heart rate variability during hemodialysis. *35nd Annual International Conference of the IEEE EMBS*. Osaka, Japan, pp. 5365-5368.
- **D. Hernando**, A. Alcaine, E. Pueyo, P. Laguna, M. Orini, A. Arcentales, B. Giraldo, A. Voss, A. Bayés-Genís, R. Bailón (2013). Influence of Respiration in the Very Low Frequency Modulation of QRS slopes and Heart Rate Variability in Cardiomyopathy Patients. *XL International Conference on Computing in Cardiology*. Zaragoza, Spain, pp. 117-120.
- F. Sandberg, R. Bailón, **D. Hernando**, P. Laguna, J.P. Martínez, K. Solem, L. Sörnmo (2013). Prediction of Intradialytic Hypotension using PPG and ECG. *XL International Conference on Computing in Cardiology*. Zaragoza, Spain, pp. 1227-1230.
- F. Sandberg, R. Bailón, **D. Hernando**, P. Laguna, J.P. Martínez, K. Solem, L. Sörnmo (2014). Prediction of hypotension in hemodialysis patients. *Physiological Measurement*. Vol. 35, pp. 1885-1898.
- **D. Hernando**, L. Sörnmo, F. Sandberg, P. Laguna, M. Llamedo, R. Bailón (2015). Identification of Hypotension Prone Patients During Hemodialysis based on the Analysis of Heart Rate Variability. *Medical & Enginering & Physics*. Vol. 37, n.12, pp. 1156-1161.

- **Chapter 6. Autonomic nervous system assessment in critically ill patients undergoing a cognitive rehabilitation therapy**: This chapter describes an exploratory study where HRV parameters are analyzed in critically ill patients who undergo neurocognitive rehabilitation to stimulate their cognitive functions. Comparing with baseline values, some patients showed an increase in the HF power after the session, suggesting an increase of parasympathetic activity, while some of them presented a decrease in the normalized LF power, suggesting a decrease of the sympathetic activity. However, critically ill patients are very diverse, have altered the ANS and take medicines which also modify its behaviour.

  - **D. Hernando**, M. Turon, R. Bailón, S. Fernandez-Gonzalo, J. Lázaro, G. Gomà, E. Gil, J. Montanyà, J. López-Aguilar, C. de Haro, P. Laguna, L. Blanch (2015). Autonomic Nervous System Assessment in Critically Ill Patients Undergoing a Cognitive Rehabilitation Therapy. *XLII International Conference on Computing in Cardiology*. Nice, France, pp. 785-788.
  - M. Turon, **D. Hernando**, S. Fernandez-Gonzalo, R. Bailón, G. Gomà, J. Lázaro, J. Montanyà, E. Gil, M. Martinez-Perez, C. de Haro, J. López-Aguilar, A. Martinez-Rubio, M. Jodar, P. Laguna, L. Blanch (2015). Effect of an early neurocognitive rehabilitation on autonomic nervous system in critically ill patients. *Intensive Care Medicine Experimental*, 3(Suppl 1):A989.
  - M. Turon, **D. Hernando**, S. Fernandez-Gonzalo, R. Bailón, G. Gomà, J. Lázaro, J. Montanyà, E. Gil, C. de Haro, M. Martinez-Perez, J. López-Aguilar, A. Martinez-Rubio, M. Jodar, P. Laguna, L. Blanch (2016). Differential effect of early neurocognitive rehabilitation on autonomic nervous system in critically ill patients with and without delirium. *American Thoracic Society (ATS) International Conference*. San Francisco.
  - M. Turon, S. Fernandez-Gonzalo, M. Jodar, G. Gomà, J. Montanyà, **D. Hernando**, R. Bailón, C. de Haro, V. Gomez-Simon, J. López-Aguilar, R. Magrans, M. Martinez-Perez, J.C. Oliva, L. Blanch. Feasibility and safety of virtual-reality-based early neurocognitive stimulation in critically ill patients. Submitted to *Annals of Intensive Care*. Under review.

- **Chapter 7. Conclusions and future work**: This chapter presents the main conclusions of the thesis and future lines of work are proposed.

1.7 Collaborations and research visits

The research conducted throughout my PhD was done in the Biomedical Signal Interpretation & Computational Simulation (BSICoS) group at University of Zaragoza, under the supervision of Raquel Bailón and Pablo Laguna. Apart from collaborations within the BSICoS group, several collaborations with other groups were also set up, which are listed below.

- *Leif Sörnmo* and *Frida Sandberg*
  Signal Processing Group, Department of Biomedical Engineering, Lund University, Lund, Sweden.
- *Beatriz F. Giraldo*
  Dept. of Automatic Control (ESAII), Universitat Politècnica de Catalunya, Barcelona, Spain.
- *Rafael Álvarez*
  Hospital Clínico Universitario Lozano Blesa, Zaragoza, Spain.
- *Alfredo Hernández*
  National Institute of Health and Medical Research (INSERM), Signal and Image Processing Laboratory (LTSI), Université de Rennes, Rennes, France.
- *Jari Viik*
  BioMediTech Institute and Faculty of Biomedical Science and Engineering, Tampere University of Technology, Tampere, Finland.
- *Rute Almeida*
  Faculdade de Ciências, Universidade do Porto & CMUP, Porto, Portugal.
- *Michele Orini*
  Institute of Cardiovascular Science, University College of London, London, UK.
- *Nuria Garatachea* and *Jose A. Casajús*
  GENUD Research Group, Faculty of Health and Sport Sciences, University of Zaragoza, Zaragoza, Spain.
- *Lluís Blanch*, *Marc Turon*, *Sol Fernandez-Gonzalo*, *Josefina López-Aguilar* and *Jaume Montanyà*
  Research Department, Institut d'Investigació i Innovació Sanitària Parc Taulí (I3PT), Fundació Parc Taulí, Sabadell, Spain.

I also had the opportunity of doing two research visits during my PhD:

- January 2014 - April 2014: Laboratoire Traitement du Signal et de l'Image (LTSI), Université de Rennes, Rennes, France. Supervised by Alfredo Hernández. Topic: *QRS Detection Optimization in Stress Test Recordings Using Evolutionary Algorithms.*

- August 2014 - December 2014: Department of Electronics and Communications Engineering, Tampere University, Tampere, Finland. Supervised by Jari Viik. Topic: *Coronary artery disease diagnosis by means of heart rate variability analysis using respiratory information.*

Chapter 2

Methodological Framework for Heart Rate Variability Analysis During Exercise: Application to Running and Cycling Stress Testing

2.1 Motivation

Heart rate variability (HRV) remains a powerful source for autonomic nervous system (ANS) assessment by using simple and non-invasive techniques. Standards of spectral analysis of HRV measurements, physiological interpretation, and clinical use have largely been published at rest [6].

In recent years, however, HRV analysis has gained increasing interest in sports and training sciences. Sports physiologists are interested in measuring HRV as a non-invasive marker of autonomic changes due to exercise training and the cardiovascular response to the stress of exercise [7]. By monitoring athletes' fatigue, fitness and performance responses to the various training phases, training load and contents can be adjusted and individualized both during and between each training cycles. Hottenrott et al. [8] show that significant differences can be observed in healthy subjects due to regular aerobic training: not only a reduction in mean heart rate both at rest and during submaximal exercise, but also an increase in autonomic efferent activity and a shift in favour of enhanced vagal modulation. Martinmäki et al. [72] also show that low-dose endurance training enhances vagal control during exercise, but does not alter resting vagal HR control.

Still, HRV interpretation during exercise is still a matter of debate. HR monitoring is yet not accepted as a gold standard due to the lack of consistency in the literature [73]. Some studies show that HRV measurements are not sensitive to fitness improvements, fatigue, overload or detraining; moreover, non expected changes have been observed, which further complicates the interpretation of the training status [74]. These contradictory results may be related to methodological inconsistencies or partial misinterpretation of the measurements [73]. It is necessary to look into the analysis methods, the characteristics of the population, training levels, intensity and duration of exercise... while interpretating the HRV indices and a multidisciplinary approach between cardiologists, exercise and pulmonary physiologists, coaches and biomedical engineers would be desirable [11].

This chapter focuses on developing an integrated methodological framework for a robust HRV analysis during exercise. One of the challenges in exercise HRV analysis is obtaining a reliable and robust QRS detection, mainly due to the significant noise levels observed in this context (Llamedo et al. [75]) and changes in beat morphology during exercise (Drezner et al. [76]). This issue will be addressed with a separate study using an evolutionary algorithm to optimize the parameters of the QRS detector.

Several approaches have been proposed to deal with the nonstationary nature of HRV during exercise, like quadratic time-frequency representations, including the Wigner-Ville distribution and its filtered versions (Mainardi [77]). In order to separate changes in ANS stimulation from changes in mean HR, which greatly varies in exercise testing, a correction of HRV parameters with time-varying mean HR should be performed, see Bailón et al. [46], Meste et al. [43] and Sacha et al. [44,45]. Respiratory

rate also increases with increasing loads of exercise and can reach frequencies above the classic HF band, thus making necessary to redefine this band as shown in Bailón et al. [78], or adding repiratory frequency information directly to the time-frequency estimation of HRV spectrum as shown in Bailón et al. [79]. Lastly, besides the LF and HF components, another component can appear in the HRV spectrum, which is synchronous with stride or pedalling frequency. This component can cause aliasing and may overlap with LF and HF bands, misleading their interpretation in terms of sympathetic or parasympathetic activation. All these methodological issues, although studied individually or partly combined, have never been approached in an integrated manner.

Another important task is the interpretation of HRV parameters during exercise. During a graded exercise test, HR and oxygen consumption rapidly increase in the beginning, following a slower increment afterwards. The increase in HR is the result of vagal withdrawal and sympathetic excitation (Sarmiento et al. [80]). There is also a significant drop in HRV in both LF and HF bands. As reported in Cottin et al. [81,82] and Bailón et al. [10, 46], there is a reduction in the LF power with exercise. Power in HF band also decreases during moderate exercise [82], but during heavy exercise, HF power is said to be related to the mechanical effect of breathing on the sinus node, with increasing power with higher intensities of exercise, see Cottin et al [81,83] and Blain et al. [84]. In the recovery phase after maximal exercise, vagal reactivation decreases HR [85] and is thought to be particularly important during the first minutes after exercise, see Arai et al. [86]. Absolute spectral LF and HF powers have shown to increase as recovery progress, while relative LF power is shown to increase as relative HF decreases during recovery, as shown in Bernardi et al. [87]. This chapter analyzes ANS response to exercise through HRV analysis in different types of exercise, namely, maximal and submaximal, running and cycling.

2.2 QRS detection optimization

Extraction of HRV during exercise remains today as an open problem in the field of cardiovascular signal processing. During exercise, it is particularly difficult to obtain a reliable and robust QRS detection, due to the highly non-stationary nature of the acquired signals and the significant levels of noise observed in this context. Although a number of QRS detectors have been proposed in the literature, most of them have been tuned for operation on rest ECG recordings, with limited noise.

A wavelet-based QRS detector [88] has been used in this thesis. The wavelet transform is a decomposition of the signal as a combination of a set of basis functions, obtained by means of dilation and translation of a single prototype wavelet. The wavelet used by our detector, described in [88], can be seen as the derivative of a low-pass function, with different cut-off frequency based on the wavelet's parameters. It is thus very useful to analyze the slopes of the different ECG waves in the different scales. For example, most of the energy of the ECG signal lies at scales 2 to 4, where different amplitude thresholds are used to identify the fiducial point of the QRS

complex. Figure 2.1 shows an example of an ECG segment and wavelet scales W_2, W_3 and W_4 correspondign to the scales 2 to 4. The first search is performed in W_4, where the peaks selected (above and below the amplitude thresholds), denoted as candidates, correspond with the maximum slope of the QRS. These candidates are then searched in scales 3 and 2, with lower scales having better time resolution. Finally, the fiducial point of the QRS complex is selected as the zero crossing between two consecutive candidates in the lowest scale.

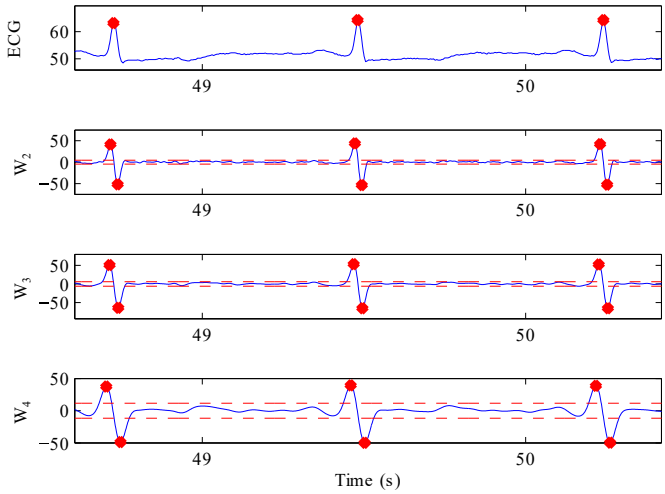

Figure 2.1: Example of an ECG segment and the wavelet scales 2 to 4 with the amplitude thresholds and final detection marks.

This detector is characterized by a great number of parameters (thresholds, time windows...) that have to be specifically tuned for it to perform correctly on exercise stress recordings. It is not an easy task to manually tune all these parameters, therefore, it is proposed to apply an optimization methodology, integrating an evolutionary algorithm (EA), based on the approach proposed in [89].

EAs are optimization techniques, inspired on the theories of evolution and natural selection. They can be used to find the optimal configuration to a system within specific constraints [90]. They have already been applied in several biomedical applications to estimate a large set of parameters and have provided quite good results [89, 91, 92].

The main objective is thus to enhance the algorithm in [88] regarding the robust QRS detection in very noisy ECG recordings, applicable to stress testing. Baseline wander, muscle artifact, and electrode motion artifact will be taken into account in the optimization of the detector parameters.

2.2.1 Databases

Training database

A training database was created using the MIT-BIH Arrhythmia Database, which contains 48 half-hour-length ECG recordings with annotated QRS complexes. The first lead of each ECG recording is artificially contaminated with 3 types of real noise recordings, leading to 144 noisy ECG recordings. A sample of this noisy database can be found online named MIT-BIH Noise Stress Test Database [93, 94]. The noise recordings were made using physically active volunteers and standard ECG recorders, leads, and electrodes; the electrodes were placed on the limbs in positions in which the subjects' ECGs were not visible. The three type noise records were assembled from the recordings by selecting intervals that contained predominantly baseline wander, muscle artifact, and electrode motion artifact, see [93]. The signal-to-noise ratios (SNRs) during the noisy segments of these recordings ranged from 24 to -6 dB.

Figure 2.2 shows an example of this database: the original ECG recording, and after the contamination of each noise recording.

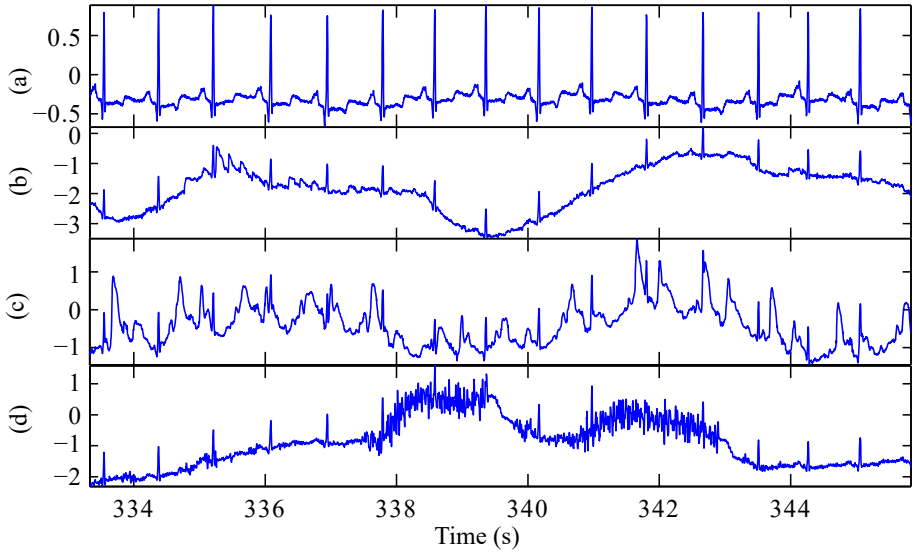

Figure 2.2: Original ECG signal (a), and the same recording contaminated with baseline wander (b), electrode motion artifact (c) and muscle artifact (d), measured in mV (SNR = 6 dB).

Evaluation database

Evaluation was performed on an exercise stress test database composed of 54 real ECG recordings, which were continuously recorded throughout exercise (ergocycle) phase at a 1000 Hz rate (Cardionics, Webster, Texas) at the University Hospital of Rennes, France. The QRS complexes were detected using the Pan & Tompkins algorithm [95] and each detection was manually verified by a trained operator with a dedicated interface.

2.2.2 Parameters to optimize

In exercise test databases, wave morphology changes are expected, in particular T waves become more peaky and can often be detected as a QRS complex. The refractory period is another parameter which should be tuned in those databases with higher expected HR. Other amplitude thresholds to detect the main peak of the QRS complex are based on the energy of the signal at different scales, obtained within a window with adjustable length. Hence, the four parameters which are going to be optimized for QRS detection are:

- Refractory period ($\mathcal{R}_P$): This parameter prevents a QRS detection within that period, restricting the minimum beat duration to a physiologically based value.

- Length of the window for amplitude threshold estimation ($\mathcal{W}_L$): window length where amplitude thresholds proportional to the RMS value of the different scales are locally adjusted. With these thresholds, the algorithm looks for candidates for the QRS detection named maximum modulus lines.

- Thresholds to reject peaky T waves ($\mathcal{T}_1$, $\mathcal{T}_2$): These two parameters are the basis to obtain the threshold $\mathcal{T}$ which is applied to avoid T waves misdetected as QRS. $\mathcal{T}_1$ acounts for the maximum slope that can be associated to a T wave, and then potentialy rejected. $\mathcal{T}_2$ acounts for the running average of the QRS slopes. The final rejection threshold $\mathcal{T}$ is set as the minimum value between $\mathcal{T}_1$ and $\mathcal{T}_2$ to remove candidates related to the T wave.

2.2.3 Evolutionary algorithm

Parameter optimization was addressed by an evolutionary algorithm [89]. These optimization algorithms are particularly adapted to problems involving cost functions that are not differentiable and presenting multiple local minima.

An initial population is created, consisting of 100 individuals. Each individual is represented as a different set of values for the parameters which are going to be optimized, being one of them the default individual (the one with the default parameters). A cost function combining a global detection error criterium (C_{err}), the mean detection jitter (ϵ), and its standard deviation (σ) was defined, in order to obtain a quantitative performance evaluation of the detector using the training database. This fitness is measured as:

$$F = \frac{C_{err}}{a} + \frac{\epsilon}{b} + \frac{\sigma}{c} \tag{2.1}$$

where a, b and c are normalization coefficients which are obtained as the mean value of each criteria in the initial population. The detection error criterium is defined as:

$$C_{err} = \sqrt{(1 - Se)^2 + (1 - PPV)^2} \tag{2.2}$$

being Se and PPV the sensitivity and positive predictive value respectively, which represent the proportion of actual QRS complexes which are correctly identified as such (Se) and the proportion of detection marks which actually correspond to QRS complexes (PPV). A true positive, i.e., a correct beat detected, is considered when a beat is detected within a 50 ms window centered in the reference QRS complex. Note that this tolerance might seem too large if our final goal is to analyze HRV, hence the inclusion of the jitter in the fitness equation.

In each iteration of the algorithm, first the best individuals are selected and then a new generation of individuals is produced using genetic operators. For the selection, a function based on the normalized geometric distribution is used. It is assigned a probability of selection P_j to each individual j based on its fitness value. A series of N random numbers is generated and compared against the cumulative probability P_j. The appropriate individual i is selected and copied into the new population if $P_{i-1} < U(0,1) \leqslant P_i$.

Then, the new generation is generated through crossovers and mutations. Crossover operations create two new individuals combining the information of two existing ones, using a number of arithmetic, heuristic and simple crossovers with a crossover probability of 0.3, 0.5 and 0.2 respectively. Mutations create one new individual from one old individual, and are less expected to happen. Mutation operator includes multi non-uniform, non-uniform and uniform mutations with a mutation probability of 0.025, 0.1 and 0.025 respectively, which change every (multi) or one parameter from one existing individual.

Finally, the algorithm is stopped when achieving a goal standard (based on the fitness value) or a maximum number of generations. In this work, the individual which present the best performance in the 25th generation is established as the optimal set of parameters.

2.2.4 Evaluation of the optimal set of parameters

The evaluation database is used to compare the detector performance using both the default and optimal parameter values, using the reference annotations as described in Section 2.2.1. The fitness value will be used to qualitative measure the detector performance in both scenarios, as described in equation (2.1). The improvement of the performance is evaluated for every recording individually, and globally within the whole database.

2.2.5 Results

The evolution of the parameters $\mathcal{R}_P$, $\mathcal{W}_L$, $\mathcal{T}_1$ and $\mathcal{T}_2$ is shown in Figure 2.3 (mean and standard deviation) for 25 iterations. It shows the default (D) and the optimized (O)

values for each parameter, as well as partial results in iterations 1, 5, 10, 15, 20, 25. Parameters $\mathcal{R}_P$ and $\mathcal{W}_L$ are measured in seconds.

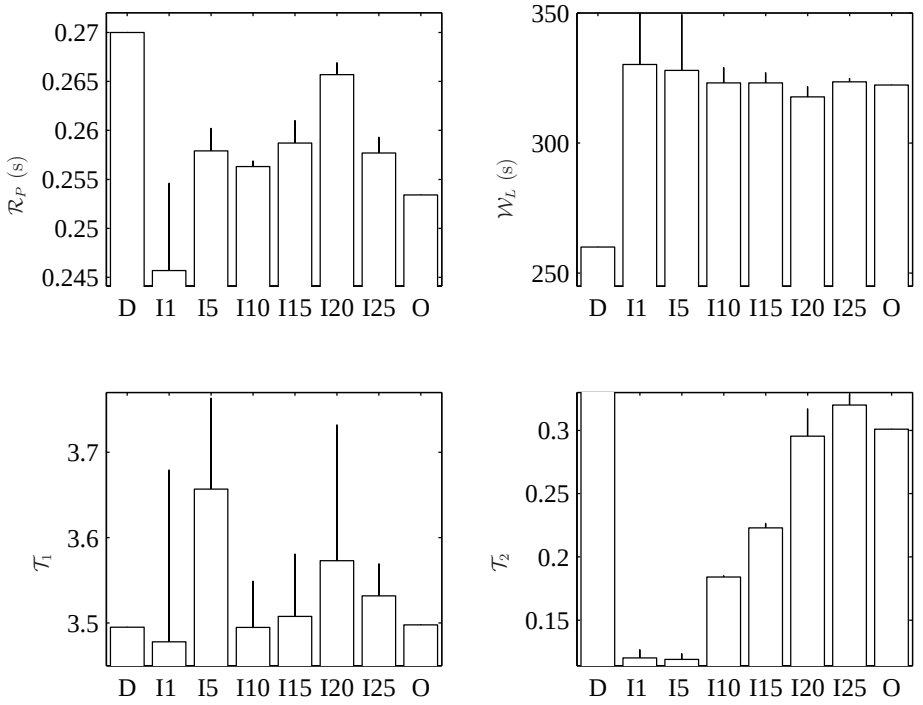

Figure 2.3: Evolution of the parameters $\mathcal{R}_P$, $\mathcal{W}_L$, $\mathcal{T}_1$ and $\mathcal{T}_2$. First and last column represent the default and optimal parameters respectively. Also the mean and standard deviation in iterations 1, 5, 10, 15, 20 and 25 are represented.

The QRS detector showed a global improvement of 4.6%, when comparing the mean fitness value from all the recordings using the optimal and default parameters. Furthermore, when analyzing each record individually, the use of optimized parameters led to at least the equivalent performance than the initial parameters for all records, and the improvement was higher (up to 19.36 %) in noisy records. It is important to remark that the performance is not lowered in standard resting condition.

The fitness value combines a global detection error criterium, the mean detection jitter, and its standard deviation. In Table 2.1, these values for the default and optimal parameters are shown. The error criterium is the one most improved (it presents a decrease of 6%), while the standard deviation of the detection jitter is the one least improved (only 1%).

Figure 2.4 shows an ECG segment from the evaluation database. Among the detections obtained with the default parameters (red marks) there are some errors, and Figure 2.4 shows the wavelet scales in one segment where the T wave has been misdetected as a QRS complex (red marks in the wavelet scales refer to the candidates for the QRS fiducial points). These errors are corrected when using the optimal parameters,

	Default set	Optimal set
C_{err}	0.3084	0.2902
ϵ (ms)	6.13	5.87
σ (ms)	9.89	9.78

Table 2.1: Values of C_{err}, ϵ and σ when using the default and optimal parameters.

see the black marks in the QRS.

2.2.6 Discussion

As it is shown in Figure 2.3, the parameter $\mathcal{W}_L$ converges towards an optimal value within few iterations, which is stable through the optimization process and presents the minimal dispersion on the final iteration, suggesting that the obtained optimal value is robust and that this parameter is particularly sensitive for detection performance. Furthermore, the obtained optimal parameter for $\mathcal{W}_L$ is quite different from the default one (a difference larger than a minute, being larger in the optimal set). This may seem contradictory with what we expected, since exercise databases are highly non-stationary and the first hypothesis was that thresholds based on the RMS of the different scales should be computed in shorter segments. On the other hand, changes in amplitude of QRS have not been taken into account, neither the progressive increase in the noise with the exercise. Parameters $\mathcal{R}_P$ and $\mathcal{T}_2$ show slower convergence and relatively low dispersions. $\mathcal{R}_P$ was expected to be shorter since during exercise, heart rate decreases and there is a risk that the next beat is missed if $\mathcal{R}_P$ is too long. Concerning parameter $\mathcal{T}_1$, it presents significant oscillations and high dispersion values, that indicate that this parameter is less sensitive than the others for this particular detection algorithm. Moreover, the optimal value for this parameter is very close to the default one. The differences in $\mathcal{T}_1$ and $\mathcal{T}_2$ suggests that in exercise database, the final threshold to avoid misdetections due to the T wave is mainly based on $\mathcal{T}_2$. It is to note, though, that the optimal parameter set is obtained from a nonlinear and complex function of these parameters, making difficult any further analytical analysis on parameter evolution. Results from Figure 2.3 suggest that an additional gain could be obtained if the EA is applied for more generations.

The obtained global detection performance improvement of 4.6% may seem low, and thus a revision of the chosen parameters is proposed. The algorithm is trained with a database containing significant noise levels of various natures (baseline wander, muscle artifact, and electrode motion artifact). While exercise stress recordings, like the evaluation database, commonly have these different kinds of noise, they also present other characteristics such as abrupt changes in the heart rate and changes in wave morphology, which were not taken into account into the optimization process. In particular, the refractory period should be trained with a database presenting such changes in heart rate. Additionally, we could have a better understanding of the impact of each parameter if we train the EA with each parameter individually, and then

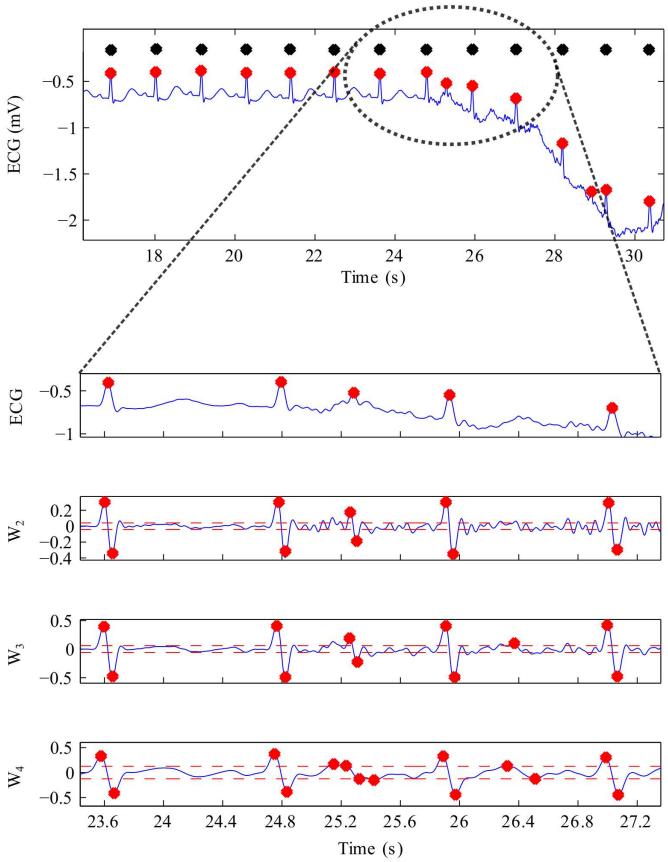

Figure 2.4: Example of an ECG segment with QRS misdetections and the wavelet scales in one segment where the T wave has been misdetected as a QRS complex. Red marks are obtained with the default parameters and black marks are obtained with the optimal parameters. In the wavelet scales, red marks refer to the candidates for the QRS fiducial points.

analyze what kind of error is corrected. These aspects are limitations of the current results and may be improved in further works. Nonetheless, as stated above, the obtained optimal parameter set provides detections performances that are at least equal to that obtained with the non-optimized parameters, with performance improvements of more than 10% on very noisy records.

2.2.7 Conclusion

This study uses an evolutionary algorithm to optimize the input parameters for a QRS detector in very noisy recordings. Problems such as the ECG morphology and the high level of noise during these tests lead to wrong detections. The input parameters of the QRS detector have been optimized by an evolutionary algorithm, which is trained with a database consisting of ECG signals contaminated with 3 types of noise, commonly found in exercise stress test recordings, such as baseline wander, electrode motion artifact and muscle artifact. After parameter optimization, the detector performance shows a global improvement. The results are, at least, the same than using the default parameters, but significantly higher in the noisier recordings. This demonstrates the advantages of the optimized parameters in noisy environments.

2.3 Materials and Methods

2.3.1 Study population and experimental protocol

The database consists of 23 male volunteers. All of them were apparently healthy, they were not taking medications and they had normal blood pressure levels and electrocardiographic patterns. They regularly participated in sports activities, doing at least 3 days/week of regular aerobic training. Written informed consent was obtained from each subject. The study protocol was approved by the institutional ethics committee and was in accordance with the Declaration of Helsinki for Human Research of 1974 (last modified in 2013). Table 2.2 shows the study population characteristics.

Age (years)	34.8 ± 5.0
Height (cm)	178.4 ± 5.7
Mass (kg)	74.8 ±7.8
Body mass index ($kg \cdot m^{-2}$)	23.5 ± 2.5
$\dot{V}O_2$ max (ml $O_2 \cdot min^{-1}$)	4216.6 ± 453.7
$\dot{V}O_2$ max $\cdot$ kg^{-1} (ml $O_2 \cdot min^{-1} \cdot kg^{-1}$)	56.4 ± 6.2

Table 2.2: Study population characteristics (23 male volunteers): age, height, mass, body mass index and maximum oxygen consumption ($\dot{V}O_2$ max). Mean ± standard deviation.

All the subjects completed three sessions in different days: a maximal test (on a treadmill) and two submaximal tests (on a treadmill and on a cycle ergometer),

denoted as MaxT, SubT and SubC, respectively. The volunteers were asked to: 1) wear comfortable, loose-fitting clothing; 2) drink plenty of fluids over the 24-h period preceding the test; 3) avoid food, tobacco, alcohol, and caffeine for 3 h prior to the test; 4) avoid exercise or strenuous physical activity on the day of the test; and 5) get an adequate amount of sleep (6-8 h) the night before the test, as proposed by Wasserman [96].

All tests were divided into three different phases: resting, exercise and recovery phase. The resting phase was common to all tests: the subjects were monitored seated for 5 min at rest, without any movement or talking, to measure resting cardiorespiratory variables.

For the exercise phase during MaxT test, the subjects performed an incremental maximal test to exhaustion on a motorized treadmill (Quasar Med 4.0, h/p/cosmos, Nussdorf-Traunstein, Germany). They began running with an initial speed of 8 km $\cdot$ h^{-1} and increased 1 km $\cdot$ h^{-1} every minute until the subjects stopped due to volitional exhaustion. From this test, the maximum HR and $\dot{V}O_2$ were noted for each subject. A physician was present during the whole session supervising the test.

For the SubC test, the exercise started at 75 W on the cycle ergometer, increasing 25 W $\cdot$ min^{-1}. The cadence frequency was fixed at 80 rpm. This phase continued until the subject reached his 90% maximum HR previously determined at the MaxT test, after that the load was kept for two more minutes. For the SubT test on the treadmill, the procedure was similar to the MaxT test, until they reached the 90% maximum HR, then they kept running two more minutes at that speed. Besides, in the SubT test the running stride was fixed at 80 strides $\cdot$ min^{-1}.

Recovery phase lasted between 3 and 5 minutes, where subjects were required to remain running at 8 km $\cdot$ h^{-1} (on the treadmill) or pedalling at 75 W (on the cycle ergometer). However, subjects did not behave in a consistent way after the stress peak, especially in the MaxT test. Some subjects continued running at a slower speed but others completely interrupted the exercise and took some seconds until they could continue. For this reason, the first 30 seconds in this phase will not be analyzed.

2.3.2 Data acquisition and pre-processing

Information about respiratory frequency and oxygen consumption ($\dot{V}O_2$) were obtained by an open-circuit sampling system (Oxycon Pro, Jaeger-Viasys Healthcare, Hoechberg, Germany). The metabolic cart was calibrated with a known gas mixture (16% oxygen, O_2, and 5% carbon dioxide, CO_2) and volume prior to the first test each day as recommended by the company. Both respiratory frequency and $\dot{V}O_2$ data were interpolated at 4 Hz and low-pass filtered with a cut-off frequency of 0.01 Hz to obtain $f_{\mathrm{R}}(n)$ and $d_{\dot{\mathrm{V}}\mathrm{O}_2}(n)$ series, respectively.

The ECG was recorded using a high resolution Holter (Mortara 48-hour H12+, Mortara Instrument, Milwaukee,Wisconsin) with a sampling frequency of 1000 Hz. For each subject, the QRS detection marks were extracted from the ECG using a multi-lead approach by the wavelet-based detector with optimized parameters for noisy

environments described Section 2.2, and each detection was manually verified by an operator with a dedicated interface. RR intervals from the ECG were obtained as the difference of each consecutive beat occurrences.

Thanks to a cadence sensor attached to the subject's shoe (Polar s3 Stride Sensor, Polar Electro, Finland), the running cadence frequency, $f_{\mathrm{C}}(n)$, was obtained in the MaxT test, after low-pass filtering the raw data with a cut-off frequency of 0.01 Hz. In the submaximal tests, this component was fixed to the requested cadence (80 rpm = 4/3 Hz).

Five intervals were established for each RR series for further analysis. In addition to the basal interval (I_{B}), which is associated to the resting phase (5 minutes prior to the exercise), the $d_{\dot{\mathrm{V}}\mathrm{O}_2}(n)$ signal from the MaxT test was used to establish 3 intervals during the exercise: 0-60%, 60-80% and 80-100% of the variation between the basal ($\dot{V}O_2^0$) and the maximum value ($\dot{V}O_2^{100}$) of $d_{\dot{\mathrm{V}}\mathrm{O}_2}(n)$ during exercise for each subject (see Figure 2.5, upper panel). $\dot{V}O_2^0$ was obtained as the mean value of $d_{\dot{\mathrm{V}}\mathrm{O}_2}(n)$ during the resting phase, while $\dot{V}O_2^{100}$ was found at the peak of $d_{\dot{\mathrm{V}}\mathrm{O}_2}(n)$, both defined at the MaxT test. These intervals were denoted as I_{60}, I_{80} and I_{100} respectively. The $\dot{V}O_2$ threshold values found in the MaxT test were used also in the SubT and SubC tests to establish the intervals, see Figure 2.5 (lower panel). Since $d_{\dot{\mathrm{V}}\mathrm{O}_2}(n)$ in SubT and SubC do not reach $\dot{V}O_2^{100}$, the last interval (usually I_{100}) lasts until the exercise phase ends. In 4 subjects, there is no I_{100} in SubC and their last interval is I_{80}. Note that each interval has different time length among the subjects. Additionally, the recovery interval (I_{R}) starts 30 s after the peak of exercise and lasts 1 min.

2.3.3 Heart rate variability estimation

From the beat occurrence times t_k, the heart rate signal is derived from t_k using a method based on the TVIPFM model [10]. The diagram of this model is shown in Figure 2.6. The input signal, $1 + m(t)$, consists of two parts: a DC component and a modulating signal with zero mean, $m(t)$, which is assumed to carry the information about ANS activity. This signal is integrated until it reaches a threshold T, which represents the mean heart period in the analyzed interval, when a beat occurs and the process is reset [42]. The advantage of TVIPFM model with respect with the original IPFM model is that it takes into account variations in the threshold, $T(t)$, which are expected during exercise. The output signal is a series event which represents the beat occurrence times t_k.

Assuming the first beat happens in $t = 0$, that $m(t)$ is casual, bandlimited, $m(t) < 1$ and that $T(t)$ is constant between two successive beats, the beat occurrence time series can be generalized as:

$$k \approx \int_0^{t_k} \frac{1 + m(t)}{T(t)} dt \tag{2.3}$$

with k and t_k being the order and occurence time of the k-th beat, respectively. The term

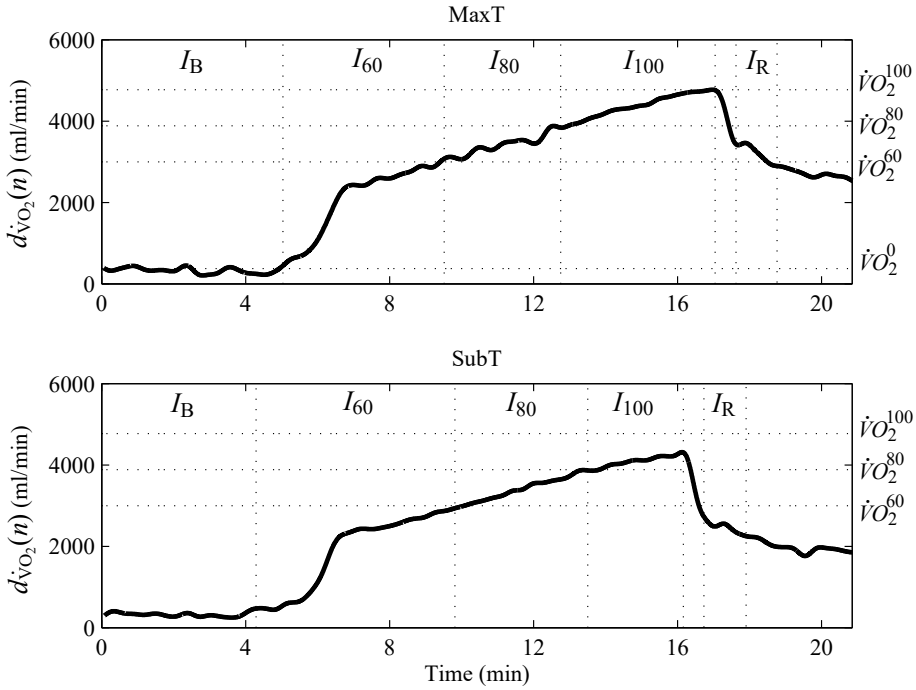

Figure 2.5: Example of oxygen consumption signal in MaxT (upper panel) and SubT (lower panel) in intervals I_B, I_{60}, I_{80}, I_{100} and I_R (basal phase, 0-60%, 60-80% and 80-100% of $d_{\dot{V}O_2}(n)$ defined by MaxT, respectively, and recovery phase) for one subject.

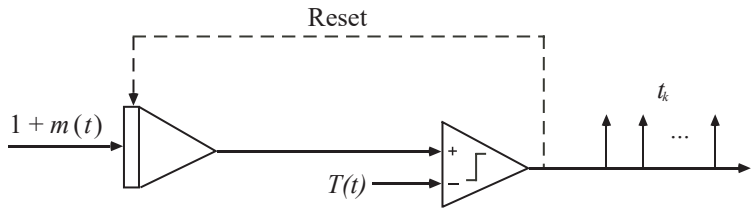

Figure 2.6: Block diagram of the TVIPFM model.

$$d_{\mathrm{HR}}(t) = \frac{1 + m(t)}{T(t)} \tag{2.4}$$

represents the instantaneous heart rate, where $1/T(t)$ represents time-varying mean heart rate and $m(t)/T(t)$ represents the heart rate variability.

Assuming that the variations of the term $1/T(t)$ are slower than those of the term $m(t)/T(t)$, and that their spectral components do not overlap, a time-varying mean heart rate $d_{\mathrm{HRM}}(n)$ can be defined as follows, and obtained by filtering:

$$d_{\mathrm{HRM}}(t) = \frac{1}{T(t)} \tag{2.5}$$

And the variability signal $d_{\mathrm{HRV}}(t)$ as:

$$d_{\mathrm{HRV}}(t) = d_{\mathrm{HR}}(t) - d_{\mathrm{HRM}}(t) = \frac{m(t)}{T(t)} \tag{2.6}$$

Then the modulating signal can be obtained by correcting $d_{\mathrm{HRV}}(t)$ by the time-varying mean heart rate $d_{\mathrm{HRM}}(t)$:

$$m(t) = d_{\mathrm{HRV}}(t)T(t) = \frac{d_{\mathrm{HRV}}(t)}{d_{\mathrm{HRM}}(t)} \tag{2.7}$$

and then it is sampled at 4 Hz to obtain $m(n)$.

2.3.4 Spectral analysis

Smoothed-Pseudo Wigner-Ville Distribution

There are several methods to estimate the spectrum of a signal. In particular, time-frequency analysis allows to study the temporal evolution of the spectral components. Among them, those belonging to the Cohen's class have interesting properties [97,98] and one particular case, the smoothed-pseudo Wigner-Ville distribution (SPWVD), has been extensively applied to the study of the cardiovascular variability [77,99,100]. One of its main advantages is that it provides an independent control over the time and frequency resolution by using separable kernels.

The SPWVD spectrum is defined in continuous time and frequency as:

$$S_{\mathrm{x}}(t,\Omega) = \int_{-\infty}^{\infty} \phi_h(\tau) \left[\int_{-\infty}^{\infty} \phi_g(t-\nu) x\left(\nu + \frac{\tau}{2}\right) x^*\left(\nu - \frac{\tau}{2}\right) d\nu \right] e^{-j\Omega\tau} d\tau \tag{2.8}$$

where the time and the frequency resolution of the SPWVD will be separately given by the shape of $\phi_g(t)$ and by the shape of (the Fourier transform of) $\phi_h(\tau)$, respectively.

In this thesis, the SPWVD will be applied in discrete time and frequency to the analytic signal of $m(n)$, $a_{\mathrm{m}}(n)$, to estimate the instantaneous power spectrum of the HRV signal as:

$$S_{\mathrm{m}}(n,f) = \sum_{k=-K+1}^{K-1} |h(k)|^2 \left[\sum_{n'=-N+1}^{N-1} g(n') a_{\mathrm{m}}(n+n'+k) a_{\mathrm{m}}^*(n+n'-k) \right] e^{-j\pi \frac{f}{F} k} \tag{2.9}$$

where $f = -F+1, \cdots, F$ and $a_{\mathrm{m}}(n)$ is defined as:

$$a_{\mathrm{m}}(n) = m(n) + j\hat{m}(n) \tag{2.10}$$

with $\hat{m}(n)$ representing the Hilbert Transform of $m(n)$ [101]. The terms $g(n)$ and $|h(k)|^2$ represent the time and frequency smoothing windows which will attenuate the interference terms, chosen to be Hamming windows of length $2N$-1=203 (about 50 s) and $2K$-1=513 samples (about 128 s), respectively, and normalized so that $\sum_{n'=-N+1}^{N-1} g(n') = 1$ and $|h(0)|^2 = 1$, respectively (Bailón et al. [10]).

Spectral components

There are three main spectral components which will be analysed. First, the instantaneous power in the LF band is extracted throughout the entire exercise test, denoted as $P_{\mathrm{LF}}(n)$, integrating the instantaneous power of the time-frequency spectrum of $m(n)$ in the range from 0.04 to 0.15 Hz. Second, $P_{\mathrm{HF}}(n)$ is obtained using a time-varying HF band: this band is centred on $f_{\mathrm{R}}(n)$ with a bandwidth of 0.125 Hz; in this database, this HF band has resulted to be always above 0.15 Hz (no overlapping with the LF band) and below half the mean HR rate, (no aliasing is produced), see Laguna et al. [102].

Lastly, the third spectral component, $P_{\mathrm{CF}}(n)$, is related to the cadence frequency (CF) component. The band for this component is centred at the running stride or pedalling frequency, $f_{\mathrm{C}}(n)$, with a bandwidth of 0.125 Hz, its upper bound limited by half the mean HR. This frequency is fixed at 80 strides $\cdot$ min^{-1} for the SubT test and at 80 rpm for the SubC test, and varying in the MaxT test, as explained before.

The intrinsic sampling frequency of HRV is the HR. Whenever the CF component exceeds half the mean HR, aliased components appear in the visible part of the spectrum and can overlap with other bands (Bailón et al. [10]). Moreover, if the CF component is not a perfect sinusoid, it will contain harmonics in the multiples of the frequency where CF appears. These harmonics also produce alias. Two main aliased components appear in this database, see Figure 2.7a. The aliased components are denoted as AF1 and AF2, and their powers are denoted as:

- $P_{\mathrm{AF1}}(n)$: in a band centered at $d_{\mathrm{HRM}}(n) - f_{\mathrm{C}}(n)$ with a bandwidth of 0.125 Hz.

- $P_{\mathrm{AF2}}(n)$: in a band centered at $-d_{\mathrm{HRM}}(n) + 2 \cdot f_{\mathrm{C}}(n)$ with a bandwidth of 0.125 Hz.

Note that $P_{\mathrm{CF}}(n)$ is obtained integrating the instantaneous power of the spectrum of $\hat{m}(n)$ in the band centered at $f_{\mathrm{C}}(n)$, but only up to half the mean HR rate. When $f_{\mathrm{C}}(n)$ exceeds it ($P_{\mathrm{AF1}}(n)$ appears in the visible spectrum), $P_{\mathrm{CF}}(n)$ is considered to be 0. In the same way, when $f_{\mathrm{C}}(n)$ is below half the mean HR rate, AF1 component does not appear.

Figure 2.7b shows an example of a time-frequency map showing some of the spectral components of HRV (HF, CF, AF1 and AF2), as well as an overlapping between HF and the aliased components.

2.3.5 Overlapping effect attenuation

While measuring the HF power, there may be overlapping zones with other components, as seen in Figure 2.7b. If an overlapping happens, the measured power reflects an artificial increase which should be corrected. Hence, several parameters are proposed to quantify the overlapping:

$$\alpha_{\mathcal{A},\mathcal{B}}(n) = \frac{P_{\mathcal{B}}(n)}{P_{\mathcal{A}}(n) + P_{\mathcal{B}}(n)}, \quad \mathcal{A}, \mathcal{B} \in \{HF, AF1, AF2\} \tag{2.11}$$

$$p_{\mathcal{A},\mathcal{B}}(n) = \frac{\Omega_{\mathcal{A},\mathcal{B}}(n)}{\Omega_{\mathcal{B}}(n)}, \quad \mathcal{A}, \mathcal{B} \in \{HF, AF1, AF2\} \tag{2.12}$$

Where parameter $\alpha_{\mathcal{A},\mathcal{B}}(n)$ represents the dominance of $P_{\mathcal{B}}(n)$ with respect to $P_{\mathcal{A}}(n)$, while parameter $p_{\mathcal{A},\mathcal{B}}(n)$ measures the ratio between the overlapped bandwidth between spectral component $\mathcal{A}$ and $\mathcal{B}$ ($\Omega_{\mathcal{A},\mathcal{B}}(n)$) and the $\mathcal{B}$ bandwidth ($\Omega_{\mathcal{B}}(n)$). The subindices $\mathcal{A}$ and $\mathcal{B}$ represents the components HF, AF1 and AF2. LF is not considered since $\alpha_{\mathrm{LF},\mathcal{B}}(n)$ is always nearly zero. This means that the considered aliased components have much less power than the LF component, thus the LF correction is not necessary.

Whenever there is an overlapping between spectral components, which is measured by parameter $p_{\mathcal{A},\mathcal{B}}(n)$, $\alpha_{\mathcal{A},\mathcal{B}}(n)$ is used to compare both powers during one minute prior to the overlapping. Hence, a time-varying M-sample mean signal, $\overline{\alpha}_{\mathcal{A},\mathcal{B}}(n)$, is defined as follows:

$$\overline{\alpha}_{\mathcal{A},\mathcal{B}}(n) = \begin{cases} \dfrac{1}{M} \displaystyle\sum_{k=n-M+1}^{n} \alpha_{\mathcal{A},\mathcal{B}}(k) & \text{if } p_{\mathcal{A},\mathcal{B}}(n) = 0 \\ \overline{\alpha}_{\mathcal{A},\mathcal{B}}(n-1) & \text{if } p_{\mathcal{A},\mathcal{B}}(n) \neq 0 \end{cases} \tag{2.13}$$

with M being the number of samples equivalent to 1 minute ($M = 240$ samples). Whenever an overlapping happens ($p_{\mathcal{A},\mathcal{B}}(n) \neq 0$), this dominance parameter does not update, maintaining the previous value, and thus avoiding errors in dominance

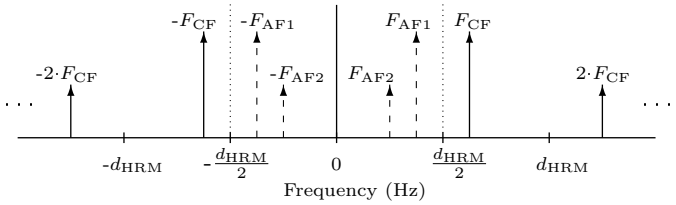

(a) Apparition of undesired aliases of F_{CF} in the spectrum of heart rate variability. Dotted lines represent the limits of the frequency range with physiological meaning in HRV analysis, defined by the mean HR, d_{HRM}. The component F_{CF} and its first harmonic produce two aliases (dashed lines) located at $F_{\mathrm{AF1}} = d_{\mathrm{HRM}} - F_{\mathrm{CF}}$ and $F_{\mathrm{AF2}} = -d_{\mathrm{HRM}} + 2 \cdot F_{\mathrm{CF}}$, respectively.

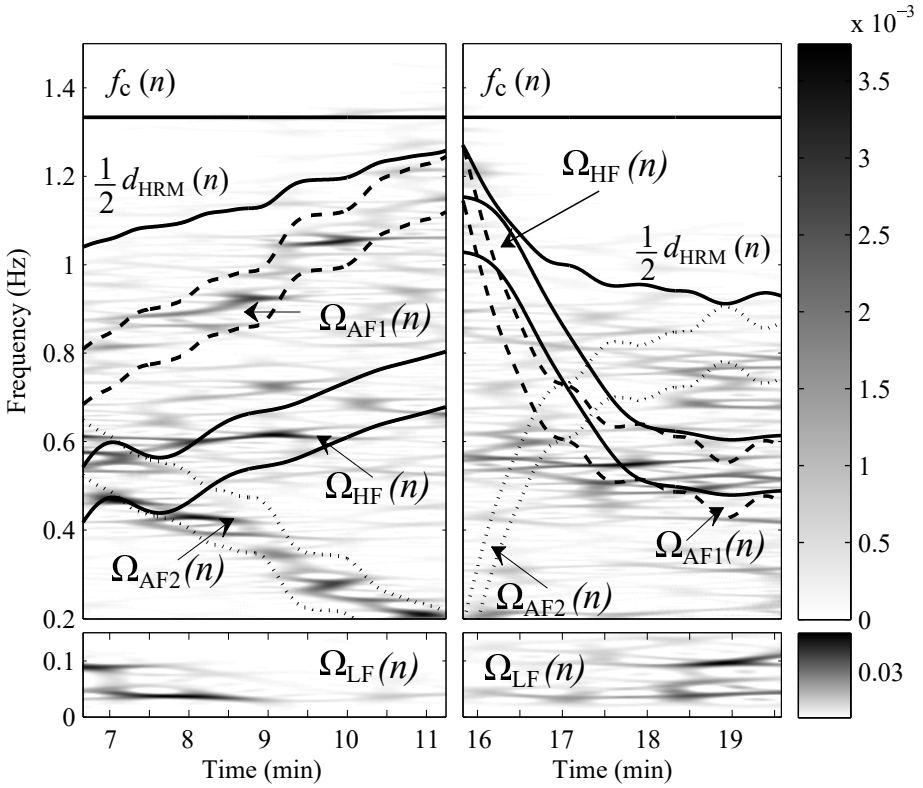

(b) Example of a time-frequency map showing some of the spectral components of HRV (HF, CF, AF1 and AF2) during the exercise phase (left) and recovery phase (right).

Figure 2.7: Spectral components.

estimation due to the overlapping. Note that this formula is valid if the overlapping happens at least one minute after the beginning of the recording, which is always the case in this database.

Then, the corrected power is estimated as:

$$\hat{P}_{\mathcal{A}}(n) = P_{\mathcal{A}}(n) - \sum_{\mathcal{B}\neq\mathcal{A}} \overline{\alpha}_{\mathcal{A},\mathcal{B}}(n) \cdot p_{\mathcal{A},\mathcal{B}}(n) \cdot P_{\mathcal{B}}(n) \tag{2.14}$$

Figure 2.8 shows an example of HF power correction. Panel a) shows $P_{\text{HF}}(n)$ (blue) and $P_{\text{AF2}}(n)$ (black), with the overlapping area marked with red dotted lines. Panel b) shows $\alpha_{\text{HF,AF2}}(n)$. Panel c) shows $\overline{\alpha}_{\text{HF,AF2}}(n)$ (blue) and $p_{\text{HF,AF2}}(n)$ (red). With these parameters, $\hat{P}_{\text{HF}}(n)$ is obtained and showed in panel a) (dashed blue).

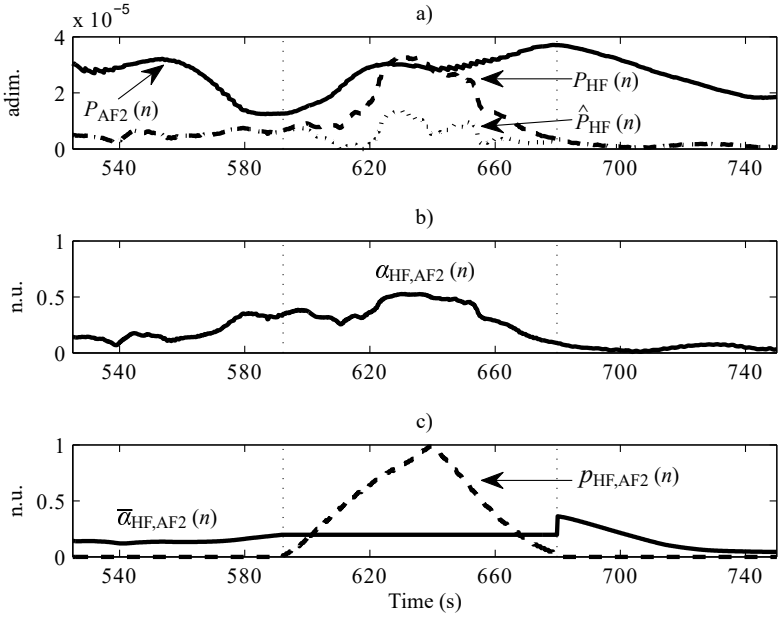

Figure 2.8: a) $P_{\text{HF}}(n)$ (dashed), $P_{\text{AF2}}(n)$ and $\hat{P}_{\text{HF}}(n)$ (dotted). b) $\alpha_{\text{HF,AF2}}(n)$. c) $\overline{\alpha}_{\text{HF,AF2}}(n)$ and $p_{\text{HF,AF2}}(n)$ (dashed). Vertical dotted lines delimit the overlapping area in all panels.

Two more parameters, T_{ov} and S_{ov}, are defined to measure the duration and severity of an overlap for each subject and for each type of test. First, $T_{\mathcal{A},\mathcal{B}}$ and $S_{\mathcal{A},\mathcal{B}}$ are defined: $T_{\mathcal{A},\mathcal{B}}$ measures the fraction of time that an overlap between the $\mathcal{A}$ and $\mathcal{B}$ components lasts ($p_{\mathcal{A},\mathcal{B}}(n) \neq 0$), and $S_{\mathcal{A},\mathcal{B}}$ measures the severity of an overlap between the $\mathcal{A}$ and $\mathcal{B}$ components and is obtained as:

$$S_{\mathcal{A},\mathcal{B}} = \frac{1}{N_{\mathcal{A},\mathcal{B}}} \sum_{n} \overline{\alpha}_{\mathcal{A},\mathcal{B}}(n) \cdot p_{\mathcal{A},\mathcal{B}}(n) \tag{2.15}$$

where $N_{\mathcal{A},\mathcal{B}}$ denotes the length (in samples) of the overlap. Then, T_{ov} and S_{ov} are obtained as the mean value of $T_{\text{AF1,HF}}$ and $T_{\text{AF2,HF}}$, and $S_{\text{AF1,HF}}$ and $S_{\text{AF2,HF}}$, respectively, for each subject.

2.3.6 Physiological indices

To denote the power related to cardiolocomotor coupling (CC) in a general way, we will use $\hat{P}_{\text{CC}}(n)$ from here onwards. This is obtained as:

$$\hat{P}_{\text{CC}}(n) = P_{\text{CF}}(n) + \hat{P}_{\text{AF1}}(n) + \hat{P}_{\text{AF2}}(n) \tag{2.16}$$

Due to the large changes of the total power for all bands, each instantaneous power is normalized by the instantaneous total power, which is defined as:

$$P_{\text{TOT}}(n) = P_{\text{LF}}(n) + \hat{P}_{\text{HF}}(n) + \hat{P}_{\text{CC}}(n) \tag{2.17}$$

Then, the studied power parameters are:

$$\overline{P}^{\text{I}}_{\mathcal{A}} = \frac{1}{N_{\text{I}}} \sum_{n \in I} \frac{\hat{P}_{\mathcal{A}}(n)}{P_{\text{TOT}}(n)}, \quad I \in \{I_{\text{B}}, I_{60}, I_{80}, I_{100}, I_{\text{R}}\} \tag{2.18}$$

Where N_{I} denotes the length of the interval I, and the subindex $\mathcal{A}$ indicates the chosen spectral component. Note that $\overline{P}^{\text{I}_B}_{\text{CC}}$ is an exception and is not defined, since at rest there is no power related to cardiolocomotor coupling.

The mean value of $d_{\text{HRM}}(n)$, $f_{\text{R}}(n)$ and $d_{\dot{\text{V}}\text{O}_2}(n)$ are also obtained for each interval as:

$$\overline{d}^{\text{I}}_{\text{HRM}} = \frac{1}{N_{\text{I}}} \sum_{n \in I} d_{\text{HRM}}(n), \quad I \in \{I_{\text{B}}, I_{60}, I_{80}, I_{100}, I_{\text{R}}\} \tag{2.19}$$

$$\overline{f}^{\text{I}}_{\text{R}} = \frac{1}{N_{\text{I}}} \sum_{n \in I} f_{\text{R}}(n), \quad I \in \{I_{\text{B}}, I_{60}, I_{80}, I_{100}, I_{\text{R}}\} \tag{2.20}$$

$$\overline{d}^{\text{I}}_{\dot{\text{V}}\text{O}_2} = \frac{1}{N_{\text{I}}} \sum_{n \in I} d_{\dot{\text{V}}\text{O}_2}(n), \quad I \in \{I_{\text{B}}, I_{60}, I_{80}, I_{100}, I_{\text{R}}\} \tag{2.21}$$

2.3.7 Statistical analysis

A Kolmogorov test showed that all $\overline{P}^{\mathrm{I}}_{\mathcal{A}}$, $\overline{d}^{\mathrm{I}}_{\mathrm{HRM}}$, $\overline{f}^{\mathrm{I}}_{\mathrm{R}}$ and $\overline{d}^{\mathrm{I}}_{\dot{\mathrm{V}}\mathrm{O}_2}$ did not follow a normal distribution. Therefore, a paired Wilcoxon test is applied for every parameter to study the differences between the different intervals within the same test, and between different tests. The difference is considered to be significantly different from zero when $p < 0.005$. Results in Figures 2.9 to 2.13 are shown as median plus median absolute deviation (MAD) values.

2.4 Results

2.4.1 Characterization of the analyzed intervals

Table 2.3 shows the mean and standard deviation of mean heart rate ($\overline{d}^{\mathrm{I}}_{\mathrm{HRM}}$), respiratory frequency ($\overline{f}^{\mathrm{I}}_{\mathrm{R}}$) and oxygen consumption ($\overline{d}^{\mathrm{I}}_{\dot{\mathrm{V}}\mathrm{O}_2}$) in the different intervals for the three tests. Significant differences were found in I_{100} between MaxT and SubT in $\overline{d}^{\mathrm{I}}_{\mathrm{HRM}}$ and $\overline{f}^{\mathrm{I}}_{\mathrm{R}}$, and between SubT and SubC in $\overline{f}^{\mathrm{I}}_{\mathrm{R}}$. In I_{R}, significant differences were found between MaxT and SubT in $\overline{d}^{\mathrm{I}}_{\mathrm{HRM}}$ and $\overline{f}^{\mathrm{I}}_{\mathrm{R}}$, and between SubT and SubC in all three parameters.

2.4.2 Characterization of HRV indices in a maximal test

As it can be seen in Figure 2.9, $\overline{P}^{\mathrm{I}}_{\mathrm{LF}}$ increases at the beginning of the exercise (I_{60}) with respect to the basal phase (I_{B}), then it decreases again when the exercise load gets more intense, and increases in the recovery phase. Wilcoxon analysis reveals that all intervals show significant differences with respect to $\overline{P}^{\mathrm{I}_B}_{\mathrm{LF}}$ and $\overline{P}^{\mathrm{I}60}_{\mathrm{LF}}$ (see the brackets in Figure 2.9). The opposite behaviour can be observed in $\overline{P}^{\mathrm{I}}_{\mathrm{HF}}$: it gets reduced at $\overline{P}^{\mathrm{I}60}_{\mathrm{HF}}$ and then it increases. However, it increases in the recovery phase. Significant differences can be observed between $\overline{P}^{\mathrm{I}_B}_{\mathrm{HF}}$ and $\overline{P}^{\mathrm{I}60}_{\mathrm{HF}}$, $\overline{P}^{\mathrm{I}60}_{\mathrm{HF}}$ and $\overline{P}^{\mathrm{I}100}_{\mathrm{HF}}$, $\overline{P}^{\mathrm{I}60}_{\mathrm{HF}}$ and $\overline{P}^{\mathrm{I}_R}_{\mathrm{HF}}$, $\overline{P}^{\mathrm{I}80}_{\mathrm{HF}}$ and $\overline{P}^{\mathrm{I}100}_{\mathrm{HF}}$, and $\overline{P}^{\mathrm{I}80}_{\mathrm{HF}}$ and $\overline{P}^{\mathrm{I}_R}_{\mathrm{HF}}$.

2.4.3 Comparison between HRV indices in the submaximal tests and the maximal test

Figure 2.10 shows $\overline{P}^{\mathrm{I}}_{\mathrm{LF}}$ and $\overline{P}^{\mathrm{I}}_{\mathrm{HF}}$ for the 3 tests in all intervals. The trending is similar for all the tests. Significant differences can be found in $\overline{P}^{\mathrm{I}100}_{\mathrm{LF}}$ in SubC test with respect to the other two tests. $\overline{P}^{\mathrm{I}}_{\mathrm{HF}}$ in SubC also shows differences with respect to SubT test during the exercise (I_{60} to I_{100}) and with respect to MaxT in I_{80} and I_{100}. No significant differences were found in I_{R}.

MaxT	I_{B}	I_{60}	I_{80}	I_{100}	I_{R}
$\overline{d}^{\mathrm{I}}_{\mathrm{HRM}}$	1.09 ± 0.14	1.98 ± 0.19	2.51 ± 0.17	2.85 ± 0.14	2.71 ± 0.18
$\overline{f}^{\mathrm{I}}_{\mathrm{R}}$	0.24 ± 0.05	0.38 ± 0.08	0.51 ± 0.14	0.69 ± 0.14	0.67 ± 0.21
$\overline{d}^{\mathrm{I}}_{\dot{\mathrm{V}}\mathrm{O}_2}$	389.2 ± 50.2	1502.7 ± 390.1	2989.2 ± 298.5	3841.0 ± 442.6	3136.4 ± 880.3
SubT	I_{B}	I_{60}	I_{80}	I_{100}	I_{R}
$\overline{d}^{\mathrm{I}}_{\mathrm{HRM}}$	1.04 ± 0.15	1.91 ± 0.15	2.40 ± 0.12	2.72 * ± 0.12	2.56 *,† ± 0.10
$\overline{f}^{\mathrm{I}}_{\mathrm{R}}$	0.25 ± 0.04	0.40 † ± 0.08	0.51 † ± 0.12	0.65 *,† ± 0.16	0.61 *,† ± 0.14
$\overline{d}^{\mathrm{I}}_{\dot{\mathrm{V}}\mathrm{O}_2}$	418.1 ± 66.0	1643.0 ± 439.4	3059.4 ± 293.9	3805.1 ± 435.7	3406.3 † ± 703.7
SubC	I_{B}	I_{60}	I_{80}	I_{100}	I_{R}
$\overline{d}^{\mathrm{I}}_{\mathrm{HRM}}$	1.06 ± 0.18	1.86 ± 0.16	2.39 ± 0.17	2.70 ± 0.18	2.46 ± 0.11
$\overline{f}^{\mathrm{I}}_{\mathrm{R}}$	0.25 ± 0.07	0.36 ± 0.05	0.47 ± 0.08	0.58 ± 0.11	0.55 ± 0.15
$\overline{d}^{\mathrm{I}}_{\dot{\mathrm{V}}\mathrm{O}_2}$	423.3 ± 69.9	1637.2 ± 197.3	2964.6 ± 307.0	3612.4 ± 325.0	2573.2 ± 485.7

Table 2.3: Median and MAD values for mean heart rate ($\overline{d}^{\mathrm{I}}_{\mathrm{HRM}}$), respiratory frequency ($\overline{f}^{\mathrm{I}}_{\mathrm{R}}$) and oxygen consumption ($\overline{d}^{\mathrm{I}}_{\dot{\mathrm{V}}\mathrm{O}_2}$) for the three tests: MaxT for maximal test on treadmill, SubT for submaximal test on treadmill, SubC for submaximal test on cycle ergometer. Different intervals are based of the oxygen consumption ($\dot{V}O_2$): I_{B}, I_{60}, I_{80}, I_{100} and I_{R} for the basal phase, 0-60%, 60-80% and 80-100% of $d_{\dot{\mathrm{V}}\mathrm{O}_2}(n)$ defined by MaxT, respectively, and recovery phase. * and †denote significant differences between MaxT and SubT, and between SubT and SubC, respectively (p value < 0.005).

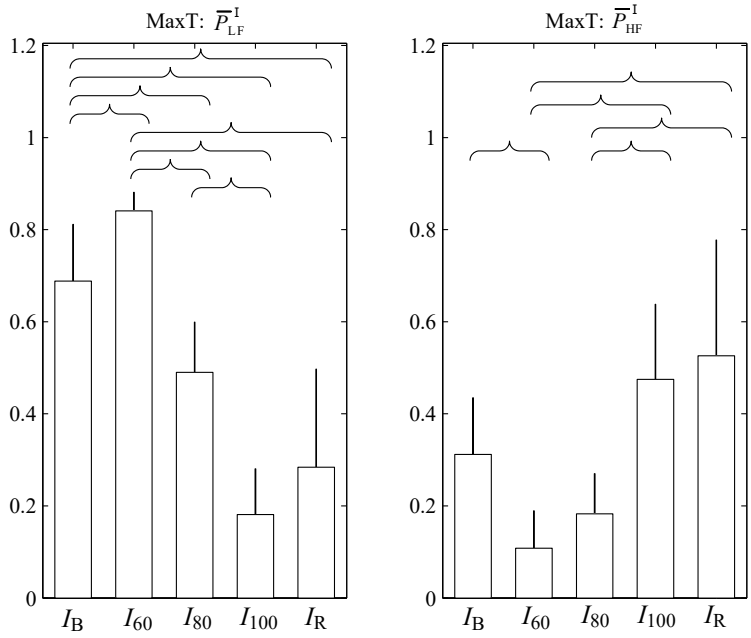

Figure 2.9: Median and MAD of $\overline{P}^{\mathrm{I}}_{\mathrm{LF}}$ (left panel) and $\overline{P}^{\mathrm{I}}_{\mathrm{HF}}$ (right panel) in intervals I_{B}, I_{60}, I_{80}, I_{100} and I_{R} (basal phase, 0-60%, 60-80% and 80-100% of $d_{\dot{V}O_2}(n)$, respectively, and recovery phase) for the MaxT test. Brackets denote significant differences (p value < 0.005).

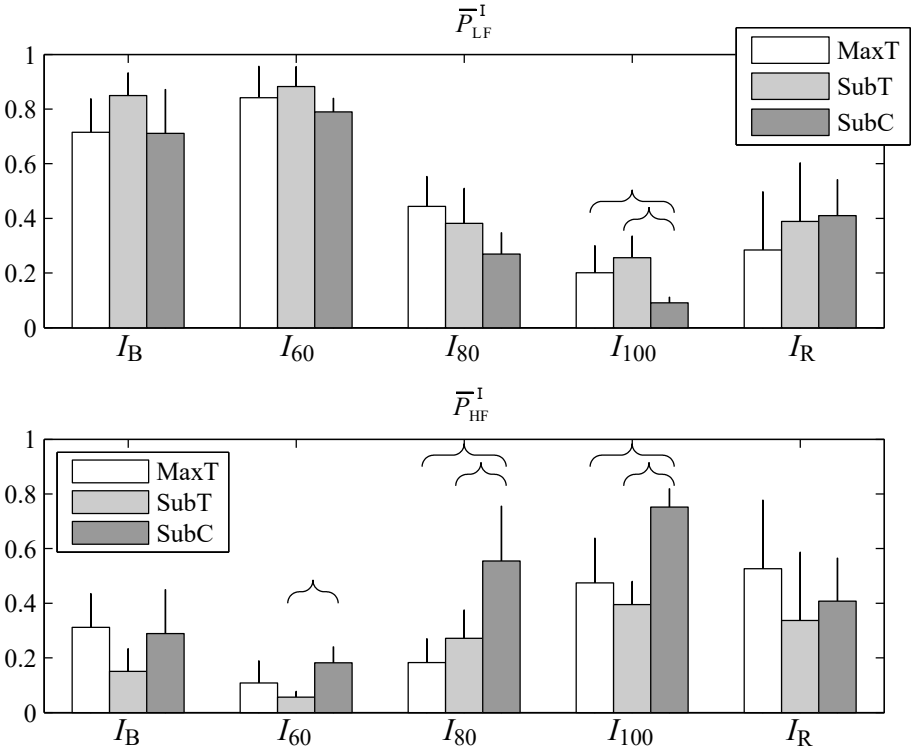

Figure 2.10: Median and MAD of $\overline{P}^{\mathrm{I}}_{\mathrm{LF}}$ (upper panel) and $\overline{P}^{\mathrm{I}}_{\mathrm{HF}}$ (lower panel) in intervals I_{B}, I_{60}, I_{80}, I_{100} and I_{R} (basal phase, 0-60%, 60-80% and 80-100% of $d_{\dot{\mathrm{V}}\mathrm{O}_2}(n)$ defined by MaxT, respectively, and recovery phase) for the MaxT, SubT and SubC tests. Brackets denote significant differences (p value < 0.005).

2.4.4 Characterization of the cardiolocomotor coupling

Figure 2.11 shows $\overline{P}^{\mathrm{I}}_{\mathrm{CC}}$ for the 3 tests in the exercise intervals ($\overline{P}^{\mathrm{I}_B}_{\mathrm{CC}}$ is not defined). At the beginning of the exercise, $\overline{P}^{\mathrm{I}}_{\mathrm{CC}}$ represents less than 10% of the total power. In the last two intervals of exercise, it reaches 20-30% of the total power. In the recovery phase, it represents about 10% of the total power. $\overline{P}^{\mathrm{I}}_{\mathrm{CC}}$ in SubC is significantly different from SubT and MaxT in I_{80} and I_{100}. No differences were found in I_{60} and I_{R}.

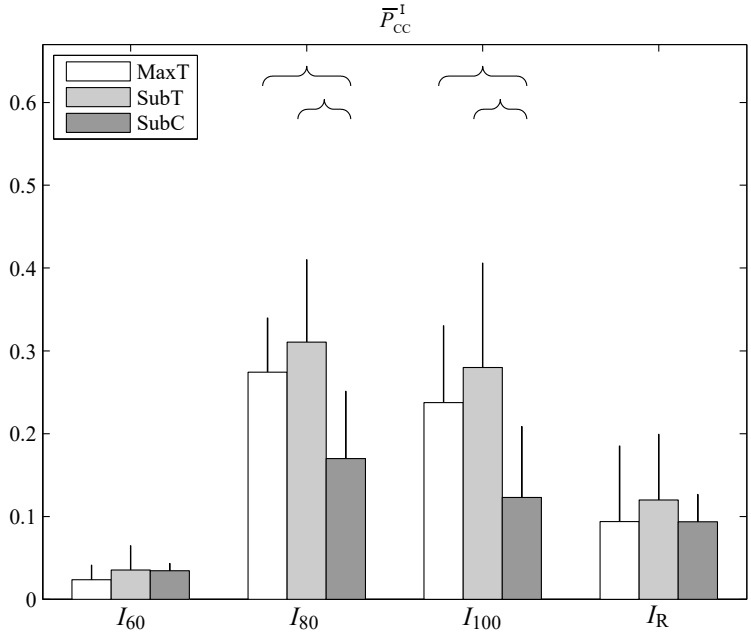

Figure 2.11: Median and MAD of $\overline{P}^{\mathrm{I}}_{\mathrm{CC}}$ in intervals I_{B}, I_{60}, I_{80}, I_{100} and I_{R} (basal phase, 0-60%, 60-80% and 80-100% of $d_{\dot{\mathrm{V}}\mathrm{O}_2}(n)$ defined by MaxT, respectively, and recovery phase) for the MaxT, SubT and SubC tests. Brackets denote significant differences (p value < 0.005).

Figure 2.12 shows different parameters to measure the severity of the overlaps. Only the two submaximal tests are compared (SubT and SubC), where $f_{\mathrm{C}}(n)$ was forced to be constant. S_{ov} is higher in SubT than SubC, which means that the power of the aliased components are higher in SubT with respect to the power in the HF band. T_{ov} is higher in SubC than SubT, which means that in SubT the overlappings happen for a longer time than in SubC. Figure 2.12 also shows the product of S_{ov} and T_{ov}, which is very similar in both tests. No significant differences are found in those parameters.

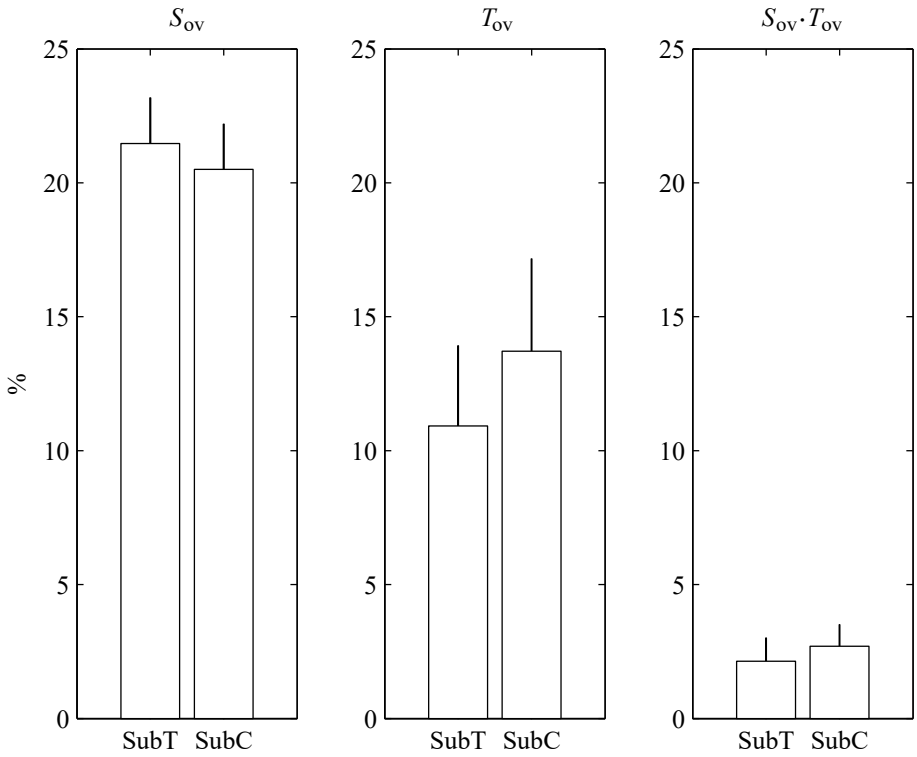

Figure 2.12: Median and MAD of S_{ov} (left), T_{ov} (middle) and the product $S_{ov} \cdot T_{ov}$ (right) for the SubT and SubC tests.

2.4.5 Influence of each methodology step

Three main methodological aspects have been included in this work to address the problems due to the characteristics of exercise test HRV: a) redefinition of HF band based on respiratory frequency, b) mean HR correction of the HRV signal, and c) correction of the overlapped aliasing components related to CF. To study the influence of each of these methods, the evolution of normalized HF power was studied in different scenarios (reported here only for SubC), where different methodologies are applied step by step.

- Scenario 0 (S0): Classical HRV analysis is applied, i.e., HF band is fixed from 0.15 to 0.4Hz, there is no mean HR correction, and CF component is not considered.
- Scenario 1 (S1): The HF band is redefined based on $f_{\mathrm{R}}(n)$.
- Scenario 1 (S2): In addition to S1, the mean HR correction is applied.
- Scenario 1 (S3): In addition to S2, the aliased components related to CF are attenuated. This is the framework used in the rest of the work.

Only the HF component is shown since LF does not change in S1 and S3. Moreover, since in S0-S2 the CF component is assumed not to exist, they will be studied separated from S3. Figure 2.13a shows the evolution of normalized HF power in S0 to S2. It is important to note that, only for this analysis, normalized power is obtained as:

$$\overline{P}_{\mathrm{HF}}^{\mathrm{I,S}} = \frac{1}{N_{\mathrm{I}}} \sum_{n \in I} \frac{P_{\mathrm{HF}}(n)}{P_{\mathrm{LF}}(n) + P_{\mathrm{HF}}(n)}, \quad S \in \{\mathrm{S0},\, \mathrm{S1},\, \mathrm{S2}\} \tag{2.22}$$

since the CF component is not taken into account in the analysis, and thus the measured powers are not comparable with those which are normalized by $P_{\mathrm{TOT}}(n)$. Significant differences can be found in S1 for all exercise intervals, and in S2 in I_{60} (always with respect to the previous scenario).

Regarding the S3 scenario, CF component is identified, as well as its alias and the overlapping zones between CC and HF components. In this scenario, $\overline{P}_{\mathrm{HF}}^{\mathrm{I}}$ is going to be redefined based on two different normalizations: only LF and HF components (HF_{n1}), and total power including CC components (HF_{n2}). The series $P_{\mathrm{HF}_{n1}}(n)$ and $P_{\mathrm{HF}_{n2}}(n)$, and their corrected version $\hat{P}_{\mathrm{HF}_{n1}}(n)$ and $\hat{P}_{\mathrm{HF}_{n2}}(n)$, are obtained as:

$$P_{\mathrm{HF}_{n1}}(n) = \frac{P_{\mathrm{HF}}(n)}{P_{\mathrm{LF}}(n) + P_{\mathrm{HF}}(n)} \tag{2.23}$$

$$\hat{P}_{\mathrm{HF}_{n1}}(n) = \frac{\hat{P}_{\mathrm{HF}}(n)}{P_{\mathrm{LF}}(n) + \hat{P}_{\mathrm{HF}}(n)} \tag{2.24}$$

$$P_{\mathrm{HF}_{n2}}(n) = \frac{P_{\mathrm{HF}}(n)}{P_{\mathrm{LF}}(n) + P_{\mathrm{HF}}(n) + P_{\mathrm{CF}}(n) + P_{\mathrm{AF1}}(n) + P_{\mathrm{AF2}}(n)} \tag{2.25}$$

$$\hat{P}_{\mathrm{HF}_{n2}}(n) = \frac{\hat{P}_{\mathrm{HF}}(n)}{P_{\mathrm{LF}}(n) + \hat{P}_{\mathrm{HF}}(n) + P_{\mathrm{CF}}(n) + \hat{P}_{\mathrm{AF1}}(n) + \hat{P}_{\mathrm{AF2}}(n)} \tag{2.26}$$

Then, the mean value is obtained in each interval, taking into account only the overlapping zones:

$$\overline{P}^{\mathrm{I_{ov}}}_{\mathrm{HF}_{nx}} = \frac{1}{N_{\mathrm{I_{ov}}}} \sum_{n \in I_{ov}} P_{\mathrm{HF}_{nx}}(n) \tag{2.27}$$

$$\overline{\hat{P}}^{\mathrm{I_{ov}}}_{\mathrm{HF}_{nx}} = \frac{1}{N_{\mathrm{I_{ov}}}} \sum_{n \in I_{ov}} \hat{P}_{\mathrm{HF}_{nx}}(n) \tag{2.28}$$

where the subindex $_{\mathrm{HF}_{nx}}$ denotes both normalizations HF_{n1} and HF_{n2}, I_{ov} denotes the overlapping zones within each interval I ($I \in \{I_{60}, I_{80}, I_{100}, I_{\mathrm{R}}\}$), and $N_{\mathrm{I_{ov}}}$ denotes the length of the overlapping zones in the interval I.

Figure 2.13b shows changes in HF power during the overlapping zones in each interval, after attenuating any aliased components related to CF. Both normalizations are presented. In the first normalization, there are no significant differences after correction, with $\overline{\hat{P}}^{\mathrm{I_{ov}}}_{\mathrm{HF}_{n1}}$ being slightly lower than $\overline{P}^{\mathrm{I_{ov}}}_{\mathrm{HF}_{n1}}$ in I_{80} and I_{100}. In the second normalization, $\overline{\hat{P}}^{\mathrm{I_{ov}}}_{\mathrm{HF}_{n2}}$ is significantly higher than $\overline{P}^{\mathrm{I_{ov}}}_{\mathrm{HF}_{n2}}$ also in I_{80}, I_{100} and I_{R}, mainly because of the correction of the CC components. No differences are found in I_{60}.

2.5 Discussion

2.5.1 Methodological aspects

This work deals with analysing HRV in an exercise test database. Standard spectral analysis may fail to properly provide ANS information during exercise, hence extra methodological steps should be taken into account. Most important challenges include a reliable and robust QRS detection, a proper method to deal with the non-stationary nature of HRV during exercise, removing the influence of the time-varying mean heart rate, adapting the HF band to the respiratory frequency, as well as taking care of additional spectral components which may interfere with the measurements.

The non-linear relation between heart rate and HRV has been addressed by several works. TVIPFM model, which is used to explain the regulation of the heart rate by the autonomic nervous system, also allows to use a time-varying threshold to remove mean heart rate influence. This way, a continuous corrected HRV series can be obtained and HRV measurements at different mean heart periods can be safely compared. Chiu et al. [103] and Meste et al. [104] deal with this problem using a different methodology named the pulse frequency modulation model, which was also applied to obtain the continuous modulating signal. Sacha et al. [44] also address this problem and propose a method to weaken the influence of HR (Sacha et al. [45]) by dividing the RR interval

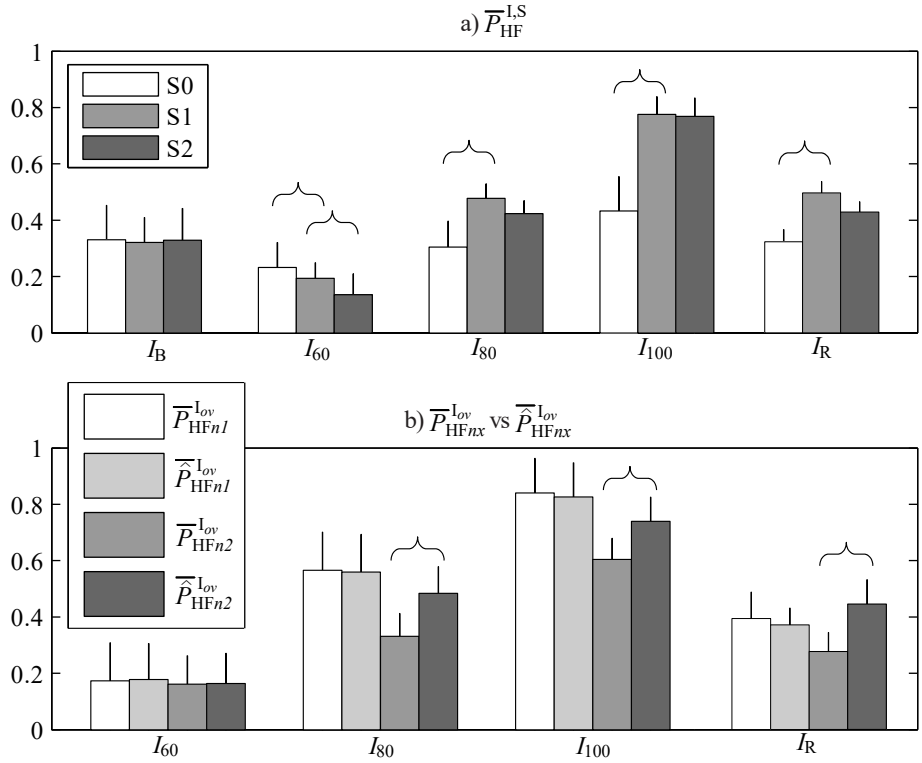

Figure 2.13: a) Median and MAD of the evolution of $\overline{P}^{\mathrm{I,S}}_{\mathrm{HF}}$ for the SubC test. 3 different scenarios are shown: S0 (classical HRV analysis), S1 (S0 + redefinition of HF band based on $f_{\mathrm{R}}(n)$) and S2 (S1 + mean HR correction). b) Median and MAD of $\overline{P}^{\mathrm{I_{ov}}}_{\mathrm{HF}_{nx}}$ (pre overlapping correction) and $\overline{\widehat{P}}^{\mathrm{I_{ov}}}_{\mathrm{HF}_{nx}}$ (post overlapping correction) for the SubC test when CC components are considered. Two different normalizations are presented: only LF and HF components (HF_{n1}), and total power including CC components (HF_{n2}). Intervals I_{B}, I_{60}, I_{80}, I_{100} and I_{R} refer to basal phase, 0-60%, 60-80% and 80-100% of $d_{\dot{\mathrm{V}}\mathrm{O}_2}(n)$ defined by MaxT, respectively, and recovery phase. Brackets denote significant differences (p value < 0.005).

tachograms or HRV spectra by the corresponding average RR intervals. This correction, however, should be performed not with the total average but with local averages in order not to lose the dynamic changes in an exercise test (Sacha et al. [105]).

Regarding the non-stationary nature of HRV during exercise, several tools have been proposed (see Mainardi [77]), such as short-time Fourier transform, time-varying autoregressive analysis and time-frequency representations. The advantage of these methodologies is that they allow to define time-varying bands for the different spectral components. In this work, one of the existing time-frequency representations has been chosen, the smoothed pseudo Wigner-Ville distribution (SPWVD), and whose capability to quantify HRV patterns in non-stationary conditions has been validated by other studies (M. Orini et al. [106], Chan et al. [103]). HF band has been defined centered at respiratory frequency since respiratory frequency increases with exercise intensity and can exceed the upper limit of classical HF band (0.4 Hz). HF bandwidth might be also dependent on respiratory spectra but in this work, a fixed band of 0.125 Hz has been used, since respiration spectra showed a very well defined and narrow peak around respiratory frequency.

Four different scenarios have been studied to evaluate the impact of each methodological approach: classical HRV analysis, the redefinition of HF band based on $f_{\mathrm{R}}(n)$ is added, the mean HR correction is added, and the attenuation of aliased cardiolocomotor coupling components is added, see Figure 2.13. At rest, there are no significant differences in the HF component in any scenario, since the mean heart rate does not significantly vary, $f_{\mathrm{R}}(n)$ is located within the classic HF band, and there is no CF component. Taking the classical HRV analysis as the reference, when the HF is located around $f_{\mathrm{R}}(n)$, there are differences in all exercise intervals, since both HF bands start to differ at the beginning of the exercise (I_{60}) when $f_{\mathrm{R}}(n)$ increases above the upper limit of the classic HF band (0.4 Hz), and maintains above it during the rest of the exercise and the recovery interval. In the next scenario, the mean HR correction is added, and there are significant differences only in I_{60}. In this interval, the mean HR greatly varies from the rest phase, while in I_{80} and I_{100} the slope of mean HR is not as steep as in I_{60}.

In the last scenario, spectral components related to cardiolocomotor coupling were identified and corrected when necessary. Two different normalizations have been studied. The first normalization, HF_{n1}, only takes into account LF and HF components. The second normalization, HF_{n2}, also includes cardiolocomotor components. While HF_{n1} is commonly used in HRV analysis at rest as a measure of sympathovagal balance, HF component during moderate-to-high exercise intensities is no longer only related to ANS activity but also to a mechanical effect. This work proposes HF_{n2} to quantify the relative HF power with respect to all components found in HRV spectrum. Comparing pre- and post- overlapping correction in HF_{n1} during the overlappings, there are no significant differences. HF_{n2} prior to the correction shows lower values because both CC and HF components are contaminated. After correction, there are significant differences in I_{80}, I_{100} and I_{R} in HF_{n2} with higher power after the attenuation of the effect of cardiolocomotor coupling. This effect is mainly due to the correction of the aliases of the CF component. However, the importance of this correction is more

evident when each subject is studied separately. As an example, in Figure 2.8, from seconds 600 to 650, HF power presents a sudden increase, which could mislead the interpretation relating it to a parasympathetic activation.

2.5.2 Physiological aspects

Regarding the maximal test, LF and HF power follow the same behaviour than reported in previous works. There is first a rapid increase of heart rate and oxygen consumption (I_{60}). In this phase of moderate exercise, there is an increase in normalized LF power and a decrease in normalized HF power. This is mainly related with both a parasympathetic withdrawal and an augmented sympathetic activity, as suggested in Sarmiento et al. [80]. During moderate-to-high exercise intensities (I_{80} and I_{100}), cardiac vagal control is no longer effective, and HF power greatly increase due to the mechanical effect of breathing [80]. This effect, together with a greater cardiolocomotor power, leads to a decrease of normalized LF power and an increase of normalized HF power. In the recovery phase, subjects are still running/cycling, and an increase in LF and a decrease in HF is expected, as described in [87], mainly due to the decrease of the mechanical effect of breathing. While there is indeed an increase in LF, HF also increases probably due to the inclusion of CC components in the normalization.

There are no significant differences in the LF and HF power indices when comparing the two tests on the treadmill (MaxT and SubT). However, in SubT there is a decrease in HF in the recovery phase as expected. Looking at Figure 2.11, it shows that CC power is always higher in SubT than MaxT. The reason may be that in MaxT, the cadence frequency was free, while in SubT it was fixed. Interestingly, the volunteers claimed that running at a fixed cadence during the incremental exercise did not feel natural. However, no significant differences were found in CC power between MaxT and SubT.

SubT and SubC are significantly different during exercise, mainly regarding HF power indices. LF power is only different in the last exercise interval, near the peak of exercise. Millet et al. [107] state that central fatigue and decrease in maximal strength are more important after prolonged exercise in running than in cycling, which may impact in HRV parameters. They also claim that running exercise induces a higher oxygen uptake than cycling at the same intensity, being the metabolic demands different for each type of exercise. This also happens in this database, where $\dot{V}O_2$ consumed in the last interval is always higher in SubT than in SubC (3825.1 ± 435.7 vs 3612.4 ± 325.1 ml $O_2 \cdot$ kg$^{-1} \cdot$ min^{-1}). Moreover, 4 subjects did not reach the last interval in SubC because the maximum value of $\dot{V}O_2$ in that test was lower than 80% of the max value in the MaxT test. However, the results of such physiological tests in cycling and running may be influenced by the athlete's original training background.

The largest differences between the submaximal tests can be found in CC power, where SubT presents higher levels of power than SubC. This component is related to cardiolocomotor coupling, which might be due to the dynamic modulation of the venous return due to leg muscle contraction (Blain et al. [84]). Running may demand

more power at muscle legs than cycling and so the effect of the arterial baroreceptors due to oscillations in venous return should be stronger in SubT. This exercise test and their related CC power at HRV could provide useful information, and has never been considered for quantification of the possible baroreflex sensitivity underlying this component, and eventually related to some pathologies related to this reflex. Another difference is that there is a reduction in the venous return during cycling compared to running, which may be due in part to peripheral muscle blood flow [107]. Moreover, subjects felt less natural to keep a fixed cadence while running on the treadmill than cycling and this additional effort may affect this component. These results suggest that this cardiolocomotor component is less strong in cyclo ergometer tests. No differences were found in the recovery phase when comparing the tests, but in MaxT and SubT there is a significant decrease from I_{100} to I_{R}, while in SubC there is no significant difference between those intervals.

Although no significant differences were found in the overlappings in SubT and SubC, it was found that S_{ov} was higher in SubT, while T_{ov} was higher in SubC. This means that the power in the aliased components is higher in SubT with respect to the HF power. However, this overlaps last shorter in SubT than SubC. If the overlapped areas are detected and removed from the study, it may be better to perform a test on a treadmill, where this overlaps are shorter. While on the other hand, if these overlaps are not detected, a test on a cycle ergometer may be preferred, since the severity of the overlaps is lower.

2.6 Conclusion

This work has proposed an integrated methodological framework for a robust HRV analysis during exercise. TVIPFM model allows to correct the HRV signal to remove the influence of the time-varying mean HR. Nonstationary nature of HRV during exercise has been solved by using the SPWVD, a time-frequency spectral analysis, which allows to extract continuous power information. HF band has been redefined and centered at the respiratory frequency. Lastly, spectral components related to the stride/pedalling cadence have been identified and, whenever they overlapped with the HF band, the measured powers have been corrected.

During the first phase of the exercise, there is a rapid increase of heart rate and oxygen consumption, together with an increase in normalized LF power and a decrease in normalized HF power. During moderate-to-high exercise intensities, however, there is an increase in normalized HF power despite the parasympathetic withdrawal, mainly due to the mechanical effect of breathing. In the recovery phase, an increase in normalized LF and a decrease in normalized HF are expected. When comparing running and cycling tests, normalized HF power differs, being greater while cycling. Power related to the stride/pedalling cadence is stronger while running, being higher if this cadence is fixed.

Chapter 3

Validation of heart rate monitor Polar RS800 for heart rate variability analysis during exercise

3.1 Motivation

The apparent ease of derivation of HRV has popularized its use in both clinical and research environments and over a broad spectrum of disciplines concerned with autonomic control of the heart ranging from cardiology to psychology. Historically, studies were confined to laboratory-based ECG systems or Holter-type monitors for both long- and short-term RR interval recordings. Such systems are expensive, time consuming, and require trained personal to operate effectively [108]. Advances in technology have

allowed the development of mobile and easy to use heart rate monitors that allow the quantification of inter-beat intervals (RR intervals) and thus analyzing heart rate variability. Commercial devices (like Polar, Garmin, Tomtom, or Suunto heart rate monitors, among others) appear as a cheaper alternative, usually providing software which allows for an affordable and a user-friendly method to determine short-term HRV outside of the laboratory setting.

These heart rate monitors have been used by scientists for HRV analysis in sport sciences, medicine and other fields of research [109–111]. Recent studies have validated these devices against different ECG systems. They show promising results and claim that, at rest, these devices are able to yield series of RR intervals for HRV analysis as reliably as those obtained by ECG [112–115]. However, [116] studied the differences according to the gender, claiming that the reliability between the heart monitor and ECG was weaker for women. Other studies have also studied and validated their reliability of HRV measurements in animals [117, 118]. Lastly, [119] shows that HRV measurements from heart monitor devices are reliable during supine and sitting rest, walking, and moderate to vigorous static exercise of the limbs. However, no study has validated HRV measurements from heart rate monitor devices during dynamic exercise of high intensity, which is characterized with a higher level of noise than in static exercise, and the variations in mean HR and respiratory frequency will also be larger. Additionally, the appearance of cardiolocomotor coupling components during high intensities may differentiate HRV measurements from ECG and from wearable heart rate monitor devices.

The aim of this study is to evaluate the agreement and reliability between the HRV analysis derived from the RR series recorded by the HR monitor Polar RS800 and HRV analysis derived from a simultaneous ECG during dynamic exercise of low, medium and high intensity.

3.2 Materials and methods

3.2.1 Subjects, experimental protocol and data acquisition

The database is the one described in 2.3.1: 23 healthy volunteers who regularly participate in sports activities. In this chapter, we focus on the SubC test also described in 2.3.1, i.e., the submaximal test on the cycle ergometer. Similarly, five different intervals are defined: I_{B}, I_{60}, I_{80}, I_{100} and I_{R}.

Data acquisition is described in 2.3.2. In addition to the ECG recording, RR intervals were recorded beat-to-beat using an HR monitor (RS800, Polar Electro Oy, Kempele, Finland) which uses a sampling frequency of 1000 Hz for the ECG signal. RR intervals from the ECG ($\mathrm{RR_{ECG}}$) were obtained as the difference of each consecutive beat occurrences. RR intervals from Polar ($\mathrm{RR_{POL}}$) were directly obtained from the device. The delay between $\mathrm{RR_{ECG}}$ and $\mathrm{RR_{POL}}$ was estimated as that lag which maximizes their cross correlation. Subsequently, the two series were synchronized by correcting this delay.

3.2.2 Heart rate variability parameters

HRV series derivation is described in 2.3.3. The SPWVD is applied to $m(n)$ to estimate the time-varying spectral properties of both HRV signals with the same parameters than 2.3.4. The instantaneous power in the low and high frequency band, $P_{\mathrm{LF}}(n)$ and $P_{\mathrm{HF}}(n)$ respectively, was extracted throughout the entire exercise test. Low frequency band ranged from 0.04 to 0.15 Hz. The high frequency band was centered on the respiratory frequency with a bandwidth of 0.125 Hz. The lower limit of the HF band was never below 0.15 Hz, and the upper limit was never above the half of mean heart rate, thus no aliasing was measured [10].

3.2.3 Reliability and agreement analysis

To study the reliability and agreement between HRV derived from the Polar records and from the ECG signal, 4 steps were proposed:

1. A Bland-Altman plot [120] was used to visualize both $\mathrm{RR}_{\mathrm{ECG}}$ and $\mathrm{RR}_{\mathrm{POL}}$ series. The bias, the limits of agreement (LOA) and the percentage of paired RR measurements that are out of the LOA were computed in each interval.

2. Pearson's correlation coefficient (ρ) [121] was used to quantify the linear relationship between the ECG and Polar following signals:

   (a) Mean heart rate: $d_{\mathrm{HRM}}(n)$
   (b) Low frequency power: $P_{\mathrm{LF}}(n)$
   (c) High frequency power: $P_{\mathrm{HF}}(n)$

   Threshold was set to 0.8, above which the two signals present a high linear correlation, providing a significant p-value (< 0.05). For reference, the correlation coefficient can also be computed in the paired RR series: Figure 3.1 shows in the upper panel a case of RR series from a subject which presents a ρ value above the threshold ($\mathrm{RR}_{\mathrm{ECG}}$ in blue, $\mathrm{RR}_{\mathrm{POL}}$ in red), while lower panel shows a case with ρ value below the threshold.

   This coefficient was evaluated in each interval (I_{B}, I_{60}, I_{80}, I_{100} and I_{R}), for every subject. Also, the relative error was computed as the the difference between the two series (from the ECG and from Polar) normalized by the mean value in the reference series (from the ECG), in absolute value. That is, if we denote any of the ECG series $x(n)$ and the Polar series $y(n)$, the relative error is computed as:

$$\epsilon(n) = \left| \frac{x(n) - y(n)}{x(n)} \right| 100\% \tag{3.1}$$

   and the mean relative error $\bar{\epsilon}$ is obtained in each interval with a ρ value above the threshold as the mean value of $\epsilon(n)$ within that interval. This is to see, in those intervals which present a high linear correlation, how much the Polar series deviate from the reference ones.

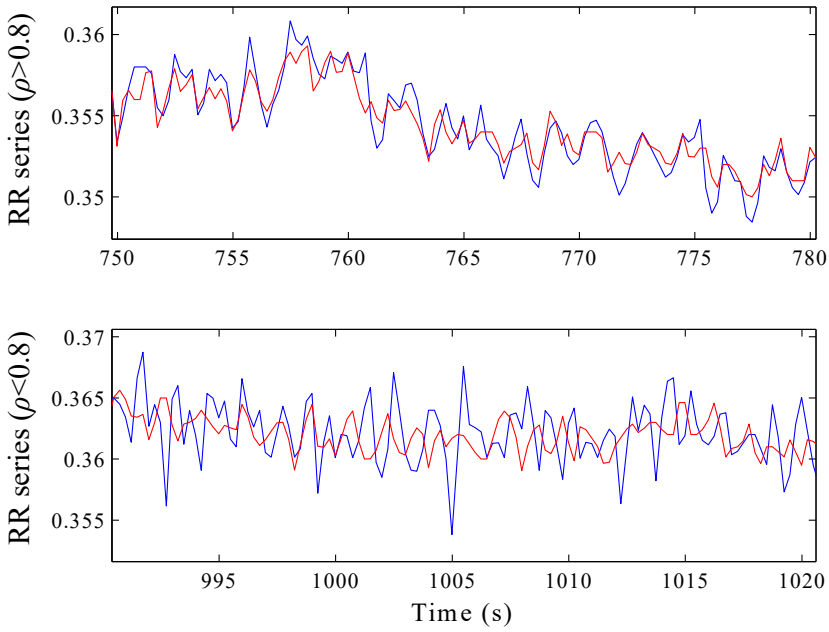

Figure 3.1: Example of an interval of the RR series with $\rho = 0.89$ (upper panel) and $\rho = 0.65$ (lower panel): RR_{ECG} in blue, RR_{POL} in red

3. To measure the interchangeability between measures, two reliability indexes were used: Lin's concordance correlation coefficient (CCC) and intraclass correlation coefficient (ICC).

   The CCC index measures the reliability between two methods [122], and it determines how far the observed data deviate from the line of perfect concordance line at 45° on a square axis scatter plot. Alternatively, ICC index which also measures reliability, represents the ratio of between-sample variance and the total variance (between- and within-sample) to measure precision under the model of equal marginal distributions [123].

4. The agreement was measured by an information-based measure of disagreement (IBMD) proposed in [124]. This measurement is based on Shannon's entropy and equals 0 when the observers agree (no disagreement: $x_i = y_i$), i.e., there is no information in the differences between methods X and Y. This measurement increases towards to 1 if the amount of information in the difference increases. The agreement (A) can be quantified as A=1-IBMD.

3.2.4 Statistical analysis for HRV parameters

Additionally, the same analysis from Chapter 2 was applied and parameters $\overline{P}^{\mathrm{I}}_{\mathrm{LF}}$, $\overline{P}^{\mathrm{I}}_{\mathrm{HF}}$ and $\overline{P}^{\mathrm{I}}_{\mathrm{CC}}$ were obtained from Polar measurements for every interval. A Kolmogorov test showed that they did not follow a normal distribution. Therefore, a paired Wilcoxon test was applied for every parameter to study the differences Polar and ECG measurements to see if they show the same ANS changes in the different intervals. The difference is considered to be significantly different from zero when $p < 0.005$.

3.3 Results

3.3.1 Bland-Altman plot

Figure 3.2 shows a Bland-Altman plot which evaluates the inter-method discrepancies between ECG and Polar RR measurements and the stability across a wider value range. The central and the upper and lower horizontal lines show the bias (mean) and the LOA ($\pm 2\sigma$), respectively, of the differences between both methods, where σ represents the standard deviation. 27552 paired RR measurements were used, from which 96.68% were contained within the range. For shorter RR, i.e. higher heart rates, the discrepancies are larger. Table 3.1 shows the bias, LOA and the percentage of paired RR measurements out of the LOA for each interval and the whole data combined. The mean RR and standard deviation associated to each interval is also shown.

RR (ms)	BIAS (ms)	LOA (ms)	Out LOA (%)
I_{R}: 369.7 ± 63.4	-0.0353	[-4.622, 4.619]	4.15
I_{100}: 359.7 ± 42.7	-0.0192	[-5.198, 5.160]	4.80
I_{80}: 435.9 ± 33.5	-0.0022	[-4.234, 4.229]	3.99
I_{60}: 507.9 ± 38.4	-0.0737	[-6.075, 5.927]	3.81
I_{B}: 1167.3 ± 442.7	0.0616	[-5.174, 5.298]	1.67
Whole range	0.0205	[-5.341, 5.382]	3.32

Table 3.1: Bias, LOA and % of paired RR measurements out of the LOA.

3.3.2 Pearson's coefficient

Figure 3.3 shows an example of $d_{\mathrm{HR}}(n)$, $P_{\mathrm{LF}}(n)$ and $P_{\mathrm{HF}}(n)$ for one subject. Due to the differences in the axes, the resting and exercise phase are represented in different plots. Left panel shows the evolution of these signals during the 5 minutes prior to the exercise (rest interval), with blue representing the signal derived from $\mathrm{RR}_{\mathrm{ECG}}$ and red is the signal derived from $\mathrm{RR}_{\mathrm{POL}}$. Right panel shows the exercise phase.

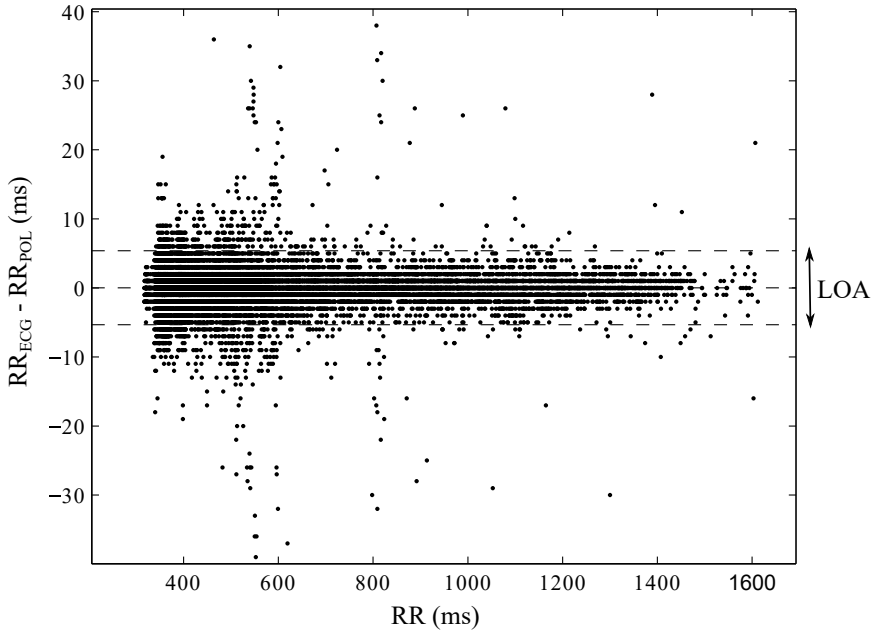

Figure 3.2: Bland-Altman plot: RR_{ECG} vs RR_{POL}

Table 3.2 shows how many subjects present a high Pearson's coefficient in each interval (ρ >0.8), for the different signals. Also, the mean relative error for those segments is computed, displayed in brackets as the mean value for those subjects.

3.3.3 Reliability and agreement coefficients (CCC, ICC and A)

Table 3.3 shows the CCC and ICC values in each interval. It can be seen lower coefficients in the rest phase than in I_{60}, which was not expected, but still excellent reliability, i.e., above 0.9. These coefficients decreases in the last intervals (near the exercise peak) for $P_{\text{HF}}(n)$, being considered poor reliability a coefficient lower than 0.8, similar to pearson's coefficient. Table 3.3 also shows the agreement between both methods in each interval. It is very similar as the reliability coefficients, with decreasing values for $P_{\text{HF}}(n)$ near the peak of exercise.

3.3.4 HRV parameters

With a study similar to Chapter 2, parameters $\overline{P}^{\text{I}}_{\text{LF}}$, $\overline{P}^{\text{I}}_{\text{HF}}$ and $\overline{P}^{\text{I}}_{\text{CC}}$ are obtained in I_{B}, I_{60}, I_{80}, I_{100} and I_{R} from the Polar measurements. Figure 3.4 shows these HRV parameters obtained from both the ECG and Polar measurements. LF power is always

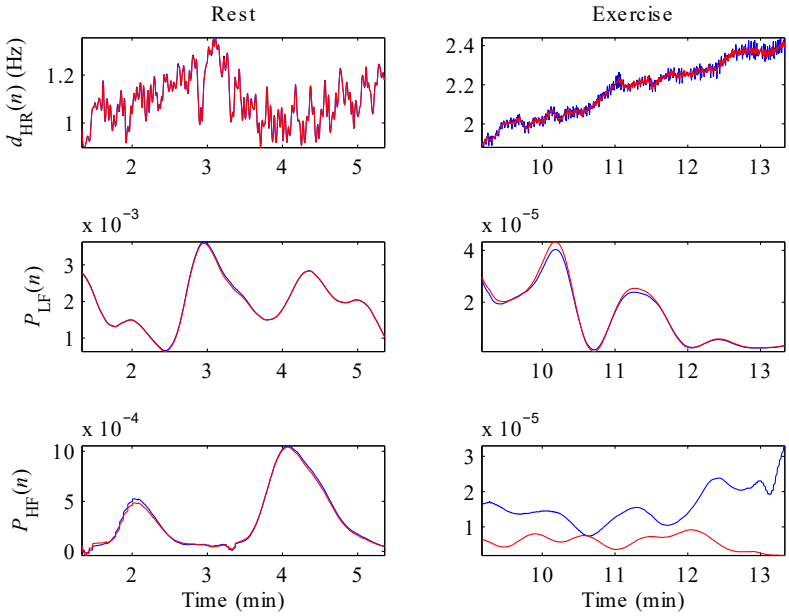

Figure 3.3: Example of $d_{\mathrm{HR}}(n)$, $P_{\mathrm{LF}}(n)$ and $P_{\mathrm{HF}}(n)$: rest phase (left) and exercise phase (right). Blue denotes signals derived from ECG and red denotes signals derived from Polar. Note that the axis have different scales.

	I_{B}	I_{60}	I_{80}	I_{100}	I_{R}
$d_{\mathrm{HRM}}(n)$	23 (0.58%)	23 (0.05%)	23 (0.06%)	23 (0.07%)	23 (0.05%)
$P_{\mathrm{LF}}(n)$	19 (3.82%)	23 (6.01%)	22 (5.49%)	22 (12.73%)	22 (9.89%)
$P_{\mathrm{HF}}(n)$	22 (9.26%)	17 (29.93%)	16 (63.91%)	12 (90.25%)	14 (70.44%)

Table 3.2: Number of subjects with a significant $\rho > 0.8$ and the relative error.

		I_{B}	I_{60}	I_{80}	I_{100}	I_{R}
RR	CCC	0.97 (0.96,0.98)	0.99 (0.99,1.00)	1.00 (1.00,1.00)	1.00 (1.00,1.00)	1.00 (1.00,1.00)
	ICC	0.99 (0.99,0.99)	0.99 (0.99,1.00)	1.00 (1.00,1.00)	1.00 (1.00,1.00)	1.00 (1.00,1.00)
	A	0.99 (0.98,0.99)	0.99 (0.99,0.99)	0.99 (0.99,0.99)	0.99 (0.99,0.99)	0.99 (0.99,0.99)
$d_{\mathrm{HRM}}(n)$	CCC	0.99 (0.99,0.99)	1.00 (1.00,1.00)	1.00 (1.00,1.00)	1.00 (1.00,1.00)	1.00 (1.00,1.00)
	ICC	0.99 (0.998,0.99)	1.00 (1.00,1.00)	1.00 (1.00,1.00)	1.00 (1.00,1.00)	1.00 (1.00,1.00)
	A	0.99 (0.98,0.99)	0.99 (0.99,0.99)	0.99 (0.99,0.99)	0.99 (0.99,0.99)	0.99 (0.99,0.99)
$P_{\mathrm{LF}}(n)$	CCC	0.96 (0.94,0.99)	0.99 (0.99,0.99)	0.99 (0.99,0.99)	0.99 (0.99,0.99)	0.99 (0.99,0.99)
	ICC	0.98 (0.96,0.99)	0.99 (0.99,0.99)	0.99 (0.99,0.99)	0.99 (0.99,0.99)	0.99 (0.99,0.99)
	CCC	0.92 (0.86,0.95)	0.95 (0.87,0.97)	0.95 (0.93,0.97)	0.92 (0.86,0.95)	0.94 (0.88,0.98)
$P_{\mathrm{HF}}(n)$	CCC	0.96 (0.95,0.98)	0.92 (0.87,0.98)	0.86 (0.75,0.96)	**0.33 (0.00,0.67)**	**0.41 (0.37,0.44)**
	ICC	0.98 (0.95,0.99)	0.96 (0.91,0.98)	0.92 (0.83,0.96)	**0.51 (0.18,0.79)**	**0.52 (0.46,0.60)**
	A	0.90 (0.85,0.94)	**0.71 (0.63,0.78)**	**0.56 (0.45,0.67)**	**0.56 (0.45,0.66)**	**0.68 (0.63,0.72)**

Table 3.3: Reliability (CCC, ICC) and agreement (A) coefficients for each interval. Values lower than 0.8 are bold.

higher in Polar measurements, while HF power is always lower with respect to the ECG measurements, but no significant differences were found between ECG and Polar measurements.

The trend of the HRV measurements is very similar to the previous Chapter. $\overline{P}^{\mathrm{I}}_{\mathrm{LF}}$ increases at the beginning of the exercise (although it is not significant in this test), then it decreases again when the exercise load gets more intense, and then it increases in the recovery phase. All pair of intervals, with the exception of the pairs I_{B} and I_{60}, and I_{80} and I_{R}, present significant differences. $\overline{P}^{\mathrm{I}}_{\mathrm{HF}}$ gets significantly reduced at I_{60}, then it increases and it decreases again in the recovery phase. I_{B} is significantly different to all intervals except I_{80} and I_{R}; I_{60} is significantly different to all intervals except I_{R}; and I_{100} is significantly different to all intervals. There is a significative increase from I_{60} to I_{80} in $\overline{P}^{\mathrm{I}}_{\mathrm{CC}}$, and a significative decrease from I_{100} to I_{R}. Hence, the same conclusions can be obtained when using the Polar measurements than with the

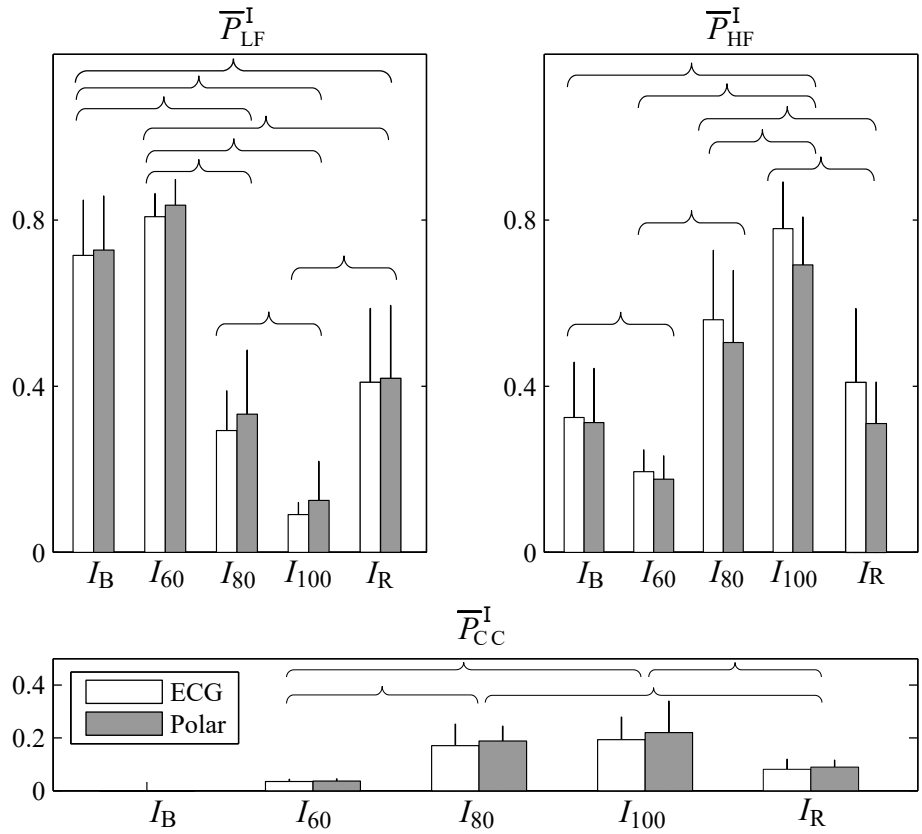

Figure 3.4: Median and MAD of $\overline{P}^{\mathrm{I}}_{\mathrm{LF}}$, $\overline{P}^{\mathrm{I}}_{\mathrm{HF}}$ and $\overline{P}^{\mathrm{I}}_{\mathrm{HF}}$ in intervals I_{R}, I_{60}, I_{80} and I_{100} for the ECG and Polar measurements. Brackets denote significant differences (p value < 0.005).

ECG ones.

3.4 Discussion

This study has corroborated the results from other studies, which support the validity of the HRV measurements derived from the RR intervals from the Polar at rest: [112] claims that a high correlation coefficient was observed in the HRV parameters, while [113] presents very similar results ($\rho > 0.99$). A recent study validated the Polar V800 at rest and showed that a strong correlation (ICC>0.999) and a narrower LOA could be achieved, when using an extra correction layer to identify errors in the Polar signal, and using the same software package for both the Polar and ECG signals [114]. From Figure 3.2, however, it can be observed that the shorter the RR is, the more differences there are between the RR series obtained from the Polar device and from the ECG. In other words, the measurements given by the Polar device are less

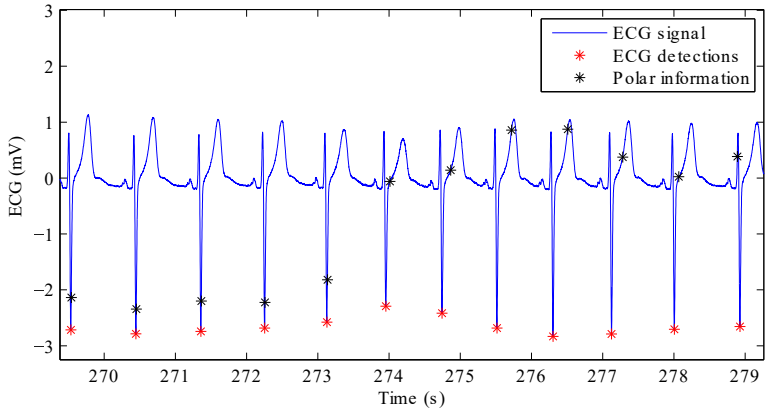

Figure 3.5: Example of ECG at rest with QRS detections (red marks) and Polar time occurrences (black marks).

accurate if the level of exercise is high, which is important if this heart rate monitor is intended to be used during intense exercise.

From Table 3.2 and Table 3.3, RR and mean HR show an excellent correlation, reliability and agreement during the whole exercise test between both measurements, which means that they can be used interchangeably. Higher loads of exercise, that is, an increase of the heart rate, do not decrease the performance of the Polar measurements.

$P_{\text{LF}}(n)$ also shows excellent correlation, reliability and agreement during the whole test, meaning that the Polar device can follow the heart rate oscillations up to 0.15 Hz as well as the ECG reference. Several studies have already demonstrated the validity of Polar measurements during the resting phase [112,113,119]. However, in this study only 19 out of 23 recordings present a correlated power in the LF band, see Table 3.2, which is unexpected. In the other 4 recordings, there are intervals where Polar detections do not match the ECG detections, possibly due to changes in QRS morphology, see Figure 3.5. This intervals, although they are short, introduce additional variation in the Polar RR-intervals which are not present in the ECG annotations, hence the lower linear correlation. Nevertheless, those were not sufficient to disrupt the excellent reliability and agreement found, as can be seen in Table 3.3. Regarding the exercise phase, these differences in the annotations do not appear.

The discrepancy in $P_{\text{HF}}(n)$ increases throughout the exercise phase. We observed that the Polar can follow the fast oscillations at the beginning of the exercise but usually underestimates the power, which can be seen in Figures 3.1 and 3.3. However, near the peak of exercise, the linear relation is much worse, with a higher error between both measurements: there are only 12 patients which present a significative high linear correlation ($\rho > 0.8$). At high exercise intensities, the Polar device cannot give a correct measurement about high frequency components of the HRV. Similar

conclusions can be extracted from Table 3.3 seeing the poor reliability and agreement coefficients during the last interval, with values lower than 0.8. Note that there is not a standard threshold for correlation, reliability and agreement [125]. Some works propose the cutoff value of 0.75 [126], others propose an interval of strong correlation was considered for (>0.75), of moderate correlation (between 0.75 and 0.5) and weak correlation for (>0.5) [112,127]. Our cutoff threshold is a bit more restrictive, but the main conclusions about HF power remains the same in the last intervals of exercise.

Besides the low values of reliability and agreement coefficients for HF power during high intensities of exercise, when calculating power parameters as the mean value in the intervals of interest, no significant differences were found in LF, HF and CC components regardless the intensity of exercise. Both Polar and ECG measurements showed an increase in normalized LF power in low intensities, a significant decrease in medium to high intensities of exercise and then a significant increase in the recovery phase; with an opposite behaviour in the case of normalized HF. CC components reached about 20% of the total power in the last exercise intervals and about 10% in the recovery phase. This suggests that the same conclusions regarding the ANS response to exercise can be derived analyzing HRV derived from RR series provided by Polar than from RR series obtained from the ECG.

In addition to the LF and HF components, another component in around 1 Hz was found when analyzing the HRV derived from the Polar device, see Figure 3.6. This component did not appear in the reference HRV from the ECG, and it was present only in 8 subjects during the exercise phase. It is still unclear neither the origin of this component, nor the reason why it only appears in some recordings, but it should be taken into account when analyzing the total power of HRV obtained from Polar.

3.5 Conclusion

A Polar RS800 device was validated in 23 healthy male volunteers during an exercise test. A high resolution ECG was simultaneously recorded to extract the RR intervals and use them as a reference. A time-frequency spectral analysis was performed to extract the mean HR and the power of LF and HF components, the latter centered on the respiratory frequency. A Bland Altman was used with the RR intervals derived from the ECG and the Polar device to graphically see the discrepancy between both measurements across the whole range. Reliability and agreement coefficients were also computed in different intervals related to the level of oxygen consumption for each subject. Both methods are interchangeable when measuring mean HR and LF power, regardless of the level of exercise (reliability and agreement > 0.9). Although the performance of the HF measurements from the Polar device decreases as the level of the exercise increases, with reliability and agreement coefficients around 0.5, the total power in the HF band in the analyzed interval was found to be not significantly different from the ECG measurement.

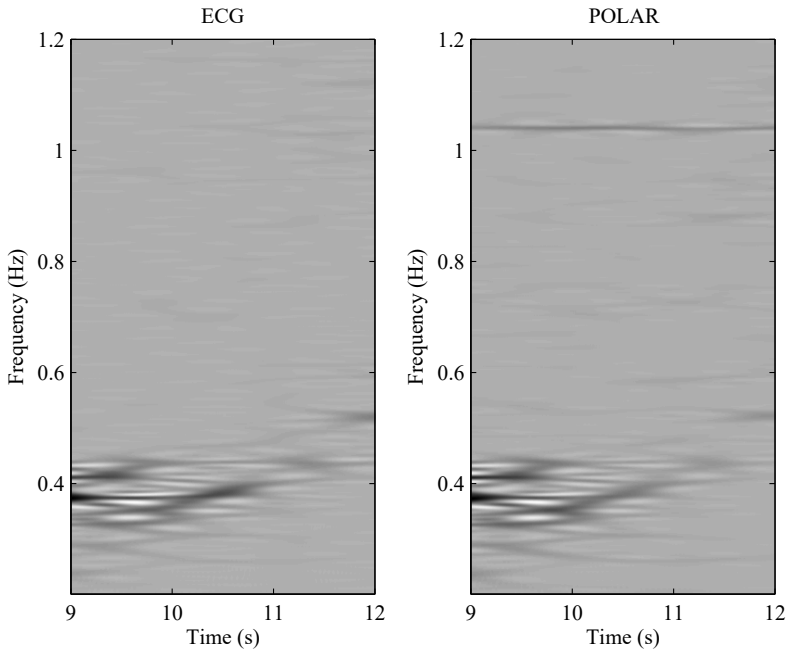

Figure 3.6: Example of the apparition of an unknown spectral component around 1 Hz when using Polar measurements.

Chapter 4

Coronary artery disease diagnosis by means of heart rate variability analysis using respiratory information

4.1 Motivation

According to the World Health Organization almost one-third of all deaths are caused by heart diseases. In 2013 the total cardiovascular diseases prevalence in America was 30.8% and in particular, coronary heart disease (CHD) was an underlying cause of death in approximately 1 of every 7 deaths in the United States [128]. The CHD is traditionally defined as various symptoms of which a large part is the result of coronary artery disease (CAD). CAD is defined as the narrowing of one or more coronary arteries, which leads to a decrease of the oxygen supply to the heart. This lack of oxygen supply to the myocardium (myocardial ischemia) may cause angina pectoris or even lead to myocardial infarction, which is defined as irreversible myocardial damage or death [129].

The narrowing of coronary arteries is affected by fat, cholesterol and other substances accumulating in walls of the arteries that are usually called stenosis in CAD. The stenosis is usually expressed as a percentage of the artery diameter or reduction in a cross sectional area of artery. Usually the cut-off limit in diagnosis of CAD is considered over 50% diameter stenosis or over 75% reduction in cross sectional area [130]. The calcification of coronary arteries is shown to begin in early stage of life but the progression of stenosis is affected by various factors, such as age, overweight, hypertension, excessive alcohol intake, smoking, diabetes, sedentary lifestyle, among others [131].

Traditional non-invasive techniques for CAD diagnosis are based on exercise ECG tests. During physical or mental stress, there is a higher metabolic demand, mainly oxygen, and as a response blood flow thorough arteries needs also to increase. If there is a significant anomaly in a coronary artery, this demand is not completely satisfied and a myocardial ischemia is produced induced by the stress. This is manifested as an alteration in the ECG signal.

Several studies have used HRV analysis during exercise, since impairment of autonomic cardiovascular regulation has been observed in ischemic CAD [132]. However, controversial results have been reported regarding HRV parameters during exercise, and the lack of a standard methodology for HRV analysis during exercise hinders a direct comparison of the results. In the study by Bailón et al. [9], HRV parameters during exercise showed accuracy values ranging from 76% to 95%, but the authors claimed that mean HR and respiratory frequency need to be taken into account. On the other hand, HRV parameters corrected by mean HR from exercise and recovery phase were reported by Virtanen et al. [133] to be inadequate for CAD detection.

The purpose of this study is to apply the methodologies described in Chapter 2, mainly the mean HR correction and inclusion of respiratory information as in [9], to an expanded version of the data set studied in [133] with the aim of determining the diagnostic performance of HRV analysis during exercise in the detection of CAD. This diagnosis performance will be evaluated with the area under the receiver operating characteristic curve method (AUC). Respiratory rate will be estimated from the ECG using an algorithm based on the QRS slopes, which has been validated in stress tests [39]. Then, HRV parameters will be extracted and their CAD diagnosis capability will be evaluated in different intervals of the exercise test.

4.2 Methods

4.2.1 Database and protocol

A subset of the FINCAVAS database [134] consisting of 457 ECG recordings was analyzed in this work. Patients underwent a maximal exercise test at Tampere University Hospital using a bicycle ergometer with electrical brakes. The initial workload varied from 20 W to 30 W, and the load was increased stepwise by 10-30 W each minute. The recovery phase after the exercise was at least five minutes. Continuous ECG was recorded at 500 Hz with CardioSoft exercise ECG system (Version 4.14, GE Health-

care, Freiburg, Germany) using the Mason-Likar modification of the standard 12-lead system. The study protocol was approved by the Ethical Committee of the Hospital District of Pirkanmaa, Finland, and all patients gave informed consent prior to the interview and measurements as stipulated in the Declaration of Helsinki.

Two groups were formed: a low likelihood of CAD (LLC) group and a CAD group. Patients for first group were chosen by detailed patient information and from symptoms from the exercise test: all patients who underwent angiography or if they reported chest pain during the exercise test were excluded from the LLC group. Patients in the CAD group underwent selective coronary angiography within 180 days of exercise testing, and they presented at least 50% luminal narrowing of the diameter of at least one major epicardial coronary artery or main branches.

Some of the patients in the CAD group were on cardiac medication (e.g., beta blockers, calcium channel blockers, diuretics...) and also several patients reported chest pain during the exercise test, leading to a shorter exercise phase.

4.2.2 Preprocessing

ECG waveforms were delineated by a multi-lead wavelet-based detector optimized to stress test recordings, as explained in Chapter 2. The beat time occurrences creates the RR series. Due to a high level of arrhythmic events in this database, several rules are imposed on the RR series as in [133]: beat intervals must be higher than 0.3 s and lower than 1.5 s, and the relative change between successive intervals must be lower than 20%. If the recording has more than 20% abnormal beats, according to the former criteria, the recording is removed from the study. In total, 48 recordings were discarded (11 from LLC and 37 from CAD). Table 4.1 shows the population characteristics for the remaining 409 recordings.

4.2.3 HRV and respiratory rate estimation

HRV series derivation is described in 2.3.3, obtaining the estimated modulating signal $m(n)$. Since in this database a simultaneous respiration signal is not available, respiratory rate is estimated from an algorithm which exploits the respiration-induced beat morphology variations on the QRS slopes of each one of the 12 Mason-Likar ECG leads. A spectral-based fusion technique is subsequently applied in order to get an estimation of the respiratory rate every 5 s, and then resampled at 4 Hz obtaining $f_{\mathrm{R}}(n)$. Further details are given in Lázaro et al. [39].

4.2.4 Physiological parameters and interval selection

Several intervals will be chosen to extract physiological parameters. For each interval, $\bar{d}^{\mathrm{I}}_{\mathrm{HRM}}$ and $\bar{f}^{\mathrm{I}}_{\mathrm{R}}$ are obtained as the mean value of $d_{\mathrm{HRM}}(n)$ and $f_{\mathrm{R}}(n)$, respectively, both measured in Hz. Subsequently, the power spectral density of $m(n)$, $S_m(n, f)$ is obtained based on SPWVD, as described in Chapter 2. Powers related to the two main

	LLC ($n = 214$)	CAD ($n = 195$)
Age (years) [a]	48 ± 9	62 ± 7 *
Gender (male/female)	124/90	149/46
BMI ($kg{\cdot}m^{-2}$) [a]	26 ± 3	27 ± 2 *
MI (patients)	0	57 *
Diabetes (patients)	12	34
Chest pain (patients)	0	67 *
Exercise length (min) [a]	7.4 ± 1.4	5.8 ± 1.2 *
ACE inhibitors	0	61
Beta blockers	0	169
Calcium channel blockers	0	38
Digitalis	0	2
Glyceryl trinitrate	0	86
Long-acting nitrate	0	90
Diuretics	0	34

Table 4.1: Population characteristics (BMI=body mass index, MI=myocardial infarction) and medication. [a] denotes median ± median absolute deviation (MAD) values, * denotes significant differences between groups (Mann-Whitney test, $p<0.005$).

components, $P_{\mathrm{LF}}(n)$ and $P_{\mathrm{HF}}(n)$ are obtained from $S_m(t, f)$. Classical LF band [0.04 Hz, 0.15 Hz] is used, while an alternative HF band centred at $f_{\mathrm{R}}(n)$ with a bandwidth of 0.15 Hz is used: [max(0.15 Hz, $f_{\mathrm{R}}(n)$ - 0.075 Hz), $f_{\mathrm{R}}(n)$ + 0.075 Hz]. Note that the chosen bandwidth is slightly wider than the previous chapters (0.15 instead of 0.125). LF component is normalized by the instantaneous total power defined as:

$$P_{\mathrm{TOT}}(n) = P_{\mathrm{LF}}(n) + P_{\mathrm{HF}}(n) \tag{4.1}$$

and thus the normalized power in LF band is defined as:

$$P_{\mathrm{LFn}}(n) = \frac{P_{\mathrm{LF}}(n)}{P_{\mathrm{TOT}}(n)} = \frac{P_{\mathrm{LF}}(n)}{P_{\mathrm{LF}}(n) + P_{\mathrm{HF}}(n)} \tag{4.2}$$

The ratio between LF and HF powers is also obtained as:

$$R(n) = \frac{P_{\mathrm{LF}}(n)}{P_{\mathrm{HF}}(n)} \tag{4.3}$$

An additional HF power is calculated, $P_{\mathrm{HFe}}(n)$, obtained within an extended band: from 0.15 Hz to half the mean HR. Extending the HF band to address the variations in respiratory frequency is an alternative used in several works [81, 135]. An example of a time-frequency map is shown in Figure 4.1, with the bands related to LF, HF and HFe, and half the mean HR.

A new instantaneous total power is defined as:

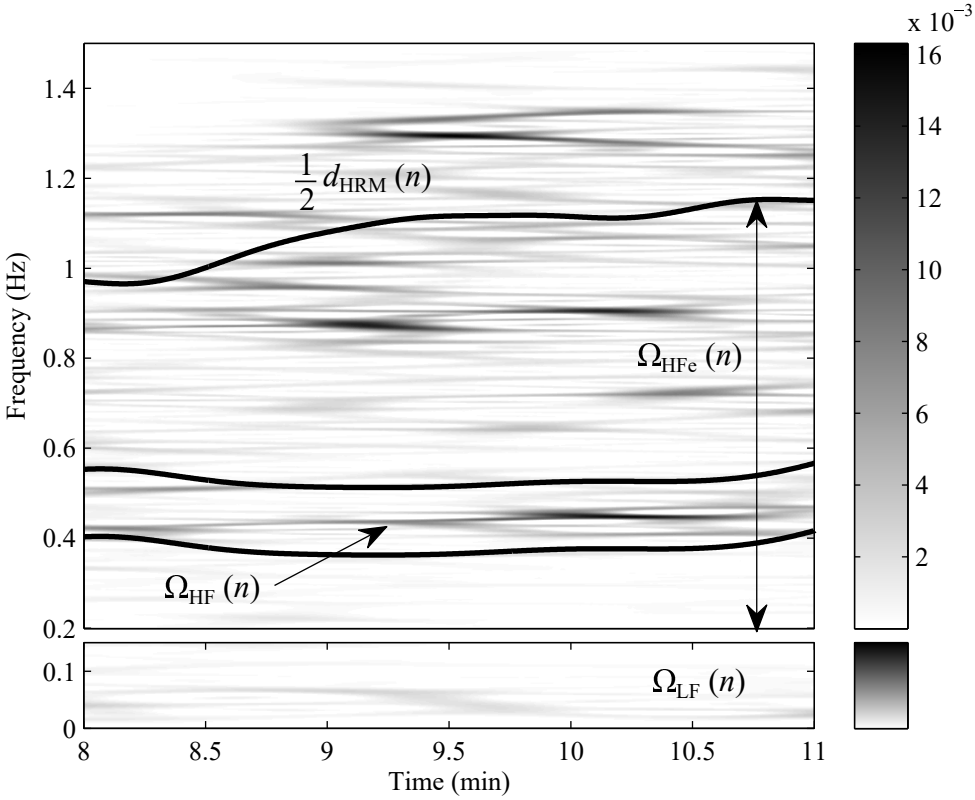

Figure 4.1: Example of a time-frequency map showing some of the spectral bands of HRV (LF, HF, and HFe) and half the mean HR ($d_{\mathrm{HRM}}(n)$) during the exercise phase.

$$P_{\mathrm{TOTe}}(n) = P_{\mathrm{LF}}(n) + P_{\mathrm{HFe}}(n) \tag{4.4}$$

To be able to compare results with those from previous chapters, the pedalling frequency is needed. Since we do not have information about this frequency and the location of its component and its alias, we will assume the following:

$$P_{\mathrm{TOTe}}(n) = P_{\mathrm{LF}}(n) + P_{\mathrm{HFe}}(n) \approx P_{\mathrm{LF}}(n) + P_{\mathrm{HF}}(n) + P_{\mathrm{CC}}(n) \tag{4.5}$$

where $P_{\mathrm{CC}}(n)$ represents the power related to cardiolocomotor coupling, including possible interfering alias. Therefore, three new normalized powers are defined as:

$$P_{\mathrm{LFne}}(n) = \frac{P_{\mathrm{LF}}(n)}{P_{\mathrm{TOTe}}(n)} \tag{4.6}$$

$$P_{\mathrm{HFne}}(n) = \frac{P_{\mathrm{HF}}(n)}{P_{\mathrm{TOTe}}(n)} \tag{4.7}$$

$$P_{\mathrm{CCne}}(n) = \frac{P_{\mathrm{HFe}}(n) - P_{\mathrm{HF}}(n)}{P_{\mathrm{TOTe}}(n)} \tag{4.8}$$

The following spectral parameters were extracted for each one of the intervals: $\overline{P}^{\mathrm{I}}_{\mathrm{LFn}}$, $\overline{P}^{\mathrm{I}}_{\mathrm{HF}}$, $\overline{R}^{\mathrm{I}}$, $\overline{P}^{\mathrm{I}}_{\mathrm{HFe}}$, $\overline{P}^{\mathrm{I}}_{\mathrm{LFne}}$, $\overline{P}^{\mathrm{I}}_{\mathrm{HFne}}$ and $\overline{P}^{\mathrm{I}}_{\mathrm{CCne}}$.

Study A: Exercise phase-dependant intervals

Following the study described in [133], four 2-min windows are selected for each patient: at the beginning of the recording (resting phase), 30 s after the exercise phase begins, just prior to the end of the exercise and 30 s after the exercise ends (recovery phase). Within these windows, a 1-min segment is searched with less than 5% abnormal beats. These segments, if found, are considered the intervals of analysis: I_{B}, I_{on}, I_{max} and I_{R}. Figure 4.2 (upper panel) shows an example of $d_{\mathrm{HRM}}(n)$ for one patient, and the windows where each interval is located. Vertical continuous lines indicates the beginning and the end of the exercise.

Study B: Heart rate-dependant intervals

In Chapter 2 and 3, intervals were chosen based on the oxygen consumption, with the aim that all subjects were in a similar metabolic demand state. Since that information is not available, heart rate will be used instead. Basal value of mean HR, d^{0}_{HRM}, is obtained as the mean value of $d_{\mathrm{HRM}}(n)$ during the resting phase, while the theoretical maximum HR, d^{100}_{HRM}, is obtained following the equation described in [136]:

$$d^{100}_{\mathrm{HRM}} = 211 - 0.64 x_{\mathrm{age}} \tag{4.9}$$

where x_{age} represents the age of the subject, and d^{100}_{HRM} is expressed in beats per minute in that equation. With these values, we obtained the percentage of increase in HR

for the intervals described in Study A. Since the most restrictive patients were those belonging to the CAD group (less duration of the exercise test, and thus lower mean HR achieved), the new intervals windows were calculated using only information from the CAD group. Taking mean values, I_{on} is equivalent to 0-30% of the mean HR range, while I_{max} is equivalent to 40-70%. Within these windows, a 1-min segment is searched with less than 5% abnormal beats. These segments, if found, are considered the intervals of analysis and denoted as I_{30} and I_{70}, respectively. I_{B} and I_{R} stay the same than in Study A. Figure 4.2 (lower panel) shows an example with the new intervals for a subject with an age of 61 years old ($d^{100}_{\mathrm{HRM}} = 2.86$ Hz).

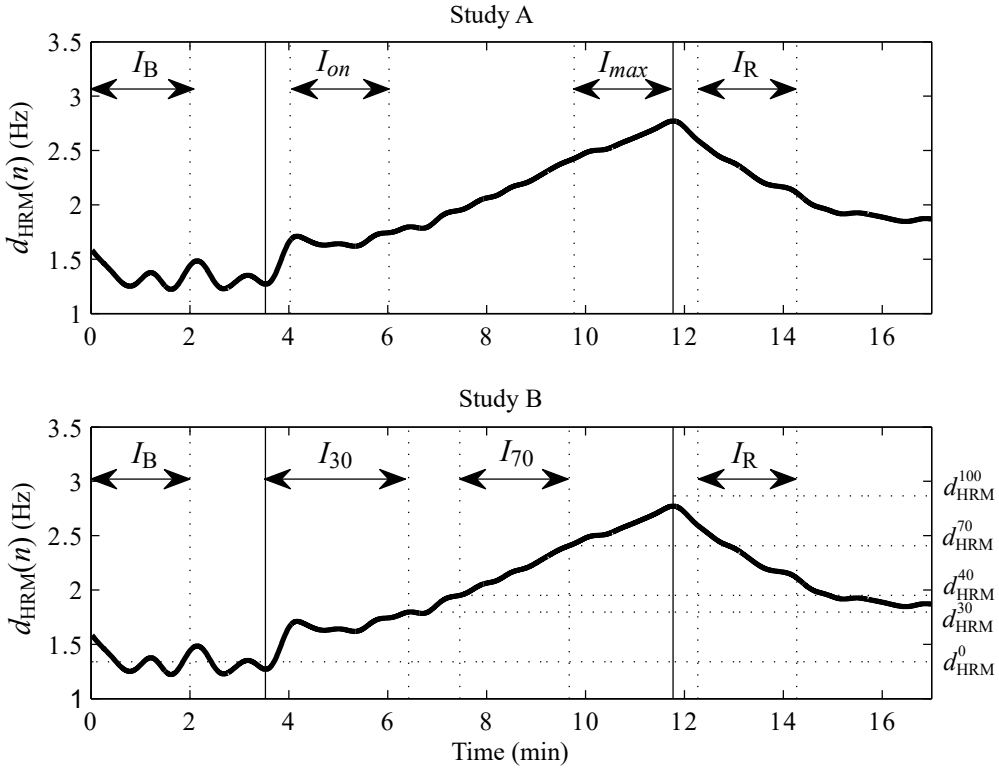

Figure 4.2: Example of $d_{\mathrm{HRM}}(n)$ for one patient. Vertical lines delimite the exercise phase, while dashed lines show the windows where the different intervals are located: exercise phase-dependant (upper panel) or heart rate-dependant (lower panel).

4.2.5 Statistical analysis

Assumption of normal distribution was rejected using a Kolmogorov-Smirnov test in all parameters. The Mann-Whitney test was used to test equality of population medians ($p<0.005$) among LLC and CAD groups. A Wilcoxon signed-rank test between $\overline{P}^{\mathrm{I}}_{\mathrm{HF}}$ and $\overline{P}^{\mathrm{I}}_{\mathrm{HFe}}$ measurements was also performed to compare these parameters ($p<0.005$).

Additionally, the area under the receiver operating characteristic curve (AUC) was obtained for each studied parameter.

4.3 Results

Study A

Statistical analysis between LLC and CAD group is shown in Table 4.2. $\bar{d}^{\mathrm{I}}_{\mathrm{HRM}}$ and $\overline{P}^{\mathrm{I}}_{\mathrm{HF}}$ are significantly different in all intervals, with $\bar{d}^{\mathrm{I}}_{\mathrm{HRM}}$ being always higher in LLC group, and $\overline{P}^{\mathrm{I}}_{\mathrm{HF}}$ being higher in LLC group in I_{B} and I_{on}, while higher in CAD group in I_{max} and I_{R}. $\overline{P}^{\mathrm{I}}_{\mathrm{HFe}}$ behaves similarly than $\overline{P}^{\mathrm{I}}_{\mathrm{HF}}$ throughout the test, but the differences between both groups are lost in I_{max}. Overall, $\overline{P}^{\mathrm{I}}_{\mathrm{HFe}}$ values are always higher than $\overline{P}^{\mathrm{I}}_{\mathrm{HF}}$ ones, and a paired Wilcoxon analysis between both HF parameters reveals that they are significantly different in I_{max} and I_{R}. Both $\overline{P}^{\mathrm{I}}_{\mathrm{LFn}}$ and $\overline{R}^{\mathrm{I}}$ are very similar, with significantly higher values for LCC group during I_{B} and I_{on}. $\bar{f}^{\mathrm{I}}_{\mathrm{R}}$ values are significantly higher in the LCC groups during I_{max} and I_{R}, but they do not differ during I_{B} and I_{on}.

		I_{B}	I_{on}	I_{max}	I_{R}
$\bar{d}^{\mathrm{I}}_{\mathrm{HRM}}$	LLC	1.35 ± 0.17	1.65 ± 0.19	2.72 ± 0.16	2.16 ± 0.21
	CAD	1.10 ± 0.12 *	1.35 ± 0.11 *	1.94 ± 0.25 *	1.48 ± 0.18 *
$\overline{P}^{\mathrm{I}}_{\mathrm{LFn}}$	LLC	0.80 ± 0.08	0.79 ± 0.12	0.16 ± 0.12	0.82 ± 0.08
	CAD	0.71 ± 0.13 *	0.70 ± 0.16 *	0.22 ± 0.14	0.76 ± 0.12
$\overline{P}^{\mathrm{I}}_{\mathrm{HF}\ (\times 10^{-5})}$	LLC	30.3 ± 18.9	7.1 ± 5.02	1.23 ± 0.8	2.56 ± 1.9
	CAD	12.5 ± 7.6 *	4.0 ± 2.6 *	2.49 ± 1.1 *	7.6 ± 5.6 *
$\overline{R}^{\mathrm{I}}$	LLC	4.23 ± 2.0	3.96 ± 2.7	0.21 ± 0.1	4.57 ± 2.9
	CAD	2.43 ± 1.3 *	2.34 ± 1.5 *	0.28 ± 0.1	3.11 ± 2.1
$\overline{P}^{\mathrm{I}}_{\mathrm{HFe}\ (\times 10^{-5})}$	LLC	38.3 ± 23.2	15.8 ± 10.4	6.6 ± 3.6	9.5 ± 5.8
	CAD	16.3 ± 9.3 *	8.7 ± 4.6 *	7.7 ± 4.6	20.0 ± 12.5 *
$\bar{f}^{\mathrm{I}}_{\mathrm{R}}$	LLC	0.20 ± 0.04	0.28 ± 0.04	0.53 ± 0.06	0.42 ± 0.05
	CAD	0.20 ± 0.05	0.27 ± 0.03	0.46 ± 0.06 *	0.38 ± 0.04 *
$\overline{P}^{\mathrm{I}}_{\mathrm{LFne}}$	LLC	0.79 ± 0.09	0.67 ± 0.14	0.04 ± 0.02	0.57 ± 0.14
	CAD	0.69 ± 0.12 *	0.52 ± 0.19 *	0.10 ± 0.06 *	0.54 ± 0.16
$\overline{P}^{\mathrm{I}}_{\mathrm{HFne}}$	LLC	0.19 ± 0.07	0.15 ± 0.09	0.27 ± 0.08	0.12 ± 0.05
	CAD	0.27 ± 0.10 *	0.19 ± 0.10 *	0.37 ± 0.10 *	0.17 ± 0.07 *
$\overline{P}^{\mathrm{I}}_{\mathrm{CCne}}$	LLC	0.01 ± 0.00	0.16 ± 0.08	0.64 ± 0.09	0.31 ± 0.11
	CAD	0.03 ± 0.01	0.22 ± 0.11	0.44 ± 0.15 *	0.24 ± 0.09

Table 4.2: Median ± median absolute deviation (MAD) values and results for the statistical analysis between LLC and CAD groups. * indicates significant differences ($p<0.005$).

When comparing $\overline{P}^{\mathrm{I}}_{\mathrm{LFn}}$ and $\overline{P}^{\mathrm{I}}_{\mathrm{LFne}}$, $\overline{P}^{\mathrm{I}}_{\mathrm{LFne}}$ is still significantly higher in the LLC group in I_{B} and I_{on} but now it is significantly lower in I_{max}. $\overline{P}^{\mathrm{I}}_{\mathrm{HFne}}$ presents significant

differences in all intervals, being always higher in the CAD group. $\overline{P}^{\mathrm{I}}_{\mathrm{CCne}}$ is only significantly different in I_{max}, being lower in the CAD group.

There are 46 diabetic patients in the database, 12 from the LLC grpup and 34 from the CAD group. If these patients are removed, no differences are found in the significant differences shown in Table 4.2. Table 4.3 shows HRV parameters for only these 46 diabetic patients. Most of the significant differences between groups are lost when comparing only diabetic patients.

		I_{B}	I_{on}	I_{max}	I_{R}
$\bar{d}^{\mathrm{I}}_{\mathrm{HRM}}$	LLC	1.32 ± 0.09	1.51 ± 0.15	2.57 ± 0.32	2.07 ± 0.24
	CAD	1.15 ± 0.15	1.37 ± 0.13	1.89 ± 0.24 *	1.49 ± 0.12 *
$\overline{P}^{\mathrm{I}}_{\mathrm{LFn}}$	LLC	0.73 ± 0.06	0.69 ± 0.14	0.03 ± 0.02	0.53 ± 0.12
	CAD	0.63 ± 0.13	0.44 ± 0.23	0.08 ± 0.04	0.46 ± 0.12
$\overline{P}^{\mathrm{I}}_{\mathrm{HF\ (x10^{-5})}}$	LLC	37.1 ± 17.1	7.25 ± 4.2	1.37 ± 1.2	3.47 ± 2.5
	CAD	9.32 ± 5.7 *	3.21 ± 1.7	2.27 ± 1.1	8.29 ± 4.7
$\overline{R}^{\mathrm{I}}$	LLC	3.58 ± 1.4	3.99 ± 2.2	0.24 ± 0.2	4.11 ± 2.4
	CAD	2.32 ± 1.3	1.89 ± 1.0	0.23 ± 0.1	2.09 ± 1.0
$\overline{P}^{\mathrm{I}}_{\mathrm{HFe\ (x10^{-5})}}$	LLC	41.1 ± 17.4	15.4 ± 8.2	5.6 ± 2.4	13.0 ± 8.3
	CAD	11.9 ± 6.8 *	7.7 ± 3.2	9.2 ± 5.1	20.4 ± 11.4
$\bar{f}^{\mathrm{I}}_{\mathrm{R}}$	LLC	0.21 ± 0.06	0.27 ± 0.06	0.52 ± 0.04	0.41 ± 0.03
	CAD	0.19 ± 0.04	0.28 ± 0.03	0.49 ± 0.06	0.38 ± 0.04
$\overline{P}^{\mathrm{I}}_{\mathrm{LFne}}$	LLC	0.73 ± 0.06	0.69 ± 0.14	0.04 ± 0.02	0.53 ± 0.12
	CAD	0.64 ± 0.13	0.44 ± 0.23	0.08 ± 0.04	0.46 ± 0.12
$\overline{P}^{\mathrm{I}}_{\mathrm{HFne}}$	LLC	0.21 ± 0.08	0.16 ± 0.06	0.28 ± 0.15	0.13 ± 0.06
	CAD	0.26 ± 0.10	0.19 ± 0.08	0.27 ± 0.12	0.22 ± 0.11
$\overline{P}^{\mathrm{I}}_{\mathrm{CCne}}$	LLC	0.02 ± 0.01	0.17 ± 0.06	0.63 ± 0.18	0.25 ± 0.09
	CAD	0.03 ± 0.01	0.27 ± 0.18	0.60 ± 0.12	0.25 ± 0.12

Table 4.3: Median ± median absolute deviation (MAD) values and results for the statistical analysis between diabetic patients from LLC and CAD groups. * indicates significant differences ($p<0.005$).

Figure 4.3 shows the AUCs for each parameter in each interval. $\overline{R}^{\mathrm{I}}$ is not represented due to the similarities to $\overline{P}^{\mathrm{I}}_{\mathrm{LFn}}$. $\bar{d}^{\mathrm{I}}_{\mathrm{HRM}}$ is the parameter with a higher value of AUCs during all the recording. Figure 4.4 shows the evolution of $\overline{P}^{\mathrm{I}}_{\mathrm{LFne}}$, $\overline{P}^{\mathrm{I}}_{\mathrm{HFne}}$ and $\overline{P}^{\mathrm{I}}_{\mathrm{CCne}}$ in each interval.

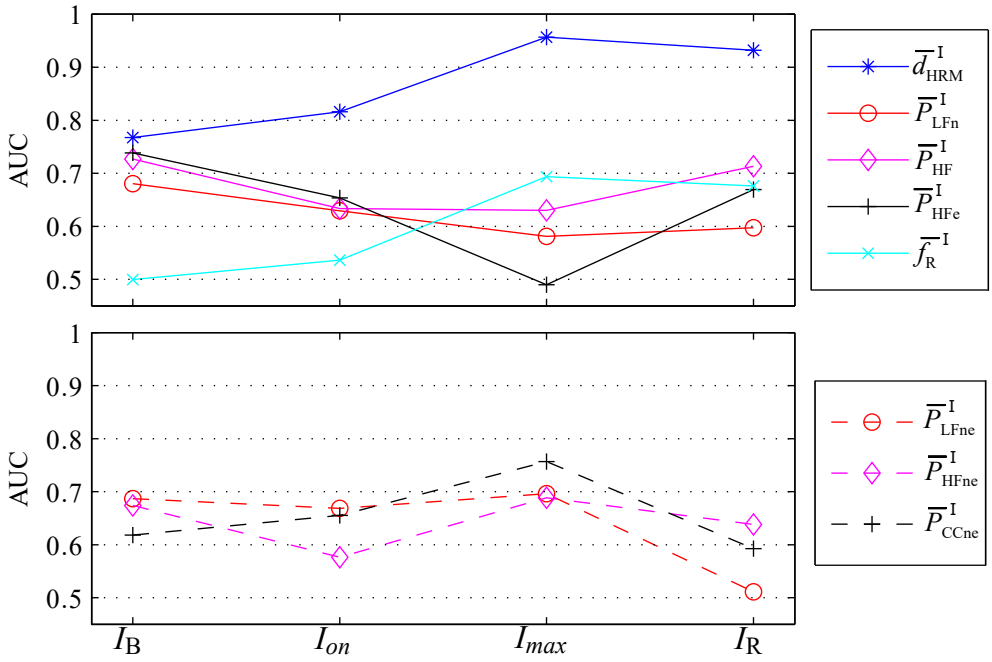

Figure 4.3: AUCs for each parameter in intervals I_{B}, I_{on}, I_{max} and I_{R}.

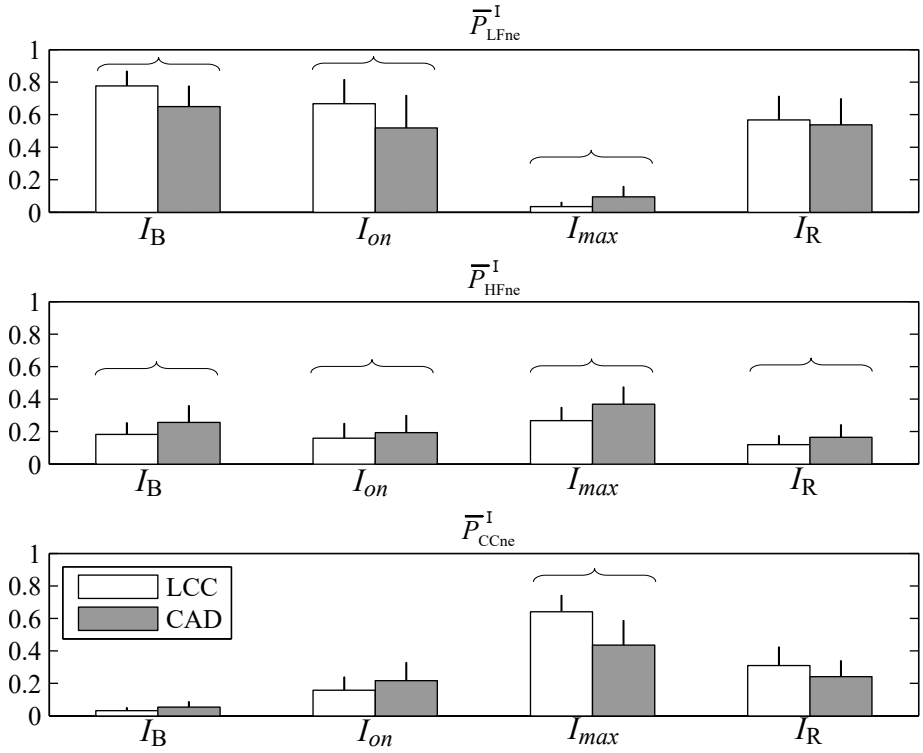

Figure 4.4: Median and MAD for $P^{\mathrm{I}}_{\mathrm{LFne}}$ (upper panel), $P^{\mathrm{I}}_{\mathrm{HFne}}$ (middle panel) and $P^{\mathrm{I}}_{\mathrm{CCne}}$ (lower panel) in intervals I_{B}, I_{on}, I_{max} and I_{R} for LLC and CAD groups. Brackets denote significant differences (p value < 0.005).

Study B

Statistical analysis between LLC and CAD group is shown in Table 4.4. Most significant differences remain the same, with I_{30} losing the differences for $\overline{P}^{\mathrm{I}}_{\mathrm{LFn}}$ and $\overline{P}^{\mathrm{I}}_{\mathrm{HFne}}$, and I_{70} being now significantly different in all parameters. Figure 4.5 shows the evolution of $\overline{P}^{\mathrm{I}}_{\mathrm{LFne}}$, $\overline{P}^{\mathrm{I}}_{\mathrm{HFne}}$ and $\overline{P}^{\mathrm{I}}_{\mathrm{CCne}}$ in the new intervals.

		I_{B}	I_{30}	I_{70}	I_{R}
$\bar{d}^{\mathrm{I}}_{\mathrm{HRM}}$	LLC	1.35 ± 0.17	1.47 ± 0.16	2.24 ± 0.16	2.16 ± 0.21
	CAD	1.10 ± 0.12 *	1.32 ± 0.12 *	1.94 ± 0.19 *	1.48 ± 0.18 *
$\overline{P}^{\mathrm{I}}_{\mathrm{LFn}}$	LLC	0.80 ± 0.08	0.70 ± 0.12	0.61 ± 0.13	0.82 ± 0.08
	CAD	0.71 ± 0.13 *	0.61 ± 0.11	0.19 ± 0.09 *	0.76 ± 0.12
$\overline{P}^{\mathrm{I}}_{\mathrm{HF\ (x10^{-5})}}$	LLC	30.3 ± 18.9	14.1 ± 8.3	1.1 ± 0.6	2.56 ± 1.9
	CAD	12.5 ± 7.6 *	7.7 ± 4.6 *	2.44 ± 1.4 *	7.6 ± 5.6 *
$\overline{R}^{\mathrm{I}}$	LLC	4.23 ± 2.0	3.21 ± 1.4	1.74 ± 1.1	4.57 ± 2.9
	CAD	2.43 ± 1.3 *	1.98 ± 0.6 *	0.38 ± 0.2 *	3.11 ± 2.1
$\overline{P}^{\mathrm{I}}_{\mathrm{HFe\ (x10^{-5})}}$	LLC	38.3 ± 23.2	19.9 ± 10.8	3.4 ± 1.2	9.5 ± 5.8
	CAD	16.3 ± 9.3 *	8.8 ± 4.6 *	5.4 ± 2.0 *	20.0 ± 12.5 *
$\bar{f}^{\mathrm{I}}_{\mathrm{R}}$	LLC	0.20 ± 0.04	0.23 ± 0.04	0.38 ± 0.05	0.42 ± 0.05
	CAD	0.20 ± 0.05	0.22 ± 0.05	0.43 ± 0.04 *	0.38 ± 0.04 *
$\overline{P}^{\mathrm{I}}_{\mathrm{LFne}}$	LLC	0.79 ± 0.09	0.69 ± 0.10	0.47 ± 0.16	0.57 ± 0.14
	CAD	0.69 ± 0.12 *	0.59 ± 0.15 *	0.18 ± 0.09 *	0.54 ± 0.16
$\overline{P}^{\mathrm{I}}_{\mathrm{HFne}}$	LLC	0.19 ± 0.07	0.21 ± 0.11	0.25 ± 0.11	0.12 ± 0.05
	CAD	0.27 ± 0.10 *	0.25 ± 0.12	0.42 ± 0.17 *	0.17 ± 0.07 *
$\overline{P}^{\mathrm{I}}_{\mathrm{CCne}}$	LLC	0.01 ± 0.00	0.05 ± 0.01	0.26 ± 0.09	0.31 ± 0.11
	CAD	0.03 ± 0.01	0.1 ± 0.12	0.39 ± 0.12 *	0.24 ± 0.09

Table 4.4: Median ± median absolute deviation (MAD) values and results for the statistical analysis between LLC and CAD groups. * indicates significant differences ($p<0.005$).

4.4 Discussion

CAD diagnosis using HRV parameters

In Study A, parameter $\bar{d}^{\mathrm{I}}_{\mathrm{HRM}}$ shows values significantly higher in the LLC group than in the CAD group, even in the resting phase. This is probably due to the fact that in the latter group, 80% of the patients took beta blocker medication. Moreover, patients in CAD group were likely affected by diminished physical capacity due to myocardial ischemia. With significantly shorter exercise sessions (5.8 min vs 7.4 min), $\bar{d}^{\mathrm{I}}_{\mathrm{HRM}}$ is expected to be lower in the CAD group. Similar conclusions can be extracted with the AUC values during I_{max}. $\bar{f}^{\mathrm{I}}_{\mathrm{R}}$ does not present significant differences between groups at rest and at the beginning of the exercise, and while it is higher in the LLC groups

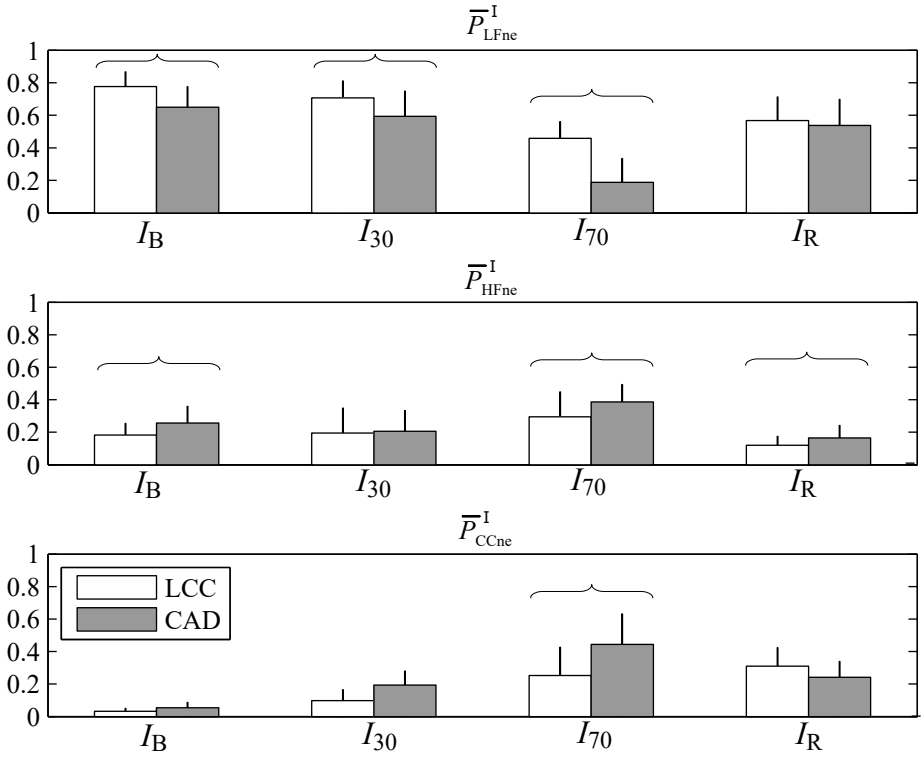

Figure 4.5: Median and MAD for $P^{\mathrm{I}}_{\mathrm{LFne}}$ (upper panel), $P^{\mathrm{I}}_{\mathrm{HFne}}$ (middle panel) and $P^{\mathrm{I}}_{\mathrm{CCne}}$ (lower panel) in intervals I_{B}, I_{30}, I_{70} and I_{R} for LLC and CAD groups. Brackets denote significant differences (p value < 0.005).

in I_{max} and I_{R}, it is again probably due to the longer duration of the exercise test, and therefore, the higher intensities reached by the LLC group.

By correcting HRV by the mean HR, we try to minimize the effect of the beta blocker medication. The fact that there is a change of trend in $\overline{P}^{\mathrm{I}}_{\mathrm{HF}}$ during exercise seems to support our hypothesis that it is reflecting differential changes in ANS response to exercise in LCC and CAD patients rather than the effect of medication. However, RSA is expected to decrease with increasing respiratory frequency [137], and patients from the LCC group have a longer exercise duration, i.e., higher $\bar{f}^{\mathrm{I}}_{\mathrm{R}}$ achieved.

When analyzing HRV during exercise, there is a need to redefine HF band since respiratory rate usually increases above 0.4 Hz. Two different bands have been presented: extended up to half the mean HR and centered at respiratory frequency. The differences between $\overline{P}^{\mathrm{I}}_{\mathrm{HF}}$ and $\overline{P}^{\mathrm{I}}_{\mathrm{HFe}}$ are more evident near the peak of exercise. By extending the frequency band to measure the HF component, there is a risk to measure other undesirable spectral components which can mislead the measures, as we have seen in previous chapters regarding the cardiolocomotor coupling. Results in Table 4.2 show that $\overline{P}^{\mathrm{I}}_{\mathrm{HFe}}$ is always higher than $\overline{P}^{\mathrm{I}}_{\mathrm{HF}}$, and while $\overline{P}^{\mathrm{I}}_{\mathrm{HF}}$ is significantly higher in the CAD group in I_{max}, this difference between both groups is lost. Moreover, $\overline{P}^{\mathrm{I}}_{\mathrm{HFe}}$ greatly increases in I_{max}, and it is reasonable to think that it is measuring the cardiolocomotor coupling, whose origin is purely mechanical. In Figure 4.1, there is a clear example that around 0.9 Hz there is an undesirable spectral component (possibly an alias of the pedalling cadence, which seems to be around 1.3 Hz) which will be reflected by $\overline{P}^{\mathrm{I}}_{\mathrm{HFe}}$ but not by $\overline{P}^{\mathrm{I}}_{\mathrm{HF}}$.

Parameters $\overline{P}^{\mathrm{I}}_{\mathrm{LFn}}$ and $\overline{R}^{\mathrm{I}}$ present very similar trends and AUCs values. While they are not able to separate LLC and CAD groups in some of the intervals, $\overline{P}^{\mathrm{I}}_{\mathrm{HF}}$ when measured guided by respiratory rate was significantly different in all intervals. Looking at the AUCs, $\overline{P}^{\mathrm{I}}_{\mathrm{HF}}$ values are higher, and even at rest it reaches an AUC above 0.7. Note that differences in age between the groups may have influenced the results. Some studies also claim that parameters like myocardial infarction or diabetes could influence to the decreased HRV in the CAD group [138, 139]. We repeated the analysis removing the 57 patients with MI and 46 diabetic patients, but no significant differences were found with respect to using all patients. However, they are very few patients, only representing 14% and 11% of the whole database, respectively. We decided to analyze only diabetic patients, from both CAD and LLC groups, and most significant differences are lost, which suggests that diabetic patients present an altered ANS activity regardless of the CAD status.

In the study by Bailón et al. [9], HRV parameters during exercise showed accuracy values ranging from 76% to 95%. We have evaluated the diagnosis capability of HRV parameters in terms of the AUC. While the two statistics measurements are likely to be correlated, they are not directly comparable since they measure different qualities of the classifier. As an example, if one classifier ranks patterns well, but selects the threshold badly, it can have a high AUC but a poor overall accuracy. Moreover, their study designed a multivariate classifier which integrated different parameters at the same time. But both their study and ours agree that when HRV parameters are

corrected by mean HR and respiratory information in included in HRV analysis, HRV parameters are able to separate LLC and CAD groups. The study by by Virtanen et al. [133], on the other hand, show that the uncorrected HRV parameters showed the best diagnostic performance in the recovery phase and that the mean HR correction decreased the correlation and the diagnostic performance. As we have seen, the mean HR alone present a high diagnostic performance due to the medication and due to the fact that the LLC group last longer in the exercise test and therefore reach higher HR. They also claim that the HRV parameters calculated from 1 min segments of exercise test ECG were not as capable as traditional ST-segment analysis. Again, the results are not comparable since they used temporal parameters instead of frequency parameters.

In Study B, we have tried to compare groups in intervals with a similar level of metabolic demand during exercise. With this purpose, two interval windows were defined: from 0 to 30% and from 40 to 70% of the range between the basal mean heart rate (obtained in the resting phase) and the theoretical d^{100}_{HRM}. Different methods have been proposed to estimate this maximum value of mean HR based on age, which deviates from the standard formula of d^{100}_{HRM} = 200 - x_{age} (beats per minute). A study by Tanaka in 2001 [140] showed that this formula often underestimated d^{100}_{HRM} in older subjects and a revised formula fitted to the data resulted in d^{100}_{HRM} = 208 - 0.7x_{age}. Another look at this by Gellish in 2007 [141] showed good correlation to stress testing results using d^{100}_{HRM} = 207 - 0.7x_{age} with a p value of <0.001. A study by Nes in 2012 [136] proposed d^{100}_{HRM} = 211 - 0.64x_{age} while finding no evidence of interaction with gender, physical activity, oxygen consumption, or BMI variables. Ultimately, the choice of any of the three different proposals did not show differences in the results.

With the new interval windows, which contained a range of 30% of the range in mean HR, 1-min length intervals are defined, I_{30} and I_{70}. We obtained the % of the range in mean HR for each interval and verified that no significative differences were found between both groups. Comparing to the intervals from Study A, the new intervals were very similar to I_{on} and I_{max} for patients belonging to the CAD group, which was expected. In the case of the LLC group, I_{70} and I_{max} were very different, with I_{70} being found near the middle stage of the exercise and I_{max} being located at the very end of the exercise by definition.

In I_{70}, LLC patients still have significantly higher $\bar{d}^{\text{I}}_{\text{HRM}}$ due to the significantly lower age in this group, and therefore, a higher d^{100}_{HRM}. $\overline{P}^{\text{I}}_{\text{LFn}}$ was found to be significantly higher in LLC group in I_{70}, which is expected in healthy subjects in the middle stage of exercise, while for CAD patients it was lower and more similar to the expected value at the final stage of exercise. Interestingly, now $\bar{f}^{\text{I}}_{\text{R}}$ is higher in I_{70} for the CAD group, which may suggest a lower RSA and thus a lower HF power, but $\overline{P}^{\text{I}}_{\text{HF}}$ is still higher than in LLC group. This corroborates that the measured power reflects the mechanical effect of breathing, which seems to be higher in the CAD group. In addition, differences in HRV parameters in I_{70} suggest that these parameters can help in diagnosing CAD before finishing the exercise test.

HRV parameters: comparison to athletes

This work presents one major difference compared to Chapter 2: the lack of a recorded pedalling frequency. Therefore, we cannot identify the alias of that component which appear in the HRV spectrum and correct them if they overlap with the HF component. To be able to compare HRV parameters between both studies, we have assumed that the extended band would cover those components. While $\overline{P}^{\mathrm{I}}_{\mathrm{CCne}}$ reached up to 30% of the total power (less than 15% in the cycle ergometer test) in Chapter 2, here it reaches 60% of total power possibly because it has a larger spectral band and it can be measuring more noise or possible harmonics of respiration. Another methodological difference from Chapter 2 is the election of the spectral band to compute $\overline{P}^{\mathrm{I}}_{\mathrm{HFn}}$, with a wider band for CAD patients to take into account wider spectra due to a more irregular breathing during exercise.

Regarding the Study A, expected changes in $\overline{P}^{\mathrm{I}}_{\mathrm{LFne}}$ and $\overline{P}^{\mathrm{I}}_{\mathrm{HFne}}$ from I_{B} to I_{on}, an increase and a decrease respectively, are not reflected in Figure 4.4. However, as commented before, there is an unexpected increase in $\overline{P}^{\mathrm{I}}_{\mathrm{CCne}}$ in I_{on} which could mislead the interpretation of the LF and HF components. In I_{max}, just prior to the peak of exercise, there is a significant decrease in $\overline{P}^{\mathrm{I}}_{\mathrm{LFne}}$ and a significant increase in $\overline{P}^{\mathrm{I}}_{\mathrm{HFne}}$, as expected. Moreover, from I_{B} to I_{max}, both LF and HF powers are significantly different from both groups. In I_{R}, $\overline{P}^{\mathrm{I}}_{\mathrm{LFne}}$ and $\overline{P}^{\mathrm{I}}_{\mathrm{HFne}}$ return to similar values than I_{B} and I_{on}, but $\overline{P}^{\mathrm{I}}_{\mathrm{CCne}}$ remains still with a high value (about 30% of the total power).

The main difference in Study B from Study A is the interval I_{70} for the LLC group. In particular, there is an increase in $\overline{P}^{\mathrm{I}}_{\mathrm{LFne}}$ and a decrease in $\overline{P}^{\mathrm{I}}_{\mathrm{CCne}}$ with respect to Study A. These changes are expected since now we are measuring in the middle stage of the exercise rather than just prior the peak of exercise. $\overline{P}^{\mathrm{I}}_{\mathrm{LFne}}$ remains very similar, however.

It is indeed difficult to compare results from different studies when the differences in methodology do not allow the same interpretations. In particular, it is dangerous to use an extended band to take measurements in the HRV spectrum during exercise due to the presence of unknown components. The lack of a pedalling frequency, however, could be addressed by estimating it using information of the baseline of the ECG or the angles series produced by the movement of the electric axe of the heart during exercise.

Limitations of the study

We have already discussed that the lack of recorded pedalling frequency hinders the analysis of HF power. Information about oxygen consumption also would help to establish the intervals to analyze HRV parameters as seen in Chapter 2. Still, the main limiations are the differences in age between both groups and the fact that most of CAD patients were taking medications which may alter ANS.

4.5 Conclusion

The CAD diagnosis capability of some HRV parameters has been studied. Respiratory rate has been estimated from the ECG and it has been included in the analysis to correctly measure the HF component. Parameters have been corrected to remove the effect of changes in mean HR in HRV. Due to the effect of medications and differences in exercise duration in this database, mean HR cannot be reliably used to diagnose CAD. HF power, when guided by respiration, achieves the highest AUC, above 0.7 both in rest and in recovery. However, if respiratory information is not used in the HRV analysis and an extended band is used instead to obtain the HF parameter, those measurements will also reflect other undesirable components which may mislead the interpretation of HRV parameters. Measuring HRV parameters at 40-70% of the range between basal and theoretical maximum value of mean HR shows significant differences in all spectral parameters, with lower normalized LF power and higher HF power (both normalized and absolute power) in CAD patients, suggesting that HRV parameters can help in diagnosing CAD before finishing the exercise test.

Chapter 5

Identification of hypotension prone patients during hemodialysis based on the analysis of heart rate variability, blood pressure variability and baroreflex sensitivity

5.1 Introduction

Blood is in charge of substances distribution, such as nutrients and oxygen, to all the cells in the body, and the removal of waste products and fluids. For this reason, it is essential for the blood to remain clean and maintain the correct balance and levels of the substances which circulate through it. This balance is controlled by the kidneys, which are in charge of the regulation of fluid and electrolyte balance in order to maintain the intra- and extracellular fluid volumes and ion compositions. If the kidneys do not work properly, fluid is retained and several ions and solutes accumulate [142]. This substances unbalance becomes life threatening. The solution for renal failure is a kidney transplantation, though finding a suitable donor is not always possible. The alternative is to undergo dialysis treatment.

The goal of dialysis is to replace the ill kidney of a patient. The hemodialysis is a process which lets the blood flow outside the patient body through an artificial kidney (dialyzer), and this process is repeated from 2 to 4 times a week, lasting each session between 2 and 5 hours, being the duration and the frequency of the treatment very dependent on each patient. The process usually consists of pumping, on the one hand, the patient's blood, and on the other hand, the dialysis fluids, both in opposite directions through the dialyzer. This two channels are separated by a semi permeable membrane which allows to filter the harmful substances in the blood. It is essential to maintain the appropriate pressure to assure the membrane filtration is performed.

The rate of fluid removal (ultrafiltration rate, UFR), is obtained based on the patient's ideal dry weight, dialysis duration, and fluid overload status at the start of dialysis. The removal fluid during a session results in relative hypovolemia and a decrease in venous return, which leads to a reduction in circulatory blood volume [142]. Compensatory mechanisms should activate to ensure the hemodynamic stability of the patient. A blood pressure level too low makes the blood not able to reach appropriately all the parts in the body through the arteries, and it causes symptoms such as dizziness, fatigue and vertigo. Not only that, but it has also been reported an increase of mortality in these patients [143–146].

Intradialytic hypotension (IDH) events occur in about 25% of the hemodialysis sessions. The primary causes of IDH are decreased blood volume, occurring as a result of fluid withdrawal of the vascular compartment during ultrafiltration, and insufficient refilling of fluid from the interstitial compartment to the vascular compartment. Other contributing factors include impaired peripheral vasoconstriction, autonomic dysfunction, arteriosclerosis, and cardiovascular pathologies such as left ventricular hypertrophy and dilated cardiomyopathy [147]. The immediate treatment includes slowing down or stopping the UFR, placing the patient in the Trendelenburg position, decreasing blood flow rate, and restoring the intravascular volume [148]. It sometimes leads to a premature termination of the treatment, which means that the patient leaves the dialysis unit still with an overloaded volume, resulting in inadequate fluid clearance and the need to extend the following sessions or even add an extra session.

Several parameters are displayed in the hemodialysis monitor to help doctors to

create personal profiles for each patient, depending on their hemodynamic stability. Dialysis duration, dialysate sodium concentration, dialysate temperature, dialysate and blood flow rates can be adjusted for each session, while parameters like body temperature, blood pressure and cardiac output are also monitored. Several bio-feedback mechanisms have been proposed along the years as IDH predictors, like short-term variability of oxygen saturation monitoring as an indirect expression of the hemodynamic stability [149].

Heart rate variability (HRV) has been extensively studied for the purpose of discriminating patients prone to IDH from resistant. Most studies have focused on the sympathovagal balance (LF/HF ratio) in hypotension-prone and hypotension-resistant uremic patients, concluding that higher values of this ratio are related to sessions without hypotension, while during a IDH event, this ratio is reduced [13]. Thus, the LF/HF ratio seems to be a useful index for discriminating between hypotension- prone and hypotension-resistant patients [15]. Still, there is room for improvement in the identification of IDH prone patients, for example using only information at the beginning of the treatment with the added value of other cardiovascular signals for an early classification of the patient.

The deficiency in the autonomic response may be originated by an impairment of the baroreceptor-mediate reflex with a consequent inefficiency in the short-term regulation of the arterial pressure [14]. Baroreflex sensitivity (BRS) parameters have been studied before in hemodialysis patients in previous studies, however there are studies which show that such indices, measured from the continuous beat-to-beat measurement of systolic blood pressure and the interbeat interval, cannot discriminate between IDH prone and resistant patients [18]. These contradictory results may be explained by the differences in the methodology. Our proposal is to include information of BRS parameters together with information of blood pressure variability (BPV) to help in the identification of IDH prone patients.

HRV and BPV are also highly influenced by respiration [21]. Respiration has not been studied in hemodialysis patients and may provide additional value to HRV and BPV analysis. In this study, we propose to include respiratory information and analyze the differences observed in prone and resistant patients. Due to the lack of a proper respiratory signal in the analyzed database, an ECG derived respiratory (EDR) signal is proposed to study wether there are differences in the respiratory frequency between IDH prone and resistant patients. The EDR signal revealed a VLF modulation which appeared occasionally. Interestingly, this modulation seemed to be synchronous with both HRV and BPV signals. To characterize this VLF modulation, the need for a spectral analysis with high frequency resolution led to the use of the minimum variance distortionless response (MVDR) method.

The hypothesis of this study is that IDH episodes are related to impaired autonomic regulation of the cardiovascular system. Several parameters will be proposed to analyze the differences between IDH prone and resistant patients. First, HRV, BPV and BRS series will be derived. Respiratory rate will be estimated from the heart's electrical axis rotation angle series obtained from the ECG. The VLF modulation found in these patients will be characterized and some parameters will be obtained to see whether

its appearance is related to impaired ANS. Additionally, a classifier will be designed, which will use information from all cardiovascular signals combined to establish if a patient is IDH prone or resistant in the first minutes of the treatment.

5.2 Database

Two databases have been used in this work, which consist of the ECG and BP signals from patients with end-stage renal failure who attended to regular sessions of hemodialysis treatment, lasting between 2 and 5 hours, 3 times a week. The continuous arterial blood pressure signal was acquired with a Finapres (Finapres Medical Systems BV, Holland) and sampled at 200 Hz with a Biopac (BIOPAC Systems Inc., USA) data acquisition system. The ECG was recorded during dialysis using the standard 12-lead configuration (first database) or a 6-lead configuration (second database), and sampled at a rate of 1000 Hz and amplitude resolution of 0.06 μV. Synchronization between the ECG and BP signals was performed manually, leading to a misalignment on the order of magnitude of a few ms, wich has negligible significance in the present application.

Symptomatic IDH is defined according to the following criteria [16]:

- if pre-dialysis systolic arterial pressure (SAP) was $\geqslant$ 100 mmHg: any event with SAP $\leqslant$ 90 mmHg, associated with complaints
- if SAP was $\leqslant$ 100 mmHg: any SAP reduction by at least 10% associated with complaints

Acute symptomatic IDH, being a subset of symptomatic IDH, is defined by a sudden drop in systolic blood pressure (30 mmHg per 10 min before hypotension).

Sweden database

This database consists of 28 sessions from 15 different patients adquired in Park Dialys, Lund, Sweden, and Helsingborg Hospital, Helsingborg, Sweden.

Each patient has been classified as being hypotension-resistant (R) or hypotension-prone (P) based on their previous clinical history. Besides, they have also been classified as being diabetic (D) or non-diabetic (ND) patients. Symptomatic hypotension occurred in 4 of the 28 sessions (one in the resistant group and the others in the prone group), of which 1 was acute (systolic blood pressure fall larger than 30 mmHg per 10 minutes prior to hypotension).

Denmark database

A second database is used, consisting of 29 sessions from 11 patients. These patients underwent hemodialysis treatments in Copenhague, Denmark. Due to the poor quality of the BP signal, 5 sessions which belonged to 2 patients were rejected from this work

and only 24 sessions from 9 patients were used. Based on clinical history, all patients are classified as being hypotension-prone, and they have also been classified as being diabetic or non-diabetic patients. Symptomatic hypotension occurred in 5 of the 24 sessions, and all of them were acute.

Global database

In total, a sum of 52 sessions from 24 patients were analyzed of which 21 sessions belonged to 10 patients with diabetes. A brief summary of the database can be seen in Table 5.1.

	Resistant	**Prone**
# Patients/# Sessions	7/11	17/41
# Ses. each patient	2,1,1,2,1,2,2	2,1,2,1,4,4,3,2,2,3,4,2,2,1,2,3,3
# Diabetic patients/# Ses.	3/4	7/17
Male/Female	6/1	9/8
Age (years)	59 ± 14	65 ± 11
Weight (kg)	87 ± 20	77 ± 20
Mean heart period (s)	0.79 ± 0.03	0.81 ± 0.02

Table 5.1: Study population characteristics

5.3 Methods

5.3.1 Heart rate variability

HRV series is derived similarly than in Section 2.3.3 with a modification. The same wavelet-based detector [88] is used to obtain the pairs (k,t_k) and then the instantaneous HR denoted as $d_{\mathrm{HR}}(n)$ is obtained. Time-varying mean HR, denoted as $d_{\mathrm{HRM}}(n)$, is extracted from $d_{\mathrm{HR}}(n)$ to obtain the variability signal $d_{\mathrm{HRV}}(n)$. In this case, contrary to Section 2.3.3, the time-varying HRV correction is not needed, since patients during hemodialysis do not expect great changes in mean HR. Besides, mean heart rate between patients in both groups are not significantly different.

5.3.2 Blood pressure variability

BPV series is obtained by detecting the systolic blood pressure of each consecutive beat. First, the blood pressure signal is low-pass filtered with a cut-off frequency of 40 Hz (forward/backward filtering) to remove noise. Then, the peaks of the low-pass filtered signal, $s(n_k)$, are found searching for the zero crossings on the derivative of the signal, implemented by regressive differences:

$$s'(n) = s(n) - s(n-1) \tag{5.1}$$

where $s(n)$ is the low-pass filtered blood pressure signal. To remove peaks which are due to noise, a time-varying threshold is applied by computing the envelope of the signal and using a portion of it as threshold, defined as:

$$u(n) = (1 + K) \cdot s_f(n) \tag{5.2}$$

where $s_f(n)$ is the result of low-pass filtering $s(n)$ with a cut-off frequency of 0.5 Hz, so it follows the envelope oscillations of the blood pressure signal. Parameter K is 0.1, this value has been chosen based on experimental observations. Figure 5.1 shows how all local maximum values of $s(n)$, as well as those related to noise, are located below the threshold.

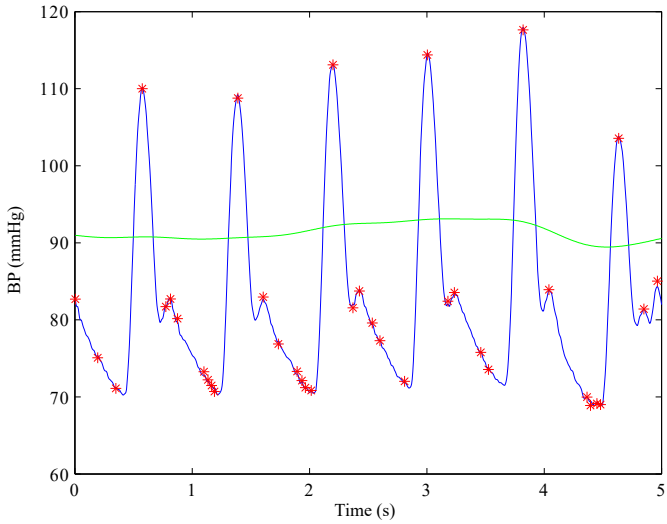

Figure 5.1: Blood pressure signal, time-varying threshold and detected peaks (systolic blood pressure).

Additionally, a protective rule is applied to the detected peaks, impossing a refractory period to make sure that a certain distance elapses between successive beat detections at times n_k:

$$|n_k - n_{k-1}| \geqslant T_{hr} \cdot F_s \tag{5.3}$$

with F_s being the sampling frequency of $s(n)$ (200 Hz) and the time T_{hr} is set to 0.5s based on expected heart rate, see Table 5.1.

One of the challenges which appears in the analysis of BP signal is signal lost segments. These "gaps" can last from seconds (due to calibration of the blood pressure

device) to minutes (while the patient is eating and the blood pressure is not being recorded), see Figure 5.2. To detect the gaps and removed them from further analysis, another amplitude threshold is used in successive 5-min segments, which is set to 10% of the minimum value of $s(n)$ in that segment, based on experimental results. A gap is found if there is more than 5 s without any valid peak above the threshold.

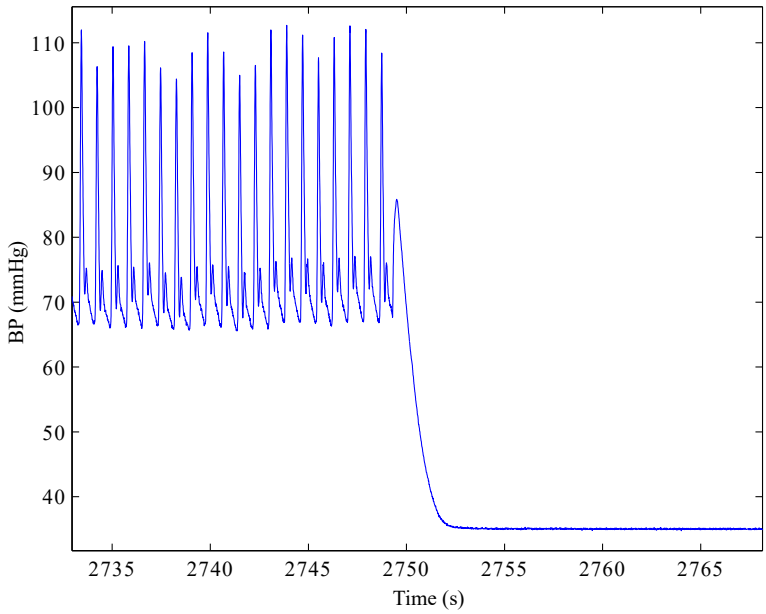

Figure 5.2: Presence of signal lost in blood pressure signal.

The pairs $(n_k,\ s(n_k))$ are interpolated using cubic splines to generate the systolic blood pressure signal $d_{\mathrm{BP}}(n)$ sampled at a rate of 4 Hz. Note that $d_{\mathrm{BP}}(n)$ is not estimated when there is a gap. In a similar way to HRV analysis, $d_{\mathrm{BP}}(n)$ is filtered to obtain $d_{\mathrm{BPM}}(n)$ and then $d_{\mathrm{BPV}}(n)$ is calculated as:

$$d_{\mathrm{BPV}}(n) = d_{\mathrm{BP}}(n) - d_{\mathrm{BPM}}(n) \tag{5.4}$$

5.3.3 Rotation angles series and respiratory frequency

Among the several EDR signals in the literature, the one used in this study exploits variations in the direction of the heart's electrical axis [40], which leads to 3 rotation angles series. Rotation angles series are estimated using the vectorcardiogram (VCG) and spatiotemporal alignment of successive QRS-VCG loops with respect to a reference loop [150]. This method consists in minimizing the normalized distance $\varepsilon(t_i)$ between a reference beat, $\mathbf{Y_R}(t_i)$, and the observed one, $\mathbf{Y}(t_i)$, with respect to the rotation transform matrix $\mathbf{Q}(t_i)$, temporal synchronization $\mathbf{J}_\tau$ and scaling $\gamma(t_i)$, for

each occurence beat time t_i. For simplicity, temporal dependence t_i will be omitted from notation: $\varepsilon = \varepsilon(t_i)$, $\mathbf{Y_R} = \mathbf{Y_R}(t_i)$, $\mathbf{Y} = \mathbf{Y}(t_i)$, $\mathbf{Q} = \mathbf{Q}(t_i)$, $\gamma = \gamma(t_i)$.

$$\varepsilon_{min} = \frac{\|\mathbf{Y_R} - \gamma \mathbf{Q}^T \mathbf{Y} \mathbf{J}_\tau\|_F^2}{\|\gamma \mathbf{Q}^T \mathbf{Y} \mathbf{J}_\tau\|_F^2} \tag{5.5}$$

$$\mathbf{Q} = \begin{bmatrix} * & \sin(\varphi_{\mathrm{Z}})\cos(\varphi_{\mathrm{Y}}) & \sin(\varphi_{\mathrm{Y}}) \\ * & * & \sin(\varphi_{\mathrm{X}})\cos(\varphi_{\mathrm{Y}}) \\ * & * & * \end{bmatrix}, \tag{5.6}$$

$$\mathbf{J}_\tau = \begin{bmatrix} \mathbf{0}_{\Delta+\tau} \\ \mathbf{I} \\ \mathbf{0}_{\Delta-\tau} \end{bmatrix} \tag{5.7}$$

The reference beat $\mathbf{Y_R}$ is a matrix 3×N whose rows contains the complex QRS in leads X, Y and Z, being N the considered analysis window for QRS complex, 120 ms in this study. The observed beat $\mathbf{Y}$ is a matrix $3\times(N + 2\Delta)$, with Δ=30 ms, being Δ the the number of symmetrically augmented samples which allow for time synchronization, and $\tau = -\Delta, \ldots, \Delta$ with increments of 1 ms. The rotation matrix $\mathbf{Q}$ can be seen as three succesive rotations around each axis, defined by the rotation angles φ_{X}, φ_{Y} and φ_{Z} . Elements in $\mathbf{Q}$ denoted as $*$ do not have any influence in this analysis. The temporal synchronization $\mathbf{J}_\tau$ is a matrix $(N + 2\Delta)\times$N. Lastly, operator $\|\cdot\|_F^2$ denotes Frobenius norm.

The normalized distance ε is minimized by finding the estimates of γ and $\mathbf{Q}$ for every value of τ, and then selecting the value of τ for which ε is minimum. With this optimum $\hat{\mathbf{Q}}$ estimated, the rotation angles $\hat{\varphi_{\mathrm{X}}}$, $\hat{\varphi_{\mathrm{Y}}}$ and $\hat{\varphi_{\mathrm{Z}}}$ are estimated using (5.6):

$$\begin{aligned} \hat{\varphi}_Y &= \arcsin(\hat{q}_{13}) \\ \hat{\varphi}_X &= \arcsin\left(\frac{\hat{q}_{23}}{\cos(\hat{\varphi}_{\mathrm{Y}})}\right) \\ \hat{\varphi}_Z &= \arcsin\left(\frac{\hat{q}_{12}}{\cos(\hat{\varphi}_{\mathrm{Y}})}\right), \end{aligned} \tag{5.8}$$

where $\hat{q_{ij}}$ represents the element in row i and column j of $\hat{\mathbf{Q}}$.

Since the QRS complex can change in morphology, a more robust estimate is applied by exponentially updating the reference beat:

$$\mathbf{Y_R}(i+1) = \alpha \mathbf{Y_R}(i) + (1-\alpha)\mathbf{Y}(i+1), \tag{5.9}$$

where i is the beat index at instant t_i. Parameter α (α=0.8) tries to follow the morphologic changes in QRS while adaptation to noise is avoided.

Once the rotation angles estimates $\hat{\varphi_{\mathrm{X}}}$, $\hat{\varphi_{\mathrm{Y}}}$ and $\hat{\varphi_{\mathrm{Z}}}$ are obtained for each beat, they are interpolated at 4 Hz, obtaining the series $\phi_{\mathrm{X}}(n)$, $\phi_{\mathrm{Y}}(n)$ and $\phi_{\mathrm{Z}}(n)$.

At this point, we found out that in some segments of the recordings, a synchronous VLF modulation appeared in $d_{\mathrm{HR}}(n)$, $d_{\mathrm{BP}}(n)$ and the angles series. Figure 5.3 shows an example of this modulation in $d_{\mathrm{HR}}(n)$, $d_{\mathrm{BP}}(n)$ and the envelope of $\phi_{\mathrm{X}}(n)$. To further analyze this modulation, the envelope of the angles series is obtained using Hilbert Transform [101] and then low-pass filtering them with a cutoff frequency of 0.03 Hz, denoted as $\phi_{\mathrm{XM}}(n)$, $\phi_{\mathrm{YM}}(n)$ and $\phi_{\mathrm{ZM}}(n)$ in order to compare them to $d_{\mathrm{HRM}}(n)$ and $d_{\mathrm{BPM}}(n)$.

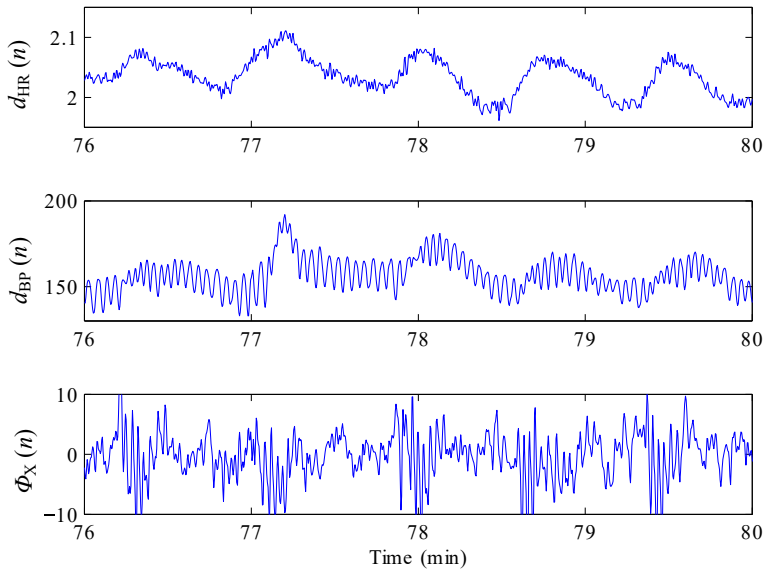

Figure 5.3: Example of $d_{\mathrm{HR}}(n)$, $d_{\mathrm{BP}}(n)$ and $\phi_{\mathrm{X}}(n)$ showing a synchronous modulation.

Lastly, the respiratory frequency f_{R} is estimated as described in [40] from the location of the largest peak in a running average of the power spectrum obtained from the EDR signals $\phi_{\mathrm{X}}(n)$, $\phi_{\mathrm{Y}}(n)$ and $\phi_{\mathrm{Z}}(n)$. The estimation procedure is divided into two parts aimed at robust performance. First, the power spectrum of each EDR signal is estimated with Lomb's method and individual running power spectra of each EDR signal are averaged in order to reduce the variance. Then,the largest peak of the average spectrum is chosen as f_{R}, obtained within a narrow interval around a reference frequency which updates using previous estimates information.

5.3.4 Spectral analysis

Among the different methods to estimate the spectrum of a signal, a non parametric method called MVDR [151, 152] was chosen since, in general, it offers higher spectral resolution than does the classical periodogram, specially in the VLF band.

Minimum variance distortionless response

Let $x(n)$ be a zero-mean stationary random process, input of K filters (denoted as $\mathbf{g}_k$) of length L.

$$\mathbf{g}_k = \begin{bmatrix} g_{k,0} & g_{k,1} & \dots & g_{k,L-1} \end{bmatrix}^T, k = 0, 1, \dots, K-1 \tag{5.10}$$

where superindex ^{T} denotes transposition. The output signals of the filters are denoted as $y_k(n)$ and obtained as:

$$y_k(n) = \mathbf{g}_k^H \mathbf{x}(n) \tag{5.11}$$

$$\mathbf{x}(n) = \begin{bmatrix} x(n) & x(n-1) & \dots & x(n-L+1) \end{bmatrix}^T \tag{5.12}$$

where superindex ^{H} denotes hermitic matrix or vector. The power of $y_k(n)$ is:

$$E\{|y_k(n)|^2\} = E\{|\mathbf{g}_k^H \mathbf{x}(n)|^2\} = \mathbf{g}_k^H \mathbf{R}_x \mathbf{g}_k \tag{5.13}$$

being $E[\cdot]$ the operator for mathematical expectation and $\mathbf{R}_x$ the covariance matrix of the input signal $x(n)$:

$$\mathbf{R}_x = E[\mathbf{x}(n)\mathbf{x}^H(n)] \tag{5.14}$$

The unitary Fourier matrix $\mathbf{F}$ is defined as:

$$\mathbf{F} = \begin{bmatrix} \mathbf{f}_0 & \mathbf{f}_1 & \dots & \mathbf{f}_{K-1} \end{bmatrix} \tag{5.15}$$

$$\mathbf{f}_k = \frac{1}{\sqrt{L}} \begin{bmatrix} 1 & e^{jw_k} & \dots & e^{jw_k(L-1)} \end{bmatrix}^T, k = 0, 1, \dots, K-1 \tag{5.16}$$

$$w_k = \frac{2\pi k}{K}, k = 0, 1, \dots, K-1 \tag{5.17}$$

where w_k represents the frequency values where the spectrum is going to be evaluated.

In the MVDR spectrum, the filter coefficients are chosen so as to minimize the variance of the filter output, subject to the commonly referred to as the distortionless constraint:

$$\mathbf{g}_k^H \mathbf{f}_k = \mathbf{f}_k^H \mathbf{g}_k = 1 \tag{5.18}$$

with the purpose that when $x(n)$ passes through the filter $\mathbf{g}_k$, there is no distortion at frequency w_k while other frequencies tend to be attenuated. The coefficients of the filter can be obtained by minimizing the following cost function J_k:

$$J_k = \mathbf{g}_k^H \mathbf{R}_x \mathbf{g}_k + \lambda[1 - \mathbf{g}_k^H \mathbf{f}_k] \tag{5.19}$$

where λ is a Lagrange multiplier. The minimization leads to:

$$\mathbf{g}_k = \mathbf{R}_x^{-1} \lambda \mathbf{f}_k \tag{5.20}$$

Using (5.20) in restriction (5.18) leads to:

$$(\mathbf{R}_x^{-1} \lambda \mathbf{f}_k)^H \mathbf{f}_k = 1 \tag{5.21}$$

$$\lambda \mathbf{f}_k^H (\mathbf{R}_x^{-1})^H \mathbf{f}_k = 1 \tag{5.22}$$

$$\lambda = \frac{1}{\mathbf{f}_k^H \mathbf{R}_x^{-1} \mathbf{f}_k} \tag{5.23}$$

With (5.23) and (5.20), the coefficients of the filter are obtained as:

$$\mathbf{g}_k = \frac{\mathbf{R}_x^{-1} \mathbf{f}_k}{\mathbf{f}_k^H \mathbf{R}_x^{-1} \mathbf{f}_k} \tag{5.24}$$

The spectrum of $x(n)$ at frequency w_k is defined as:

$$S_x(w_k) = E\{|y_k(n)|^2\} = \mathbf{g}_k^H \mathbf{R}_x \mathbf{g}_k \tag{5.25}$$

And using (5.24) in (5.25):

$$S_x(w_k) = \frac{1}{\mathbf{f}_k^H \mathbf{R}_x^{-1} \mathbf{f}_k} \tag{5.26}$$

If $K > 2L - 1$, then the MVDR filter has enough degrees of freedom to cancel all the other input frequencies [153]. In this study, the MVDR method has been applied with a resolution of K =2048 samples and a window length of L =300 samples.

Spectral coherence

When there exists a linear relationship between two signals $x_1(n)$ and $x_2(n)$, the cross spectrum $S_{x_1x_2}(w)$ can be used to characterize the related spectral components. The cross spectrum, $S_{x_1x_2}(w)$, is defined as the discrete-time Fourier transform of the cross-correlation function $r_{x_1x_2}(k)$. Spectral coherence function, $\Gamma_{x_1x_2}(w)$, is defined as the normalized cross spectrum density:

$$\Gamma_{x_1x_2}(w) = \frac{S_{x_1x2}(w)}{\sqrt{S_{x_1}(w) S_{x_2}(w)}} \tag{5.27}$$

Percentile	WELCH	MVDR
90%	0.7731	0.6617
95%	0.8157	0.6769
99%	0.8727	0.7163

Table 5.2: Results of statisical threshold for coherence.

Magnitude Squared Coherence (MSC) is an index which measures the linear correlation between two signals at a given frequency w:

$$|\Gamma_{x_1x_2}(w)|^2 = \frac{|S_{x_1x2}(w)|^2}{S_{x_1}(w)S_{x_2}(w)}. \tag{5.28}$$

Using MVDR method to estimate both spectra and cross-spectra, we obtain:

$$S_{x_1x_2}(w_k) = \frac{\mathbf{f}_k^H \mathbf{R}_{x_1x_1}^{-1} \mathbf{R}_{x_1x_2} \mathbf{R}_{x_2x_2}^{-1} \mathbf{f}_k}{[\mathbf{f}_k^H \mathbf{R}_{x_1x_1}^{-1} \mathbf{f}_k][\mathbf{f}_k^H \mathbf{R}_{x_2x_2}^{-1} \mathbf{f}_k]} \tag{5.29}$$

$$|\Gamma_{x_1x_2}(f)|^2 = \frac{|\mathbf{f}_k^H \mathbf{R}_{x_1x_1}^{-1} \mathbf{R}_{x_1x_2} \mathbf{R}_{x_2x_2}^{-1} \mathbf{f}_k|^2}{[\mathbf{f}_k^H \mathbf{R}_{x_1x_1}^{-1} \mathbf{f}_k][\mathbf{f}_k^H \mathbf{R}_{x_2x_2}^{-1} \mathbf{f}_k]} \tag{5.30}$$

with $\mathbf{R}_{x_1x_2} = E[\mathbf{x}_1(n)\mathbf{x}_2^H(n)]$, being the cross correlation matrix.

Statistical threshold for coherence

When measuring the spectral coherence between two signals, a statistical threshold ρ_s must be determined to decide if there exist a linear correlation at a given frequency between them. A fixed threshold can be misleading, since two uncorrelated signals present random coherence which is not equal to zero. Moreover, estimators used to calculate auto and cross-spectra also affect coherence values [154, 155]. The statistical threshold ρ_s is determined as follows: the coherence between two segments of white noise, assumed to be uncorrelated, is first computed and then, after 1000 repetitions, the maximum coherence value in each iteration is obtained and sorted. The percentile η % is chosen to obtain ρ_s, with an error of (100-η) %.

Since this threshold is dependant of the method used to estimate the spectrum of the signal, the MVDR method is compared with Welch periodogram as a reference. For Welch periodogram, a Hamming window was chosen, and the following values have been used: L=2 minutes and D=1 minute. Table 5.2 shows the results of the 90, 95 and 99th percentile. For the same error, the needed threshold for Welch periodogram is always higher. The final threshold chosen, ρ_s, is set to 0.7, and the error is assumed to be less than 3% if the MVDR method is used.

5.3.5 HRV, BPV and BRS parameters

The ECG and BP signals were registered during several hours, coinciding with the duration of the hemodialysis session. It is decided to segment the variability signals associated to them in 5-min segments, where stationarity has been assumed. For each segment of $d_{\mathrm{HRV}}(n)$ and $d_{\mathrm{BPV}}(n)$, the spectra are estimated, denoted as $S_{\mathrm{HR}}(w)$ and $S_{\mathrm{BP}}(w)$ respectively, and the spectral indices are obtained integrating the spectrum in the desired band. The following spectral indices of HRV and BPV were considered, reflecting spectral band power:

$$P_{\mathrm{S}}^{\mathrm{B}}, \quad \mathrm{B} = \{\mathrm{LF}, \mathrm{HF}\}, \mathrm{S} = \{\mathrm{HR}, \mathrm{BP}\}$$

with Ω_{LF} ranging from 0.04 to 0.15 Hz and Ω_{HF} from 0.15 to 0.4 Hz; the spectral ratio

$$R_{\mathrm{S}} = \frac{P_{\mathrm{S}}^{\mathrm{LF}}}{P_{\mathrm{S}}^{\mathrm{HF}}}, \tag{5.31}$$

and the normalized spectral ratio

$$R_{\mathrm{S}}^{\mathrm{n}} = \frac{P_{\mathrm{S}}^{\mathrm{LF}}}{P_{\mathrm{S}}^{\mathrm{LF}} + P_{\mathrm{S}}^{\mathrm{HF}}}, \tag{5.32}$$

MSC index is used to identify the relationship between HRV and BPV to obtain the BRS parameters, which are defined from the spectral power of HRV and BPV in the LF and HF bands as:

$$\alpha^{\mathrm{B}} = \sqrt{\frac{P_{\mathrm{HR}}^{\mathrm{B}}}{P_{\mathrm{BP}}^{\mathrm{B}}}}, \quad \mathrm{B} = \{\mathrm{LF}, \mathrm{HF}\} \tag{5.33}$$

Since BRS quantifies the HR response due to changes in BP, α^B is only computed when the MSC index between $d_{\mathrm{HRV}}(n)$ and $d_{\mathrm{BPV}}(n)$ is above the threshold ρ_s.

5.3.6 VLF parameters

To characterize VLF modulation shown in Figure 5.5, the following steps are followed:

- The spectral coherence is obtained from all possible combinations between $d_{\mathrm{HRM}}(n)$, $d_{\mathrm{BPM}}(n)$, $\phi_{\mathrm{XM}}(n)$, $\phi_{\mathrm{YM}}(n)$ and $\phi_{\mathrm{ZM}}(n)$. This is performed for all 5-min segments.
- For each segment, the maximum coherence value is anotated, as well as its frequency, denoted as $\Gamma_{\mathrm{x_1x_2}}^{\mathrm{max}}$ and $f_{\mathrm{x_1x_2}}^{\mathrm{max}}$ respectively, with $\mathrm{X_1}$,$\mathrm{X_2}$ $\epsilon\{d_{\mathrm{HRM}}, d_{\mathrm{SBPM}}, \phi_{\mathrm{M}}\}$. ϕ_{M} denotes the angle with the highest coherence with $d_{\mathrm{HRM}}(n)$ and $d_{\mathrm{BPM}}(n)$. For the segment to be included in the study, 3 conditions must be fulfilled:

  1. All $\Gamma_{\mathrm{x_1x_2}}^{\mathrm{max}}$ must be above the threshold ρ.

2. All $f^{\max}_{x_1x_2}$ must coincide (therefore, denoted simply as $f^{\max}$) in a range no more than 0.002Hz.
3. The spectrum of $d_{\mathrm{HRM}}(n)$, $d_{\mathrm{SBPM}}(n)$, $\phi_{\mathrm{M}}(n)$ are "peaky" enough, that is, at least 50% of the total power in the VLF band is contained in an interval centered around the largest peak $f^{\max}$: [$f^{\max}$-0.01Hz,$f^{\max}$+0.01Hz] and power spectral density values at the interval extremes do not exceed 75% of the value at $f^{\max}$.

- The median value of $\Gamma^{\max}_{x_1x_2}$ and $f^{\max}$ are obtained for each recording, denoted as $\overline{\Gamma^{\max}_{x_1x_2}}$ and $\overline{f}^{\max}$, respectively. Moreover, the duration of the VLF modulation is quantified as the total segments with a coherence value above the threshold divided by the total number of segments, denoted as $T_{\%}$.

5.3.7 Statistical analysis

Statistical analysis is performed to determine whether the indices differ between prone and resistant patients. Kolmogorov test is applied to all parameters to know if they follow a normal distribution, and the result is negative. Therefore, a Mann Whitney analysis is used to test equality of population medians among prone and resistant groups. Two groups are considered to be significantly different when p <0.05. Results will be shown as median ± MAD values.

To characterize the VLF modulation, significant differences are studied between prone and resistant patients (P and R) as well as diabetic and non diabetic patients (D and ND). Results will be shown in P, R, D and ND groups, as well as the subgropus P+D, P+ND, R+D and R+ND, which are formed as the combination of each pair of groups.

5.3.8 Features selection

Feature selection is a process commonly used when there are a lot of features in a classifier and not all of them are important. In this context, features are the spectral indices obtained from HRV, BPV and BRS. This process consists of selecting a subset of features that performs the best under some classification system. There are several methods to do this, and in particular, the sequential methods begin with a previous subset and iteratively either add or remove features until some termination criterion is met. The drawback of these methods is that they are not guaranteed to produce the optimal result.

There are two main subgroups: sequential forward selection and sequential backward selection. The former starts with no features and adds them one at each step, adding the one that decreases the error the most, and it stops when any addition does not decrease significantly that error. The latter starts with the full set of features and in each step, the feature whose removal decrease the most the error is removed, until any further removal increases the error significantly. To reduce overfitting, this error is validated in a different set than training set.

The sequential floating selection method is a combination of both groups, and it is able to remove features which become obsolete with the addition of new ones, or reevaluate features that had been previously removed. In this work, the Sequential Floating Forward Selection (SFFS) method has been used, which consist of applying one forward step following several conditional backward steps as long as the error decreases [156], as follows:

1. Start with the empty set $Y = \{\varnothing\}$
2. Select the best feature
   $x^+ = \underset{x \notin Y_k}{\operatorname{argmax}}[J(Y_k + x)]$
   $Y_k = Y_k + x^+;\ k = k + 1$
3. Select the worst feature
   $x^+ = \underset{x \in Y_k}{\operatorname{argmax}}[J(Y_k - x)]$
4. If $J(Y_k - x^-) > J(Y_k)$ then
   $Y_{k-1} = Y_k - x;\ k = k - 1$
   go to Step 3
   else
   go to Step 2

being Y_k the pool of the k selected features, J the criterion function to maximize and x one element of the feature set.

In this work, the idea of the leave–one–out method, which will be explained in the next section, is used in the features selection: the search is performed in all the observations but one, and the search is repeated until every observation has been left out once. In this way, in a database with N observations, $N - 1$ different feature subsets are obtained. The most K repeated features are selected for the final model.

Regarding the value of K, a commonly used rule is not to use more than $\sqrt{m_k}$ features, being m_k the number of observations which belong to the smallest group. The database used in this work consist of 41 sessions from 17 prone patients, and 11 sessions from 7 resistant patients. Since the resistant group is the smaller one, it determines the upper limit for K, whose value in this work is $K = 2$.

5.3.9 Classifier design and evaluation

A linear discriminant analysis method has been chosen, which consists of searching some linear combinations of the selected features which provide the best separation between the considered classes. These different combinations are called discriminant functions [157]. This analysis assumes normal densities with equal covariance matrices in the classes.

Classifier evaluation

The optimal framework in classification is determining two non-overlapping groups: one training group for selecting the optimal features and training the classifier, and a validation group for testing the classifier. Unfortunately, not always is possible to have two different groups due to the low number of data, since the feature selection and classifier training would be overfitted to the training data, which may not be representative enough, and the classifier would not work properly for the validation data and, consequently, for additional databases. However, using all the observations for the training group and then for the evaluation group would give biased results, since the features and the classifier would be optimal only for that data and would not be general.

One of the most common approaches to solve this problem is the leave–one–out method [158]. For classifier training, this method uses all observations to train the classifier but one, which is used for evaluation, and process is repeated such that each observation in the database is used once as the validation data.

The leave–one–out method works with observations, which in this work is the same as patients, therefore called leave–one–patient–out. A patient can have 1, 2, 3 or even 4 different sessions, corresponding to different days. Both feature selection and classifier training are performed with all the sessions from all patients but one, being the sessions from this patient left out, repeating the process with all the patients.

The classification framework in this work is as follows:

- The whole database is used for feature selection, following the leave–one–patient–out method. The criterion used for the features search is to minimize the error of the classifier, which is the same to maximize the accuracy of the classifier.

- Once the features set is determined, a linear classifier is trained and evaluated using the leave–one–patient–out method. The performance of the classifier is measured with sensitivity (Se), specificity (Sp) and accuracy (Acc), defined as:

$$Se = \frac{TP}{TP + FN}$$

$$Sp = \frac{TN}{TN + FP}$$

$$Acc = \frac{TP + TN}{TP + TN + FP + FN}$$

  with TP, TN, FP and FN being the number of true positives, true negatives, false positives and false negatives respectively. In this work, prone patients are classified as positive while being a resistant patient is classified as being negative.

During the evaluation, each session will be treated as an independent observation.

5.4 Results

5.4.1 VLF modulation characterization

VLF modulation has been studied in $d_{\mathrm{HRM}}(n)$, $d_{\mathrm{SBPM}}(n)$ and rotation angles $\phi_{\mathrm{XM}}(n)$, $\phi_{\mathrm{YM}}(n)$ and $\phi_{\mathrm{ZM}}(n)$. Figure 5.5 shows an example of a segment of these series with a visible VLF modulation. For a comparison to Welch periodogram, Figure 5.4 shows the spectral coherence between $d_{\mathrm{HRM}}(n)$ and $\phi_{\mathrm{XM}}(n)$ using MVDR method (left) and Welch periodogram (right) for comparison, where MVDR method shows better spectral resolution.

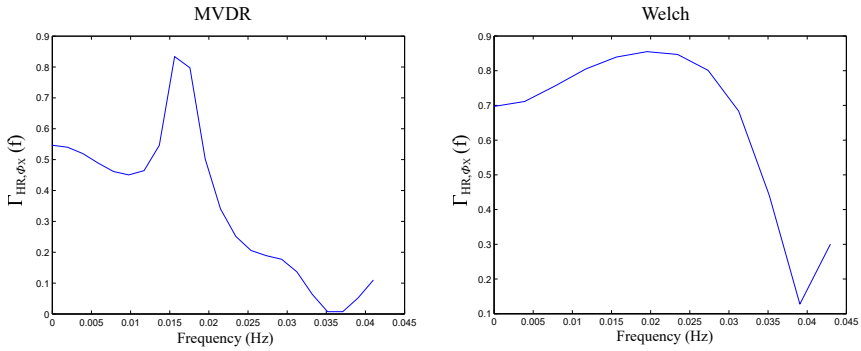

Figure 5.4: Spectral coherence between $d_{\mathrm{HRM}}(n)$ and $\phi_{\mathrm{XM}}(n)$ using the MVDR method (left) and Welch periodogram (right).

Once the statistical threshold has been set for coherence between signals, $\overline{\Gamma^{\max}_{\mathrm{x_1x_2}}}$ is obtained for each combination, as well as $\overline{f}^{\max}$ and $T_{\%}$. Table 5.3 shows the median $\pm$ MAD values of VLF parameters in P and R groups, and D and ND groups. Significant differences are found in $\overline{\Gamma^{\max}_{\mathrm{HR},\phi}}$, $\overline{\Gamma^{\max}_{\mathrm{BP},\phi}}$, $\overline{f}^{\max}$ and $T_{\%}$ when comparing P and R groups; and in $\overline{f}^{\max}$ and $T_{\%}$ when comparing D and ND groups. Median values for subgroups P+D, P+ND, R+D and R+ND are also shown, and significant differences (not shown in Table 5.3) were found in $\overline{f}^{\max}$ between R+D and R+ND, and between P+D and R+ND, and in $T_{\%}$ between P+D and P+ND, and between P+D and R+ND.

5.4.2 Discriminative indices

Table 5.4 shows the results for the statistical analysis. Parameters related with VLF modulation are omitted since they were already shown in the previous section.

Another analysis is performed using only the first 30 minutes of the treatment (the first 6 segments). The aim is to know wether these parameters are able to discriminate between IDH prone and resistant at the beginning of the treatment, and see the differences with the previous analysis. Results can be seen in Table 5.5. VLF modulation

Group (# sessions)	$\overline{\Gamma^{\max}_{\mathrm{HR},\phi}}$	$\overline{\Gamma^{\max}_{\mathrm{HR,BP}}}$	$\overline{\Gamma^{\max}_{\mathrm{BP},\phi}}$	$\overline{f}^{\max}$ (Hz)	$T_{\%}$
P (20)	0.797 * ± 0.014	0.776 ± 0.019	0.738 * ± 0.016	0.015* ± 0.002	6.16 * ± 4.3
R (6)	0.744 ± 0.008	0.79 ± 0.015	0.776 ± 0.003	0.023 ± 0.003	3.38 ± 2.1
D (15)	0.782 ± 0.011	0.79 ± 0.012	0.763 ± 0.010	0.015* ± 0.0004	11.62 * ± 4.9
ND (11)	0.757 ± 0.009	0.749 ± 0.0009	0.749 ± 0.011	0.021 ± 0.002	5.76 ± 4.7
P+D (12)	0.787 ± 0.009	0.794 ± 0.011	0.763 ± 0.007	0.014 ± 0.001	12.06 ± 6.8
P+ND (8)	0.753 ± 0.011	0.716 ± 0.0003	0.738 ± 0.008	0.016 ± 0.001	6.35 ± 2.3
R+D (3)	0.749 ± 0.001	0.786 ± 0.001	0.751 ± 0.0001	0.017 ± 0.001	5.45 ± 3.9
R+ND (3)	0.779 ± 0.008	0.83 ± 0.020	0.804 ± 0.020	0.023 ± 0.003	3.51 ± 1.8

Table 5.3: VLF modulation characterization: coherence values ($\overline{\Gamma^{\max}_{\mathrm{HR},\phi}}$, $\overline{\Gamma^{\max}_{\mathrm{HR,BP}}}$ and $\overline{\Gamma^{\max}_{\mathrm{BP},\phi}}$), frequency ($\overline{f}^{\max}$) and % of time ($T_{\%}$) of the modulation. Number of sessions where the VLF modulation appears is shown in brackets for each group. Asterisks denote p-values lower than 0.05.

Variable	Prone	Resistant
$P^{\mathrm{LF}}_{\mathrm{HR}}$	0.0009 ± 0.002	0.0022 ± 0.004 $*$
$P^{\mathrm{HF}}_{\mathrm{HR}}$	0.0009 ± 0.003	0.0018 ± 0.004
$R^{\mathrm{n}}_{\mathrm{HR}}$	0.42 ± 0.21	0.75 ± 0.14 ‡
R_{HR}	1.04 ± 0.88	4.5 ± 2.3 ‡
$P^{\mathrm{LF}}_{\mathrm{BP}}$	0.0011 ± 0.001	0.0006 ± 0.0005 $*$
$P^{\mathrm{HF}}_{\mathrm{BP}}$	0.001 ± 0.001	0.0003 ± 0.001 †
α^{LF}	0.55 ± 1.04	1.38 ± 1.83 †
α^{HF}	0.62 ± 1.01	1.67 ± 3.38
f_{R}	0.19 ± 0.03	0.21 ± 0.02

Table 5.4: Median ± MAD of HRV, BPV, BRS and EDR indices for prone and resistant patients. The symbols $\{*, \dagger, \ddagger\}$ represent p-values less than $\{0.05, 0.01, 0.001\}$, respectively.

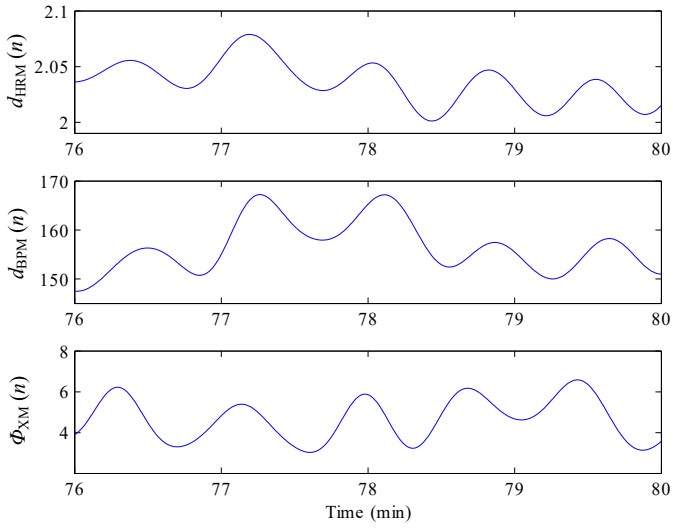

Figure 5.5: Example of $d_{\mathrm{HRM}}(n)$, $d_{\mathrm{BPM}}(n)$ and $\phi_{\mathrm{XM}}(n)$ showing a synchronous modulation.

appearence is inconsistent, and it usually appears after this period of time, therefore they are not shown.

5.4.3 Classification of prone and resistant patients

Feature selection using the leave–one–patient–out method leads to $R^{\mathrm{n}}_{\mathrm{HR}}$ and R_{HR}. The performance of the classifier can be seen in Table 5.7, where it can be seen the high sensitivity (Se=97.5%) but a low specificity. The cause may be that the P and R groups in the database are strongly unbalanced (17P and 7R).

5.4.4 Division into diabetic and non diabetic subgroups

The dataset is divided into diabetic and nondiabetic subgroups due to the fact that the diabetes state in patients may lead to an impairment in the ANS activity. In this scenario, two classifiers are trained, one for the diabetic subgroup, and another for the non diabetic subgroup. In this way, the diabetic group consists of 10 patients (21 sessions) of which 7 are hypotension–prone, while the non diabetic group consists of 14 patients (31 sessions) of which 10 are hypotension–prone.

In each subgroup, feature selection is repeated and the classifier is trained and evaluated. Results can be seen in Table 5.6 and Table 5.7. For the diabetic group, the selected features are $R^{\mathrm{n}}_{\mathrm{HR}}$ and $P^{\mathrm{LF}}_{\mathrm{HR}}$, while for the non diabetic group the features are $R^{\mathrm{n}}_{\mathrm{HR}}$ and α^{LF}.

Variable (30 min)	Prone	Resistant
$P_{\mathrm{HR}}^{\mathrm{LF}}$	0.0028 ± 0.008	0.0034 ± 0.005
$P_{\mathrm{HR}}^{\mathrm{HF}}$	0.0012 ± 0.002	0.0021 ± 0.004
$R_{\mathrm{HR}}^{\mathrm{n}}$	0.46 ± 0.23	0.76 ± 0.17 ‡
R_{HR}	1.39 ± 1.44	6.12 ± 5.05 ‡
$P_{\mathrm{BP}}^{\mathrm{LF}}$	0.0012 ± 0.002	0.0009 ± 0.002
$P_{\mathrm{BP}}^{\mathrm{HF}}$	0.0008 ± 0.001	0.0006 ± 0.001 †
α^{LF}	1.05 ± 1.63	1.84 ± 2.32 ∗
α^{HF}	0.85 ± 1.07	2.08 ± 3.91
f_{R}	0.23 ± 0.05	0.26 ± 0.07

Table 5.5: Median ± MAD of HRV, BPV and BRS indices for prone and resistant patients using information from the first 30 minutes. The symbols $\{*, \dagger, \ddagger\}$ represent p-values less than $\{0.05, 0.01, 0.001\}$, respectively.

Although they are two different classifiers, they can be seen as a decision tree where the diabetes variable decides which branch is activated. This way it can be considered as a global classifier whose performance improves by splitting diabetic and non diabetic patients (Acc=92.1%).

	Features selected	
	All indices	HRV indices
All patients	$R_{\mathrm{HR}}^{\mathrm{n}}$, R_{HR}	-
Diabetic	$R_{\mathrm{HR}}^{\mathrm{n}}$, $P_{\mathrm{HR}}^{\mathrm{LF}}$	$R_{\mathrm{HR}}^{\mathrm{n}}$, $P_{\mathrm{HR}}^{\mathrm{LF}}$
Non–diabetic	$R_{\mathrm{HR}}^{\mathrm{n}}$, α^{LF}	$R_{\mathrm{HR}}^{\mathrm{n}}$, R_{HR}

Table 5.6: Selected features using either all indices or only the HRV indices.

	All indices			HRV indices		
	Se	Sp	Acc	Se	Sp	Acc
All patients	97.5	54.5	88.2	-	-	-
Using diabetes information	97.5	72.7	92.1	95	72.7	90.2

Table 5.7: Classifier perfomance using all indices and HRV indices only

5.4.5 Classification based on HRV indices only

The results in the previous subsections shows that HRV indices carry most of the information for discriminating IDH prone and resistant patients, and therefore we constrain the analysis to only HRV indices, with diabetes information included. In this scenario, we also included the 2 patients (both diabetic and prone) which were

removed due to poor quality in the blood pressure signal (see Section 5.2), since blood pressure information is not used in this case, increasing the study population size.

The selected features are shown in Table 5.6, being $R^{\mathrm{n}}_{\mathrm{HR}}$ and $P^{\mathrm{LF}}_{\mathrm{HR}}$ for diabetic patients, and $R^{\mathrm{n}}_{\mathrm{HR}}$ and R_{HR} for non-diabetic patients. These results are very similar to the ones involving all types of indices where three out of four selected features were HRV-related. The performance of the HRV-based classifier is shown in Table 5.7: a slight decrease in accuracy (Acc = 90.2%) is observed.

5.4.6 Patient balance

The next step is to balance the P and R groups, by replicating information of each resistant patient two times. The goal is to minimize the effect of being the prone group much bigger than the resistant one, leading to a bias in the performance. The new R group consists of 21 patients (33 sessions) of which 9 are diabetic. The P group consists of 19 patients (46 sessions) of which 9 are diabetic.

The classification is repeated using only HRV indices and results can be seen in Table 5.8. Selected features are again $R^{\mathrm{n}}_{\mathrm{HR}}$ and $P^{\mathrm{LF}}_{\mathrm{HR}}$ for diabetic patients, and $R^{\mathrm{n}}_{\mathrm{HR}}$ and R_{HR} for non-diabetic patients. In this case, an increase in specificity is observed (72.7 to 83.4) at the expense of a decrease in sensitivity (95 to 87.8); the accuracy increases from 90.2 to 93.2.

5.4.7 Session balance

There is still an imbalance in the number of sessions per patient, with P patients having more sessions than R patients. By discarding sessions so that all patients had up to two sessions, the results were recomputed for the classifier based on HRV indices only and including diabetes information. A total of 10 sessions were discarded, chosen randomly for those patients with 3 and 4 sessions (all IDH prone). The database is still divided into diabetic (upper panel) and non diabetic (lower panel), while blue and orange represent IDH resistant and prone patients, respectively. The sensitivity increased from 87.8% to 94.3% and, and the specificity and accuracy decreased from from 83.4% to 70.5%, and from 93.2% to 88.7%, respectively, see Table 5.8. No differences were found in the selected features.

	Se	Sp	Acc
Patient balance	87.8	83.4	93.2
Session balance	94.3	70.5	88.7

Table 5.8: Classifier perfomance when balancing the groups.

5.5 Discussion

VLF modulation origin

The origin of this VLF modulation is still controversial. Several authors have studied this VLF modulation in HRV, relating it to fields like termoregulation mechanisms [159], renin-angiotensin-aldosterone systems and/or parasympathetic outflow [160]. It has also been reported during dry supine immersion and exposure to non-hypoxic hypobaria, as well as in sleep apnea events [161]. Our hypothesis is that this VLF modulation, which also appears in BPV and other series related to the ECG signal and respiration, may be related to an altered ANS response during hemodialysis treatment. P and R groups show significantly different maximum coherence values, although prone patients present a higher coherence between HRV and EDR, but lower coherence between BPV and EDR. The modulation frequency and the duration are also different, with prone patients having a lower frequency but longer duration. Diabetic patients also present a significantly lower frequency and longer duration than non diabetic patients. Looking at the subgroups, P+D and R+ND present the same differences in frequency and duration. These differences suggest that there are differences in the VLF modulation in patients prone and/or diabetic, which have altered ANS. However, these results are only based on the segments where the coherence was high enough. The VLF modulation only appears in short periods of time, which is less than 15% of the time for the majority of the patients, and it is very irregular, ranging from 5 minutes to one hour and a half, depending on the patient.

The main restriction in the VLF modulation characterization is that it needs to appear synchronously in HRV, BPV and angles series. When studying each signal separately, there are several segments where this modulation appears in HRV and angles series, but not in BPV. If the BPV series is removed and the duration ($T_{\%}$) is again computed, there is no significative differences with the previous value. Still, there are very few cases to extract a robust conclusion about this phenomenon.

The significant differences in the coherence values appear in the interaction between the rotation angles series with the other two series. The angles series are strongly related to respiration, which suggests that respiration may be one of the origins of this modulation. Actually, these very low frequency components in HRV have previously been associated to the modulation observed in periodic breathing [162]. The relation of this VLF modulation and respiration was further investigated in two works [163, 164], where the hypothesis was that the source of that modulation is respiration, either directly or through ANS which controls respiration, and that other non linearly related autonomic regulation effects are secondary. Both works tried to remove the influence of respiration using partial coherence between HRV and QRS slopes, [163] using the Sweden database described in Section 5.2 and the angle series as a surrogate of respiration, and [164] using a database consisting of patients with dilated cardiomyopathy and ischemic cardiomyopathy and the real respiratory signal. The results shows that after removing the influence of respiration, partial coherence presented a significative drop, sometimes dropping below the threshold, compared to ordinary coherence. This

decrease suggests that the origin of the VLF modulation can be partially explained by the linear effect of respiration. Still, there may be other effects, such as a nonlinear relation with respiration in the periodic breathing events, which contribute to the genesis of the observed VLF modulation.

The MVDR method has demonstrated to better characterized this VLF modulation compared to Welch periodogram thanks to its better frequency resolution, and it has been shown to perform well when the signal can be modelled as a sum of sinusoids [153]. However, this estimator is not a true power spectral density in the sense that the area under the MVDR spectrum does not represent the total power in the measured process, which should be a characteristic of a true power spectral density [165]. What it does correctly is to describe relative component powers over frequency, and it is particularly useful to obtain coherence values between different signals. Nevertheless, power parameters in LF and HF bands were also computed with Welch periodogram, and there were no different results than those presented in this work using MVDR method.

Discriminative indices

HRV indices have been thoroughly studied in the past, especially the ratio R_{HR} since it assesses cardiovascular autonomic regulation and reflects the activity of the sympathetic versus the parasympathetic branch [16]. It has been shown that patients prone to IDH exhibit a much lower ratio than do resistant patients [14]. Similar information is conveyed by $R^{\mathrm{n}}_{\mathrm{HR}}$, since it represents the normalized value of the power in the LF band relative to the sum of the LF and HF bands. Since this index also conveys information about the balance between the two ANS branches, it is expected to exhibit significant differences between the two patient groups.

Note that the election of the HF band was the classic 0.15-0.4 Hz instead of centering it around f_{R}. This decision was made to be able to compare with other similar works where the classic HF band is used. Moreover, we made sure that f_{R} was located within that band to make sure we are measuring correctly. In hemodialysis patients, f_{R} rarely goes up to high frequencies, but instead it may be the case that patients fall asleep and f_{R} decreases to frequencies in the LF band. In our database, during the first 30 minutes of the treatment this never happens. However, for the study where we analyze parameters from all the treatment, we removed any segments where this happened.

Regarding BRS, α^{LF} is significantly different between the two groups, implying impaired regulation of the heart rate in prone patients when a sudden drop in blood pressure occurs, i.e., at IDH. However, other studies have obtained conflicting results, claiming that the baroreflex mechanism is preserved and adequately activated during intradialytic hypotension [17]. In one BP parameter used in BRS, $P^{\mathrm{HF}}_{\mathrm{BP}}$, there are significant differences between prone and resistant patients (Table 5.4), reflecting that the blood pressure in prone patients is more unstable. This suggests that even though the vessels have reduced parasympathetic innervation, potentially not affecting BPV, it still can exist a secondary modulation given by the HRV that implies variability in

the blood volume at the ventricles leading to variability in the BP.

The statistical analysis based on the initial 30 min of the dialysis session is aiming to label the patient at the beginning of the treatment. Hence, the ECG and BP signals are not needed to be recorded during the whole treatment. The statistical analysis shows very similar results, with $R^{\mathrm{n}}_{\mathrm{HR}}$, R_{HR}, $P^{\mathrm{HF}}_{\mathrm{BP}}$ and α^{LF} being also discriminative. However, it is interesting that the analysis based on entire dialysis sessions will yield a slightly different result since the spectral indexes changes during the dialysis session. In particular, there are also differences in $P^{\mathrm{LF}}_{\mathrm{HR}}$ and $P^{\mathrm{LF}}_{\mathrm{BP}}$ between prone and resistant patients when using information of the whole dialysis session. This may mean that some differences between prone and resistant patients get larger as the treatment goes on.

Prone and resistant classification

The preferred classification framework is to have two disjunct groups: one for selecting the features and training the classifier, and another for evaluating the classifier. However, when only sparse data is available, feature selection and classifier training can be overfitted to the training data. This may not be representative enough, and thus the classifier would not work properly for the evaluation data. Using all data for training and evaluation leads to optimistically biased results, and thus we decided to use the k-fold crossvalidation method [158]. A value of $k = 1$ leave–one–patient–out crossvalidation was adopted for both feature selection and classifier training.

It should be noted that the standard leave-one-out method is not appropriate to use on the present database. This method involves "observations" which in this study translates to "patients". A patient can have 1, 2, 3 or even 4 different sessions, corresponding to different days. Different sessions from the same patient should not be treated as independent measurements. Due to this, the leave-one-out method analyzes patients instead of sessions in the present study.

The use of a linear classifier which is based in LDA makes results not optimal, since the features do not follow the assumption of normality and they are not independent. However, the data distribution is not known, and using any other non parametric method to estimate that distribution from the data may imply a risk of overfitting which could lead to a positive bias of the result. In this case, that risk is high due to the reduced number of patients.

Regarding the first classifier performance, the obtained specificity is lower than the sensitivity, influenced by the unequal numbers of prone and resistant patients. When taking information on diabetes into account, the specificity increases, and the overall accuracy improves. This result agrees with the hypothesis that the ANS of diabetic patients is dysfunctional. Furthermore, this result means that information on diabetes should be treated as another feature when training the classifier.

Since almost all of the selected indices are HRV related, it was natural to investigate classification performance solely based on HRV indices. Such a restriction is of interest since it has been shown that HRV can be estimated using finger photoplethys-

mography [166], a technology which is easier to use than the ECG. The present results show that just a minor drop in accuracy is observed for an HRV-based classifier, i.e., from 92.1% to 90.2% (Table 5.7).

An important limitation of the present study is that the dataset is rather small, and that the prone and resistant group are highly imbalanced. In order to avoid the bias in the results due to the P group being much larger than the R group, a simple replication technique has been employed [167], with which each R session is used three times. The replicated data has been assumed to be representative enough of the resistant group, which may be not true with such a small database. Using the replication technique, an increase in specificity is observed (72.7 to 83.4) at the expense of a decrease in sensitivity (95 to 87.8); the accuracy increases from 90.2 to 93.2.

Another limitation of the database is that the number of sessions varies from patient to patient. Limiting the number of sessions per patient yields to an increase in sensitivity but a decrease in specificty and accuracy. Since the removed sessions are considered to be dependent measurements, the performance is not expected to be very different.

HRV indices can be divided into linear (temporal and spectral, the latter used in this work) and non-linear indices. Temporal HRV indices were first also included in the analysis, but they showed a lower discriminative power between P and R patients, and they were removed from the study. Non-linear indices have previously shown good capability to predict arrhythmic risk [168], but their physiological interpretation is less clear than the one related to spectral indices. Although non-linear indices are related to certain methodological concerns, e.g, data length, such indices provide complementary information which may improve the classification of P and R patients, and therefore should be part of a future study.

Other information could also be used to improve classifier performance. Some authors claim that prone patients suffer from a decrease in peripheral vascular resistance, suggesting a possible cardiac underfilling [169]. It has also been reported that every patient has a relative blood volume which for prone patients is stable with low variability [170]. Other studies suggest that the count of ventricular premature beats and heart rate turbulence are related to IDH [16]. In addition to that, it is important to note that these results are obtained from a database composed of elderly renal failure patients, whose age, pathology and medication also affect ANS regulation over the heart.

Since the main limitation of this work is the small size of the database, it is proposed for a future work to repeat this analysis with a bigger data set. The use of other classifiers, such as quadratic classifiers or neural networks, could also improve the results [171]. Besides, it is proposed to use other features, derived from the photoplethysmographic (PPG) signal and heart rate turbulence signal [12, 172], premature ectopic beats analysis [173] or short term variability of oxygen saturation [146]. With more hypotension events, a feature selection could be performed to detect hypotension events.

5.6 Conclusion and extended work

Hemodialysis is a well-established treatment for patients with severe kidney problems. A serious problem during treatment is intradialytic hypotension (IDH), which occur in about 25% of all sessions, causing symptoms such as dizziness and vertigo, and possibly also premature termination of the session. The occurrence of IDH not only leads to higher costs and increased need for medical service, but, more seriously, to increased mortality. This study has focused in the non-invasive assessment of autonomic nervous system in patients undergoing hemodialysis treatment through cardiovascular signals variability analysis.

The VLF modulation observed in some patients has been characterized. This modulation has been observed in HRV, BPV and EDR signals (rotation angles series). To estimate the spectrum and cross-spectrum of the series in the VLF band, a high-resolution method has been used since it provides better resolution than Welch periodogram. With indices related to the VLF modulation, a statistical analysis has been performed to identify differences between IDH prone and resistant patients. Some differences have been found in the coherence values and the duration, the latter being higher in prone patients. However, only 2 sessions showed a modulation longer than 25% of the treatment, being in general much shorter and irregular. No relation has been found neither with the clinic history of the patients, nor with the hypotension events.

Additionally, the heart rate variability, blood pressure variability, baroreflex sensitivity and respiratory rate derived from the ECG have been analyzed and several indices have been extracted in order to study if they are able to discriminate between being IDH prone or resistant. They were analyzed using information from all the treatment, but also using only the first 30 minutes of the treatment, in both cases there were parameters related to HRV, BPV and BRS which could discriminate the patients. The latter was decided since it would be more efficient to develop a method to classify patients in the beginning of the treatment, when hypotensive events are unlikely to occur.

For the classifier, a leave–one–patient–out technique has been applied due to the small size of the database. A division into diabetic and non diabetic subgroups has been proved to improve the results, leading to a global classifier with Acc=92.1%. Using only HRV parameters, a patient can be classified as IDH prone or resistant with an accuracy of 90.2%, having the advantage of only needing the ECG signal. Balancing the groups to avoid biased results, as well as the number of sessions per patient, has lead to similar results, with accuracy values of 93.2% and 88.7% respectively.

Extended work

- **VLF modulation**

  As mentioned in 5.5, the relation of the VLF modulation and respiration was further investigated in two works [163, 164]. In [164], this modulation was stud-

ied in HRV and QRS slopes in patients with dilated cardiomyopathy and ischemic cardiomyopathy. A VLF modulation has been reported in the upward and downward QRS slopes series of patients with stable angina pectoris [174], synchronous with the VLF component of HRV [175]. In [163], the database used is the same as the database from Sweden used in this thesis. Ordinary coherence was obtained between HRV and QRS slopes in both studies. Then, to remove respiratory information, the partial coherence was computed removing the influence of the respiratory signal and the EDR signal (angles series), respectively. Results showed a significant decrease in partial coherence, which suggests that this modulation is explained, at least partially, by respiration.

- **IDH prediction**

  This study has focused in identifying IDH prone patients using cardiovascular signals to adapt the treatment for each patient. Even though, IDH events still happen everyday, and an early prediction and prevention can dramatically improve the quality of life for patients with an end stage renal disease. HRV parameters described in this work, together with heart rate turbulence (HRT) parameters were also used for predicting IDH events. The predictor is based on the one proposed in [12], which used the photoplethysmography signal. A patient-dependant threshold was added to this predictor based on HRV and HRT parameters, and doing so, the threshold can be adjusted to the patient's propensity to IDH. These results were published in [176].

Chapter 6

Autonomic Nervous System Assessment in Critically Ill Patients Undergoing a Cognitive Rehabilitation Therapy

6.1 Introduction

Autonomic nervous system plays an important role in the maintenance of systemic homeostasis, exerting a control on essential functions such as cardiac and respiratory functions, thermoregulation and hormonal secretion. Recent clinical and electrophysiological studies reveal a high incidence of ANS dysfunction in patients treated in medical and surgical intensive care unit (ICU) [177, 178]. Although the incidence of ANS dysfunction in critically ill patients is not exactly established, it is clear that its occurrence adversely impacts on clinical prognosis, mortality and morbidity [179].

ANS disturbances may produce diverse and unexpected consequences beyond the common deficits associated with the dysfunction of parasympathetic system. For in-

stance, critically ill patients are also at risk of neurocognitive impairments that may persist after hospital discharge. ICU-related neurocognitive impairments are particularly pronounced in regard to memory, executive functioning, attentional functions and speed processing [180, 181]. Consequences of these long-term neurocognitive impairments are far-reaching and adversely impact on patients' life, contributing to impaired ability to perform activities of daily living, to decreased quality of life of patients and relatives, to increased medical costs, and inability to return to work [182]. Although neurocognitive impairments are long-lasting and devastating for survivors, rehabilitation rarely occurs during or after critical illness.

Among various pathophysiological mechanisms proposed to explain neurocognitive impairments in critically ill patients, parasympathetic dysfunction leading cholinergic deficiency seems one of the most viable to explain the development of long-term sequelae. During critical illness a release of inflammatory mediators (e.g., cytokines) can spread to distant organs, including the brain through circumventricular organs and the choroid plexus, which have no blood brain barrier [183]. Increased levels of cytokines and other inflammatory mediators have been associated with neurocognitive impairments [184].

Studies have shown that the parasympathetic nervous system acts as a physiological regulator of the inflammatory response to immune system activation. Recently, a potential role of vagus nerve (i.e. vagal anti-inflammatory pathway) in inflammatory conditions has emerged, and it has been postulated that parasympathetic stimulation via vagus nerve reduces production of systemically active cytokines [185]. Decreased vagus nerve activity is associated with increased morbidity and mortality [186]. HRV analysis has been used successfully to assess vagal activity [187] and could serve to detect physiological deterioration or response to therapy in critically ill patients. Furthermore, prefrontal activation, which has also been related to changes in HRV, could help to strengthen the ANS integrity via the vagus nerve stimulation.

A cognitive rehabilitation (CR) is a behavioral therapy that has proven to be effective improving cognitive deficits in clinical populations with abnormalities in brain activation patterns. In a recent review authors conclude that neural changes associated with CR converge in frontal regions, including cingulate cortex, prefrontal and middle frontal areas [188], the same areas involved in the balance of sympathetic and parasympathetic branches of ANS.

The objective of this chapter is to explore the effect of the neurocognitive intervention targeted to improve prefrontal activation over ANS measured by HRV in a sample of critically ill patients.

6.2 Methods and materials

6.2.1 Database

17 critically ill patients were included in this study with the following inclusion criteria: patients aged 18 to 85 years, having received mechanical ventilation for at least

24 hours, scoring more than 8 on the Glasgow Coma Scale (GCS) and −1 to +1 on the Richmond Agitation Sedation Scale (RASS) and haemodynamically stable. Patients with previous neurologic pathology or focal brain injury before ICU admission, patients with serious psychiatric pathology or mentally retarded, and patients with sensory impairments were excluded from the study. Also, closest relatives agreed the subject to be included in the study. The clinical study was approved by the human subjects protection committe (CEIC). Diagnosis and clinical and sociodemographic characteristics of the sample are summarized in Table 6.1, presented as mean (M) and standard deviation (SD), unless otherwise noted.

Age (M,SD)		64.31	10.47
Gender (N,%)	Male	12	70.59
	Female	5	29.41
Diagnosis (N,%)	Intestinal perforation	3	17.65
	Peritonitis	3	17.65
	Septic shock	2	11.76
	Politrauma	2	11.76
	Pneumonia	2	11.76
	Hemorrhagic shock	1	5.88
	Toxic intake	1	5.88
	Pancreatitis	1	5.88
	Esophageal perforation	1	5.88
	Acute respiratory failure	1	5.88
APACHE-II (M,SD)		24.31	9.53
SOFA (M,SD)		9.5	4.53
RASS (M,SD)		1.13	2.26
Length of ICU stay, days (M,SD)		24.94	30.17
Duration of intubation, days (M,SD)		18.69	31.27
Duration of sedation, days (M,SD)		7.69	8.55
Septic Shock (N,%)		9	52.94
Cardiac arrest (N,%)		1	5.88

Table 6.1: Descriptives. *APACHE-II: Acute Physiology and Chronic Health Evaluation II; SOFA: Sequential Organ Failure Assessment; RASS: Richmond Agitation-Sedation Scale.*

Patients received the CR sessions in their own beds when they were alert and calm until discharge from the ICU. Sessions were guided by a neuropsychologist and supervised by an ICU nurse. Sessions aimed to provide cognitive stimulation and engagement through exercises, not necessarily obtaining correct answers. The exercises included in each session were determined by patients' alertness level and ability to raise each arm separately with elbow straight against gravity. Physiological data were

recorded 20 minutes before sessions (PRE), during sessions (SES), and after sessions (POS). During the monitorization, the ECG and the respiratory signal $r(n)$ were obtained at a sampling rate of 200 Hz using the BetterCare® system [189]. Other information include if the patients had a forced termination of the CR due to feeling tired, if patients were still mechanically ventiled (MV) during the CR and if they suffered from delirium.

6.2.2 Neurocognitive intervention

The Early Neurocognitive Rehabilitation in Intensive Care -ENRIC protocol- has been develop in Parc Tauli Hospital in order to apply cognitive stimulation in critically ill patients during ICU stay. The neurocognitive intervention is supported by an interactive platform of advanced signals and image computation, and includes a relaxation and low cognitive load exercises software specifically designed for critically ill patients. One of the main objectives of the module is to offer intuitive interaction, as well as a logical and natural response. Kinect, a Microsoft gesture recognizing device, capable of tracking an image of the distance between the user and the camera in real time, thus capturing user movements and gestures, is used. The stimulation module shows a pleasant and relaxing virtual environment where the patient can walk through. During the session time a virtual avatar goes along with the patient, orienting, motivating and inviting him/her to relax. In order to get this objective, different active and passive exercises through the virtual environment have been developed:

Passive exercises: These exercises focus on relaxation of the patient while simple attentional functions are stimulated. These passive exercises have been especially designed for patients with difficulties of mobility and alertness, due to their low interaction level.

Active exercises: These exercises focus on the cognitive stimulation of complex functions (i.e. complex attentional functions and executive functions), and therefore, these exercises involve high level of cognitive requirement.

The aim of these sessions was to provide cognitive stimulation and engagement through the exercises, not necessarily obtaining correct answers. Inclusion of exercises on each session was determined by alertness level and the patient's ability to raise each arm separately with elbow straight against gravity.

6.2.3 Data analysis

Spectral analysis is performed in consecutive 2 minute segments with an overlap of 1 minute. The classic periodogram is applied to the HRV and respiratory signal to obtain their power spectral densities.

Respiratory signal

The respiratory frequency in each interval is set as the frequency at which the power spectral density of the respiratory signal, $S_r(f)$, is maximum within the band [0.15, 0.8] Hz, and denoted as $f_{\mathrm{R}}^{\mathrm{I}}$. ICU patients usually have a high respiratory rate, usually above 0.4Hz, hence the necessity of an extended band. Additionally, due to the irregular pattern of respiration, specially from ventilated patients, there may not be a predominant component associated to respirtory rate.

To define the HF band, 2 eligible bands are proposed, always centered around $f_{\mathrm{R}}^{\mathrm{I}}$ and within the band between 0.15 Hz and half the mean heart rate. These 2 bands are: $\Omega_{\mathrm{HF}} = [f_{\mathrm{R}}^{\mathrm{I}}\text{-}0.075,\ f_{\mathrm{R}}^{\mathrm{I}}\text{+}0.075]$ Hz and $\Omega_{\mathrm{HFe}} = [f_{\mathrm{R}}^{\mathrm{I}}\text{-}0.15,\ f_{\mathrm{R}}^{\mathrm{I}}\text{+}0.15]$ Hz. Subsequently, the following ratio is obtained:

$$R_r = \frac{P_{\mathrm{HF}}^{\mathrm{R}}}{P_{\mathrm{HFe}}^{\mathrm{R}}} \tag{6.1}$$

where $P_{\mathrm{HF}}^{\mathrm{R}}$ is the power obtained within the spectral band Ω_{HF} and $P_{\mathrm{HFe}}^{\mathrm{R}}$ is the power obtained within the spectral band Ω_{HFe}. The superindex $^{\mathrm{R}}$ means that these powers are obtained from $S_r(f)$. If this ratio is above 0.7, it is considered that most of the power is located narrowly around $f_{\mathrm{R}}^{\mathrm{I}}$ and Ω_{HF} is used as the final HF band, otherwise the spectrum is more spread out and Ω_{HFe} is used to cover it.

Figure 6.1 and Figure 6.2 show example where Ω_{HF} and Ω_{HFe} are chosen, respectively.

HRV signal

The HRV signal, $m(n)$, is obtained using the TVIPFM model as described in Chapter 2. From the spectral density of each interval, $S_m(f)$, the power in the low and high spectral bands are obtained: P_{LF} for the LF band (0.04-0.15 Hz) and P_{HF} for the chosen HF band (centered at $f_{\mathrm{R}}^{\mathrm{I}}$). In addition, the total power in both LF and HF bands (P_{TOT}), and the normalized power in LF band with respect to P_{TOT} (P_{LFn}) are also computed. Figure 6.3 and Figure 6.4 show the HRV signal of the same patients shown in Figure 6.1 and Figure 6.2, respectively, with the chosen HF bands.

Each patient is characterized with each parameter computed as the median value of the central 5 segments before the CR ($P_{\mathrm{S}}^{\mathrm{PRE}}$), during the CR ($P_{\mathrm{S}}^{\mathrm{SES}}$) and after the CR ($P_{\mathrm{S}}^{\mathrm{POS}}$), with $S = \{LF, HF, LFn, TOT\}$. For the analysis, the changes in the power during SES with respect to the basal state (PRE) is obtained as $\Delta P_{\mathrm{S}}^{\mathrm{SES}} = (P_{\mathrm{S}}^{\mathrm{SES}} - P_{\mathrm{S}}^{\mathrm{PRE}})/P_{\mathrm{S}}^{\mathrm{PRE}}$. For changes in POS, the analysis are similar: $\Delta P_{\mathrm{S}}^{\mathrm{POS}} = (P_{\mathrm{S}}^{\mathrm{POS}} - P_{\mathrm{S}}^{\mathrm{PRE}})/P_{\mathrm{S}}^{\mathrm{PRE}}$.

6.3 Results

Results are presented for 3 different groups of patients: patients who did not suffer from delirium and were not MV (G1, 11 patients), patients who were MV (G2, 4

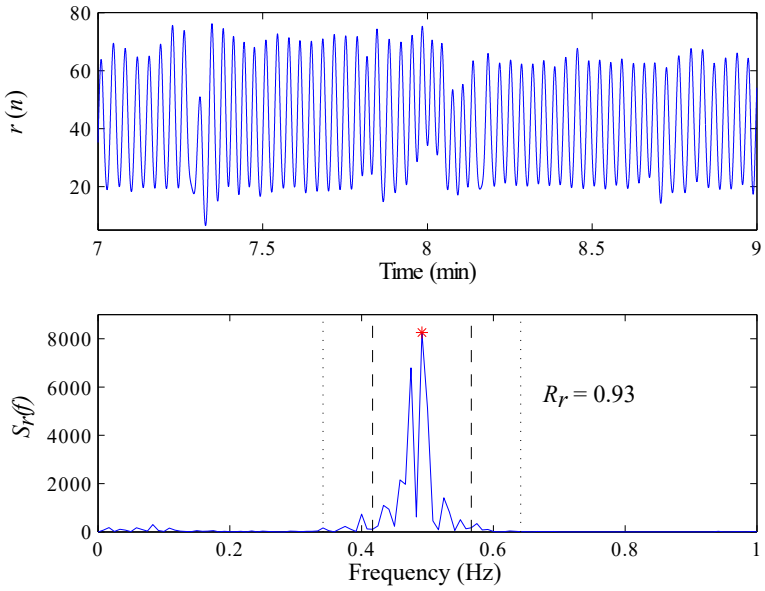

Figure 6.1: Example of an interval of respiratory signal $r(n)$ (upper panel) and its power spectral density $S_r(f)$ (lower panel) with R_r =0.93. Dashed lines delimit the spectral band Ω_{HF} and dotted lines delimit the spectral band Ω_{HFe}. $f_{\mathrm{R}}^{\mathrm{I}}$ is marked with a red asterisk.

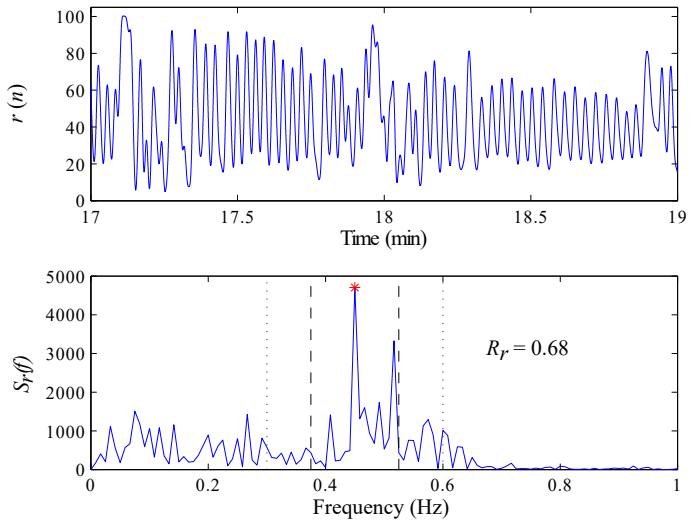

Figure 6.2: Example of an interval of respiratory signal $r(n)$ (upper panel) and its power spectral density $S_r(f)$ (lower panel) with R_r =0.68. Dashed lines delimit the spectral band Ω_{HF} and dotted lines delimit the spectral band Ω_{HFe}. $f_{\mathrm{R}}^{\mathrm{I}}$ is marked with a red asterisk.

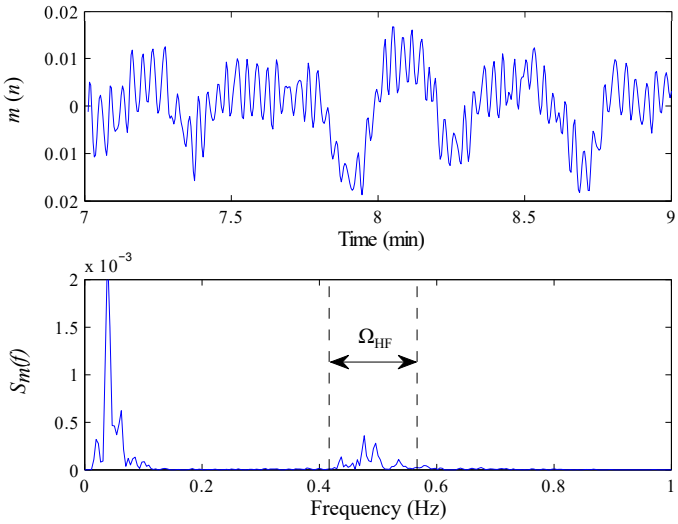

Figure 6.3: Example of an interval of $m(n)$ (upper panel) and its power spectral density $S_m(f)$ (lower panel). Dashed lines delimit the spectral band Ω_{HF}.

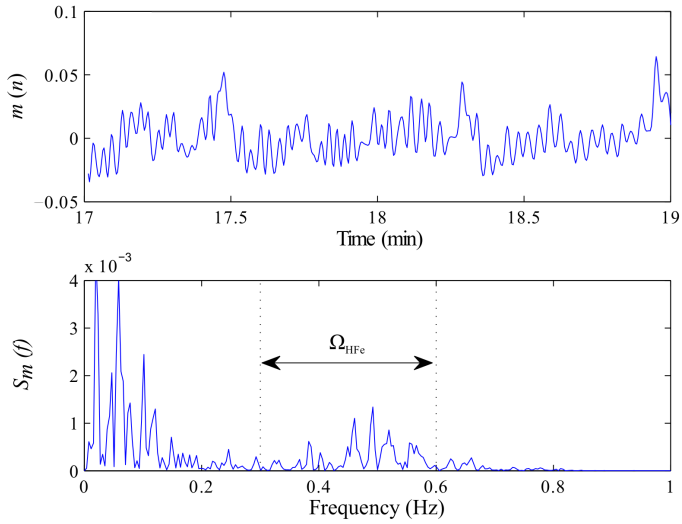

Figure 6.4: Example of an interval of $m(n)$ (upper panel) and its power spectral density $S_m(f)$ (lower panel). Dashed lines delimit the spectral band Ω_{HFe}.

patients), and patients who suffered from delirium (G3, 2 patients).

G1: During the session, 4 out of 11 patients present an increase in $\Delta P_{\mathrm{HF}}^{\mathrm{SES}}$ and $\Delta P_{\mathrm{TOT}}^{\mathrm{SES}}$ and a decrease in $\Delta P_{\mathrm{LFn}}^{\mathrm{SES}}$, 4 present the opposite response, and 3 present a decrease in the three parameters. 6 out of 11 patients show an increase in $\Delta P_{\mathrm{HF}}^{\mathrm{POS}}$ after the session and 4 of them also present a decrease in $\Delta P_{\mathrm{LFn}}^{\mathrm{POS}}$ and an increase in $\Delta P_{\mathrm{TOT}}^{\mathrm{POS}}$.

G2: 2 out of 4 patients had a forced termination of the cognitive rehabilitation due to feeling tired. The 2 patients who underwent the whole session present a decrease in all parameters during the intervention. After the session, those patients with a forced termination present a decrease in all parameters. The other two patients present opposite changes: one of them has an increase in $\Delta P_{\mathrm{HF}}^{\mathrm{POS}}$ and a decrease in $\Delta P_{\mathrm{LFn}}^{\mathrm{POS}}$, while the other has a decrease in $\Delta P_{\mathrm{HF}}^{\mathrm{POS}}$ and an increase in $\Delta P_{\mathrm{LFn}}^{\mathrm{POS}}$; however both present an increase in $\Delta P_{\mathrm{TOT}}^{\mathrm{POS}}$.

G3: There are 2 patients with delirium and both were also MV. Also, one of them had a forced termination of the session. During the session, both patients present an increase in $\Delta P_{\mathrm{HF}}^{\mathrm{SES}}$ and $\Delta P_{\mathrm{TOT}}^{\mathrm{SES}}$ and a decrease in $\Delta P_{\mathrm{LFn}}^{\mathrm{SES}}$. After the session, both patients present an increase in $\Delta P_{\mathrm{LFn}}^{\mathrm{POS}}$ and a decrease in $\Delta P_{\mathrm{HF}}^{\mathrm{POS}}$ while $\Delta P_{\mathrm{TOT}}^{\mathrm{POS}}$ decreases.

6.4 Discussion

HRV parameters are widely used to assess the ANS activity. In this work, power in the HF band is used as an index of the parasympathetic activity in critically ill patients, while the sympathetic activity is related to the normalized power in the LF band. Also, the total power is used as a measure of the variance of the HRV. Several researchers have demonstrated that low or decreasing HRV in ICU patients reflects greater severity of illness and predicts subsequent deterioration and mortality [190]. During mental and physical tasks, an increase in sympathetic activity has been observed [191]. Therefore, our hypothesis is that an activation of the sympathetic activity should be observed during the neurocognitive session due to the mental and physical effort. After the session, when cognitive and physical demands disappear, vagal system takes over and we expect that the parasympathetic activity should be increased.

Results during the session do not seem to follow any clear pattern. Results after the session are more promising, since there are 6 patients with a higher P_{HF} associated with a higher parasympathetic activity, and 4 of them also present a reduced sympathetic activity. This behavior dominates in the "moderately ill" patients, i.e., those who were not MV, did not suffer from delirium and did not have an abrupt termination of the neurocognitive intervention. This suggests that this therapy could improve the ANS balance in these patients, while other patients with worse conditions could need more sessions or even a different kind of intervention.

Some MV patients present a very irregular breathing signal. They do not adapt to the reference frequency and they are constantly fighting against the machine. These patients had also a forced termination of the session, and present a decrease in all parameters. However it is not clear if this decrease in the HRV power is related to

the irregular breathing or to the medication, there are very few MV patients in this database to extract any conclusion.

It remains unclear if delirium can be caused by an autonomic dysfunction. The only study published to date found no differences comparing patients with and without delirium in HF and low to high frequency ratio [192]. In our sample, patients suffering from delirium in the moment of the CR session showed an inverse pattern as we expected. It is possible that patients with delirium showed severe impairs in their attentional capacities that did not allow to follow the CR session, so intervention had no effect over ANS in these patients. Further investigations are needed to elucidate if neurocognitive therapies might have any effect on cognition in patients suffering from delirium states. It is important to consider that delirium patients in our sample were also MV, so interpretation of these results should be taken carefully.

Critically ill patients in medical and surgical ICUs are a highly heterogeneous group of patients (including a wide range age, ICU admission diagnosis and comorbidities). Therefore, HRV in critically ill patients may be affected by various factors (sedation, ventilator pattern, effect of drugs administered...); thus, the heterogeneity of the sample patients and the different clinical practices used are important limitations of this study. The extension of this work is to analyze subsequent sessions for each patient, and correlate the effect of the neurocognitive intervention on the ANS with the severity of the disease or other factors such as the effect of drugs they are taking. Also, further studies are needed involving a large number of critically ill patients.

Moreover, since this is an exploratory study, we decided to use simple methodologies to extract HRV parameters. However, these signals are highly non-stationary and can change very suddenly, which is expected in patients staying in the ICU. Other spectral methods which address the non-stationary nature of these signals are required, like the SPWVD distribution used in previous chapters. Regarding the choice of the width of the HF spectral band, Figure 6.4 suggests that increasing the band symmetrically may not be always the best option. It can be improved by continuously adapting the band based on the instantaneous power in the respiratory signal spectrum using techniques like spectral coherence. Additionally, the measurement in the HF band in MV patients needs to be explored to better understand the relation of HF spectral components and ANS activations. More robust methods will be used when extending this work to the new database.

6.5 Conclusion

This study analyses the autonomic nervous system activity by analysing the spectral parameters of the heart rate variability in critically ill patients who undergo cognitive rehabilitation. The neurocognitive intervention using virtual reality is feasible to deliver, safe, tolerable and well-accepted for critically ill patients, and suitable for stimulating cognitive functions. Comparing with baseline values, 7 patients showed an increase in the HF power after the session, suggesting an increase of parasympathetic activity, while 5 of them presented a decrease in the normalized LF power, suggesting

a decrease of the sympathetic activity. However, critically ill patients are very diverse, already have altered the ANS and they take medicines which also modify its behaviour. These preliminary results establish the first stage in implementing such intervention on a larger scale aimed to evaluate their efficacy.

Chapter 7

Conclusions and future work

7.1 Summary and conclusions

The objective of this thesis was to extract information about ANS state from cardiovascular signals, mainly HRV, and respiratory information in non-stationary environments. For this purpose, we have addressed the necessity to develop robust methodologies adapted to each scenario to make sure that measurements allow us to correctly interpret changes in ANS activity.

Three different scenarios have been presented. The first scenario is *HRV in exercise testing*: a methodological framework has been presented which addresses all the main limitation in exercise databases. It was applied to study ANS response of athletes to running and cycling stress testings. Then, the clinical value of exercise HRV assessed using the proposed methodology was studied in coronary artery disease diagnosis. The second scenario is *HRV in hemodialysis*: HRV, BPV, BRS and respiration were studied with the aim to identify hypotension prone and resistant patients. The third scenario is *HRV in ICU patients*: HRV measurements were proposed in an exploratory study as markers of ANS integrity after early cognitive rehabilitation in critically ill patients.

7.1.1 HRV in exercise testing

The main contribution in this part has been the development of a robust methodological framework suitable for HRV analysis during exercise. The limitations in HRV

analysis during exercise include the noisy and non-stationary nature of HRV during exercise, changes in mean HR and high and varying respiratory rate. To have a better QRS detection in the noisy ECG, an evolutionary algorithm has been applied to optimize some of the parameters of the detector. The HRV signal has been computed based on the TVIPFM model, which takes into account the high variations in the mean heart rate expected during exercise. Also, to extract the spectral parameters, the SPWVD method has been applied, which is a time-frequency analysis that allows to extract instantaneous power parameters. Since the respiratory frequency varies during exercise, usually reaching high frequencies, the HF band is needed to be redefined. Moreover, spectral components related to cardiolocomotor coupling have been identified in the HRV spectrum, and a correction has been applied whenever this component overlaps with the HF component.

This framework has been applied to three different exercise tests in order to study the response of ANS to the stress of exercise in healthy subjects: one maximal test on a treadmill, and two submaximal tests on a cyclo ergometer. Information about the maximal test is used to extract each subject's maximum value of oxygen consumption. Different intervals are determined in each test: one related to the resting phase, and the rest based on the level of oxygen consumption. Normalized powers related to LF and HF components are analyzed in these intervals: in the first exercise interval, during low intensities of exercise, LF increases as a response of an activation of the sympathetic nervous system, while there is a decrease in HF following the inhibition of the parasympathetic activity. During high intensities of exercise, however, HF increases while LF decreases since now HF power does not only reflect autonomic response, but also the increasing mechanical effect of breathing. CC power, related to the cardiolocomotor coupling, increases with the intensity of exercise, reaching up to 30% of the total power in the last intervals, being higher in the treadmill tests.

Additionally, a heart rate monitor has been validated in terms of HRV measurements. RR series were adquired simultaneously from the ECG and a Polar device during dynamic exercise of low, medium and high intensity. Reliability and agreement coefficients show that both methods are interchangeable when measuring instantaneous mean heart rate and LF power, regardless of the level of exercise (reliability and agreement > 0.9). However, instantaneous HF power measurements present reliability and agreement coefficients lower than 0.7 in the last intervals of the exercise phase. In spite of this low agreement and reliability, when computing the HRV parametrs as the mean value in the analyzed intervals and addressing the CC spectral components, no significant differences were found between the ECG and Polar measurements. Both parameters describe the same ANS response to the exercise stress. As a result, the use of HRV measurements from the Polar device is appropriate regardless the intensity of exercise.

HRV analysis has also been applied to exercise test with the aim of determining the diagnostic performance of HRV measurements during exercise in the detection of CAD. These patients present a high number of abnormalities in the RR series, mainly due to arrhythmic events, therefore special care is needed in the selection of the interval to analyze. Moreover, due to the effect of medications and differences in

exercise duration between CAD and low-likelihood CAD groups (CAD vs LLC), it was seen that mean HR and respiratory frequency cannot be reliably used to diagnose CAD: the former presents significant differences even at rest, and the latter presents differences at the peak of exercise, since LLC group have longer exercise phases and thus the respiratory frequency is higher. HF power, when guided by respiration, achieves the highest AUC, above 0.7 both in rest and in recovery. When measuring in intervals with a similar metabolic demand, based on the increment in the mean HR, a significant difference can be observed in the last interval of exercise between LLC and CAD patients, with lower normalized LF power and higher HF power (both normalized and absolute power) in CAD patients, suggesting that HRV parameters can diagnose CAD before finishing the exercise test. Due to the lack of cadence frequency information, the CC component cannot be corrected, and the use of an extended band for HF power will surely measure additional spectral components. This emphasizes the necessity of a standard methodology for HRV analysis during exercise.

7.1.2 HRV in hemodialysis

The hypothesis behind this study is that intradialytic hypotension (IDH) prone patients present an impairment in autonomic regulation of the cardiovascular system. Different parameters have been proposed to differenciate between IDH prone and resistant patients. HRV parameters have previously demonstrated their capability in this goal, but we have also added information from blood pressure variability (BPV) and respiration by means of ECG derived respiratory (EDR) signals to improve the IDH state diagnosis. In particular, the EDR signals are the rotation angles series which describes the rhythmically movements of the electric axis of the heart due to respiration. A VLF was found presented in HRV, BPV and angles series, and it was characterized with the hypothesis that it was caused by the hemodinamic inestability of IDH patients. A MVDR method was applied to extract parameters in the VLF band since, in general, it presents a better frequency resolution than other spectral estimators. All these parameters were analyzed individually, where respiratory frequency showed no apparent correlation with the IDH status of the patient. VLF parameters showed that this modulation appears more often in prone patients and may be related with an altered ANS. Some of the parameters related to HRV (normalized LF and ratio), BPV (HF) and BRS (LF) were indeed able to discriminate between both groups.

The rest parameters from HRV, BPV and BRS were used to design a classifier that, using information of the first 30 minutes of the treatment, is able to classify IDH prone and resistant patients. With an early identification of IDH prone patients, the treatment can be properly adjusted to their necessities. The classifier was trained using a leave-one-patient-out method (due to the small size of the database), where all recordings belonging to the same patients were left out of the training, and the process was repeated for each patient. The process of features selection was performed using a SFFS approach, with both selecting and removing features until the best set is found. We also found that including information of the diabetes state of the patients, the overall performance of the classifier improved, reaching values of sensitivity and

accuracy of Se=97.5% and Acc=92.1%. Since the majority of parameters were found to be HRV related, mainly the ratio of LF/HF powers and the normalized LF power, we proposed to design a classifier with only HRV parameters, having the advantage of not needing to record blood pressure. This new classifier achieved Se=95% and Acc=90.2%.

7.1.3 HRV in ICU patients

Critically ill patients present alterations in ANS which can persist even after hospital discharge. In particular, it has been observed an increasing number of cases of neurocognitive impairments. Several studies have shown that the parasympathetic nervous system acts as a physiological regulator of the inflammatory response to immune system activation, and suggested that a parasympathetic stimulation could avoid the neurocognitive impairments. A neurocognitive rehabilitation has been suggested for these patients to effectively improve cognitive deficits in clinical populations with abnomalities in brain activation patterns. In this scenario, HRV parameters have been proposed to explore the impact of this neurocognitive rehabilitation in ICU patients and as a novel marker of ANS integrity in these patients.

HRV analysis for ANS assessment in ICU patients has not been fully explored, mainly due to the numerous limitations. ICU patients takes a great number of medication which alter ANS activity, some of them are mechanically ventilated, other suffer from delirum (which is unclear if it is caused by an autonomic dysfunction), and in general they are a highly heterogeneous group of patients. In this exploratory study, we have tried to analyze HRV parameters in the most possible homogeneous groups of the initial database. Respiratory information has been included in the HRV analysis, and to address the highly irregular breathing pattern of some patients, the spectral band related to HF component has been accordingly adapted for each patient. Comparing with baseline values, 7 patients showed an increase in the HF power after the session, suggesting an increase of parasympathetic activity, while 5 of them presented a decrease in the normalized LF power, suggesting a decrease of the sympathetic activity. These results need to be interpretated with special care due to the patients characteristics, who already have altered the ANS and they take medicines which also modify its behaviour. A larger database with more controlled factors is being recorded at the moment with the aim to continue exploring the capability of HRV measurements to assess ANS integrity in these patients.

7.2 Conclusion

HRV is the most used tool to study ANS activity. However, many different studies present contradictory results when analyzing HRV in non stationary signals, mainly due to a lack of a standard methodology. This thesis has presented a methodological framework to analyze HRV in non stationary environments to assess ANS activity. This framework has been adapted for each application to address the different limitations

presented for each scenario. As we have seen, HRV analysis needs to be guided by respiratory information, and other cardiovascular variability signals can add value to the interpretation of the ANS activity. We want to emphasize the necessity to choose a proper methodology to make sure that measurements allow us to correctly interpret changes in ANS activity.

7.3 Future work

Future research lines derived from this thesis are:

- Parameters from the QRS detector have been optimized to correctly perform on exercise recordings. The training database has been chosen to deal with noise from baseline wander, muscle artifact and electrode motion artifacts. These types of noise, although present in exercise databases, could not be the only source of misdetections of our detector. The new proposal is to additionally train the algorithm with real noise from different exercise databases to better optimize the parameters, explore more parameters to optimize, or even redefine the detector and include changes in beat morphology induced by exercise.

- HRV analysis during sport has different applications. A follow up study of subjects who often practice sport would show how the ANS adapts to maintained level of physical activity. Following this adaptation to the stress of exercise, HRV parameters measured could be used to try to predict the maximum value of oxygen consumption and aerobic and anaerobic thresholds, very important parameters for athletes. Moreover, one limitation of our study is that our analysis was applied to only men subjects. This analysis should be extended also to women, and groups with different range of ages and physical activity to better understand how the ANS respond to the stress of exercise.

- The study of CAD diagnosis by means of HRV could improve if we include information of medication. Moreover, spectral analysis would improve with the cadence frequency, which was not recorded. It could however be estimated from changes in the baseline wander or the angles series. This approach can be validated with the athletes' database, from which we have the cadence frequency information.

- Autonomic imbalance may trigger mechanical and electrical complications, leading to sudden cardiac death (SCD). The overall annual incidence of SCD based on extrapolation of data from the United States is approximately 1 in 1000 adults over the age of 35 years [193]. Several studies have proposed HRV analysis as a predictor of sudden cardiac death, from temporal-domain, frequency domain and non-linear indices, suggesting that HRV paramters can be used as a predictor of SCD [194–196]. Our proposed methodology could be applied to FINCAVAS database and study HRV paramters during exercise in patients who suffered sudden cardiac death.

- The main limitation of the critically ill patients study was the small size of the database and its heterogeneity. Currently, a new database is being recorded in Parc Tauli Hospital with more patients and HRV will be used to explore the ANS integrity in these patients before and after the neurocognitive intervention. Additionally, HRV can be influenced by certain drugs typically prescribed in ICU (among which include anticholinergic drugs, agents with effect on adrenergic receptors, angiotensin-converting enzyme inhibitors or even calcium channel blockers), as well as the severity level of critical illness (APACHE-II score at ICU admission and SOFA scores during ICU stay), so the effect will be considered while analyzing HRV in all subsequent analysis.

- Disposing information about autonomic function, via HRV analysis, in a large sample of critically ill patients in ICU could lay the groundwork for implementing HRV analysis in other clinical decisions in the routinely management of critically ill patients. For example, since autonomic dysfunction has been associated with extubation failure in mechanically ventilated patients, results of HRV could be useful in predicting success of weaning from mechanical ventilation in critically ill patients, thereby decreasing reintubation rate and the adverse effects associated.

Bibliography

[1] L. McCorry, "Physiology of the autonomic nervous system," *Am J Pharm Educ*, vol. 71(4), p. 78, 2007.

[2] A. Zygmunt and J. Stanczyk, "Methods of evaluation of autonomic nervous system function," *Arch Med Sci*, vol. 6(1), pp. 11–18, 2010.

[3] W. A. Scott, "Assessment of the autonomic nervous system," in *Moss and Adams heart disease in infants and adolescents including the fetus and young adult* (Williams & Wilkins, ed.), 1995.

[4] C. J. Mathias, "Autonomic diseases: clinical features and laboratory evaluation," *J Neurol Neurosurg Psychiatry*, vol. 74(3), pp. iii31–41, 2003.

[5] A. E. Draghici and J. A. Taylor, "The physiological basis and measurement of heart rate variability in humans," *J Physiol Anthropol*, vol. 35(22), 2016.

[6] Working group of ESC, "Heart rate variability. Standards of measurement, physiological interpretation, and clinical use," *Eur Heart J*, vol. 17, pp. 354–381, 1996.

[7] J. Borresen and M. Lambert, "Autonomic control of heart rate during and after exercise: measurements and implications for monitoring training status," *Sports Med*, vol. 38(8), pp. 633–646, 2008.

[8] K. Hottenrott, O. Hoos, and H. Esperer, "Heart rate variability and physical exercise. Current status," *Herz*, vol. 31(6), pp. 544–552, 2006.

[9] R. Bailón, P. Serrano, and P. Laguna, "Influence of time–varying mean heart rate in coronary artery disease diagnostic performance of heart rate variability indices from exercise stress testing," *J Electrocardiol*, vol. 44, pp. 445–452, 2011.

[10] R. Bailón, N. Garatachea, I. de la Iglesia, JA. Casajús, and P. Laguna, "Influence of running stride frequency in heart rate variability analysis during treadmill exercise testing," *IEEE Trans Biomed Eng*, vol. 60(7), pp. 1796–1805, 2013.

[11] A. Aubert, B. Seps, and F. Beckers, "Heart rate variability in athletes," *Sports Med*, vol. 33(12), pp. 889–919, 2003.

[12] K. Solem, B. Olde, and L. Sörnmo, "Prediction of intradialytic hypotension using photoplethysmography," *IEEE Trans Biomed Eng*, vol. 57, pp. 1611–1619, 2010.

[13] G. Pelosi, M. Emdin, C. Carpeggiani, M. A. Morales, M. Piacenti, P. Dattolo, T. Cerrai, A. Macerata, A. L'Abbate, and Q. Maggiore, "Impaired sympathetic response before intradialytic hypotension: A study based on spectral analysis of heart rate and pressure variability," *Clin. Sci. (Lond)*, vol. 96, pp. 23–31, 1999.

[14] S. Cavalcanti, L. Chiari, S. Severi, and G. Avanzolini, "Spectral analysis of heart rate variability during hemodialysis in stable and unstable patients," *Proc. of Computers in Cardiology*, pp. 119–122, 1995.

[15] S. Cavalcanti, S. Severi, and G. Enzmann, "Analysis of oscillatory components of short-term heart rate variability in hemodynamically stable and unstable patients during hemodialysis," *Artif. Organs*, vol. 22, pp. 98–106, 1998.

[16] L. Sörnmo, F. Sandberg, E. Gil, and K. Solem, "Noninvasive techniques for prevention of intradialytic hypotension," *IEEE Rev Biomed Eng*, vol. 5, pp. 45–59, 2012.

[17] D. Sapoznikov, R. Backenroth, and D. Rubinger, "Baroreflex sensitivity and sympatho–vagal balance during intradialytic hypotensive episodes," *J Hypertension*, vol. 28(2), pp. 314–324, 2010.

[18] L. J. Chesterton, M. N. Selby, J. O. Burton, and C. W. McIntyre, "Cool dialysate reduces asymptomatic intradialytic hypotension and increases baroreflex variability," *Hemodial. Int.*, vol. 13, pp. 189–196, 2009.

[19] J. Saul, R. Berger, P. Albrecht, S. Stein, M. Chen, and R. Cohen, "Transfer function analysis of the circulation: unique insights into cardiovascular regulation," *Am. J. Physiol. Heart Circ. Physiol*, vol. 261(4), pp. H1231–H1245, 1991.

[20] R. Barbieri, A. Bianchi, J. Triedman, L. Mainardi, S. Cerutti, and J. Saul, "Model dependency of multivariate autoregressive spectral analysis," *IEEE Eng. Med. Biol. Mag.*, vol. 16(5), pp. 74–85, 1997.

[21] M. Orini, R. Bailón, P. Laguna, L. Mainardi, and R. Barbieri, "A multivariate time-frequency method to characterize the influence of respiration over heart period and arterial pressure," *EURASIP Journal on Advances in Signal Processing*, p. 214, 2012.

[22] J. Jackson, R. Hart, S. Gordon, A. Shintani, B. Truman, L. May, and E. Ely, "Six–month neuropsychological outcome of medical intensive care unit patients," *Crit Care Med.*, vol. 31, pp. 1226–1234, 2003.

[23] A. Guyton and J. Hall, *Textbook of Medical Physiology.* Philadelphia: Elsevier Inc., 2006.

[24] R. Hainsworth, "The control and phisiological importance of heart rate," in *Heart rate variability* (M. Malik and J. A. Camm, eds.), ch. 1, Futura Publishing Company, Inc., 1995.

[25] L. Sörnmo and P. Laguna, *Bioelectrical Signal Processing in Cardiac and Neurological Applications*. Amsterdam: Elsevier, 2005.

[26] S. R. Braun, "Respiratory Rate and Pattern. Clinical Methods: The History, Physical, and Laboratory Examinations.," in *Clinical Methods: The History, Physical, and Laboratory Examinations.* (H. K. Walker, W. D. Hall, and J. W. Hurst, eds.), ch. 43, Boston: Butterworths, 3 ed., 1990.

[27] C. Guilleminault, J. G. Briskin, M. S. Greenfield, and R. Silvestri, "The impact of autonomic nervous system dysfunction on breathing during sleep," *Sleep*, vol. 4(3), pp. 263–278, 1981.

[28] K. Narkiewicz and V. K. Somers, "The sympathetic nervous system and obstructive sleep apnea: implications for hypertension," *J Hypertens*, vol. 15(12), pp. 1613–1619, 1997.

[29] M. J. Lewisa, A. L. Shorta, and K. E. Lewisb, "Autonomic nervous system control of the cardiovascular and respiratory systems in asthma," *Respir Med*, vol. 100(10), pp. 1688–1705, 2006.

[30] J. Kallenbach, T. Webster, R. Dowdeswell, S. Reinach, R. Millar, and S. Zwi, "Reflex heart rate control in asthma. Evidence of parasympathetic overactivity," *Chest*, vol. 87, pp. 644–648, 1985.

[31] J. P. Ribeiro, "Periodic breathing in heart failure: bridging the gap between the sleep laboratory and the exercise laboratory," *Circulation*, vol. 113(1), pp. 9–10, 2006.

[32] D. L. Eckberg, "Point:counterpoint: respiratory sinus arrhythmia is due to a central mechanism vs. respiratory sinus arrhythmia is due to the baroreflex mechanism," *J Appl Physiol*, vol. 106(5), pp. 1740–1742, 2009.

[33] R. W. deBoer, J. M. Karemaker, and J. Strackee, "Hemodynamic fluctuations and baroreflex sensitivity in humans: a beat-to-beat model," *Am. J. Physiol.*, vol. 253, pp. H680–H689, 1987.

[34] S. B. G. Blain, O. Meste, "Influences of breathing patterns on respiratory sinus arrhythmia in humans during exercise," *Am. J. Physiol. Heart Circ. Physiol.*, vol. 288(2), pp. H887–H895, 2005.

[35] C. Julien, M. J. Parkes, S. Y. C. Tzeng, P. Y. W. Sin, P. N. Ainslie, P. van de Borne, J. O. Fortratand, M. A. Custaud, C. Gharib, A. Porta, F. Vallais, G. Baselli, M. Pagani, D. Lucini, R. L. Hughson, J. A. Taylor, C. O. Tan, D. M. Baekey, T. E. Dick, J. F. R. Paton, and B. Taha, "Comments on point:counterpoint: respiratory sinus arrhythmia is due to a central mechanism

vs. respiratory sinus arrhythmia is due to the baroreflex mechanism," *J Appl Physiol*, vol. 106(5), pp. 1745–1749, 2009.

[36] A. E. Hedman, K. U. Tahvanainen, J. E. Hartikainen, and M. O. Hakumäki, "Effect of sympathetic modulation and sympatho-vagal interaction on heart rate variability in anaesthetized dogs," *Acta Physiol Scand*, vol. 155, pp. 205–214, 1995.

[37] M. Kollai and G. Mizsei, "Respiratory sinus arrhythmia is a limited measure of cardiac parasympathetic control in man," *J Physiol.*, vol. 424, pp. 329–342, 1990.

[38] R. Bailón, L. Sörnmo, and P. Laguna, "Ecg-derived respiratory frequency estimation," in *Advanced methods and tools for ECG data analysis* (G. Clifford, F. Azuaje, and P. E. McSharry, eds.), ch. 8, Artech House, 2006.

[39] J. Lázaro, A. Alcaine, D. Romero, E. Gil, P. Laguna, E. Pueyo, and R. Bailón, "Electrocardiogram derived respiratory rate from QRS slopes and R-wave angle.," *Annals Biomedical Enginnering*, vol. 40(10), pp. 2072–2083, 2014.

[40] R. Bailón, L. Sörnmo, and P. Laguna, "A robust method for ECG-based estimation of the respiratory frequency during stress testing," *IEEE Trans Biomed Eng*, vol. 53, no. 7, pp. 1273–1285, 2006.

[41] N. Charkoudian and J. A. Rabbitts, "Sympathetic neural mechanisms in human cardiovascular health and disease," *Mayo Clin Proc*, vol. 84(9), pp. 822–830, 2009.

[42] E. J. Bayly, "Spectral analysis of pulse frequency modulation in the nervous systems," *IEEE Trans. on Biomedical Engineering*, vol. 15, pp. 257–265, 1968.

[43] O. Meste, H. Rix, and G. Blain, *ECG processing for exercise test.* Advanced Biosignal Processing, Springer, 2009.

[44] J. Sacha and W. Pluta, "Alterations of an average heart rate change heart rate variability due to mathematical reasons," *Int. J. Cardiol*, vol. 128, pp. 444–447, 2008.

[45] J. Sacha, S. Barabach, G. Statkiewicz-Barabach, K. Sacha, A. Müller, and J. Piskorski, "How to strengthen or weaken the hrv dependence on heart rate â Description of the method and its perspectives," *Int. J. Cardiol*, vol. 168, pp. 1660–1663, 2013.

[46] R. Bailón, G. Laouini, C. Grao, M. Orini, P. Laguna, and O. Meste, "The integral pulse frequency modulation with time–varying threshold: Application to heart rate variability analysis during exercise stress testing," *IEEE Trans Biomed Eng*, vol. 58(3), pp. 642–652, 2011.

[47] R. Sassi, S. Cerutti, F. Lombardi, M. Malik, H. V. Huikuri, C. K. Peng, G. Schmidt, and Y. Yamamoto, "Advances in heart rate variability signal analysis: joint position statement by the e-Cardiology ESC Working Group and

the European Heart Rhythm Association co-endorsed by the Asia Pacific Heart Rhythm Society," *Europace*, vol. 17(9), pp. 1341–1353, 2015.

[48] A. U. Rajendra, J. K. Paul, N. Kannathal, C. Lim, and J. Suri, "Heart rate variability: a review," *Med Biol Eng Comput*, vol. 44, pp. 1031–1051, 2006.

[49] M. Pagani, F. Lombardi, and S. Guzzetti, "Power spectral analysis of heart rate and arterial pressure variabilities as a marker of sympatho–vagal interaction in man and conscious dogs," *Circulation Research*, vol. 59, pp. 178–193, 1986.

[50] A. Malliani, M. Pagani, F. Lombardi, and S. Cerutti, "Cardiovascular neural regulation explored in the frequency domain," *Circulation*, vol. 84, pp. 482–492, 1991.

[51] J. A. Wijbenga, A. H. Balk, S. H. Meij, M. L. Simoons, and M. Malik, "Heart rate variability index in congestive heart failure: relation to clinical variables and prognosis," *Eur Heart J*, vol. 19(11), pp. 1719–1724, 1998.

[52] M. Rothschild, A. Rothschild, and M. Pfeifer, "Temporary decrease in cardiac parasympathetic tone after acute myocardial infarction," *Am J Cardiol*, vol. 18, pp. 637–639, 1988.

[53] B. Wennerblom, L. Lurje, J. Solem, H. Tygesen, M. Udén, R. Vahisalo, and A. Hjalmarson, "Reduced heart rate variability in ischemic heart disease is only partially caused by ischemia. An HRV study before and after PTCA," *Cardiology*, vol. 94(3), pp. 146–151, 2000.

[54] M. K. Mandawat, D. R. Wallbridge, S. D. Pringle, A. A.Riyami, S. Latif, P. W. Macfarlane, A. R. Lorimer, and S. M. Cobbe, "Heart rate variability in left ventricular hypertrophy," *Br Heart J*, vol. 73(2), pp. 139–144, 1995.

[55] F. H. Messerli, H. O. Ventura, D. J. Elizardi, F. G. Dunn, and E. D. Frohlich, "Hypertension and sudden death. Increased ventricular ectopic activity in left ventricular hypertrophy," *Am J Med*, vol. 77(1), pp. 18–22, 1984.

[56] D. J. Ewing and R. Winney, "Autonomic function in patients with chronic renal failure on intermittent haemodialysis," *Nephron*, vol. 15(6), pp. 424–429, 1975.

[57] R. I. Lowensohn, M. Weiss, and E. H. Hon, "Heart–rate variability in brain–damaged adults," *Lancet*, vol. 1, pp. 626–628, 1977.

[58] R. M. Carney, J. A. Blumenthal, P. K. Stein, L. Watkins, D. Catellier, L. F. Berkman, S. M. Czajkowski, C. O'Connor, P. H. Stone, and K. E. Freedland, "Depression, heart rate variability, and acute myocardial infarction," *Circulation*, vol. 104, p. 2024, 2001.

[59] H. Bonnemeier, U. K. H. Wiegand, A. Brandes, N. Kluge, H. A. Katus, G. Richardt, and J. Potratz, "Circadian profile of cardiac autonomic nervous modulation in healthy subjects: Differing effects of aging and gender on heart rate variability," *J Cardiovasc Electrophysiol*, vol. 14, pp. 8791–8799, 2003.

[60] Y. Yamasaki, M. Kodama, and M. Matsuhisa, "Diurnal heart rate variability in healthy subjects: effects of aging and sex differences," *Am J Physiol*, vol. 271, pp. 303–310, 1996.

[61] P. Coumel, J. S. Hermida, B. Wennerblom, A. Leenhardt, P. Maison-Blanche, and B. Cauchemez, "Heart rate variability in left ventricular hypertrophy and heart failure, and the effects of beta–blockade," *Eur Heart J*, vol. 12, pp. 412–422, 1991.

[62] S. C. Malpas, E. A. Whiteside, and T. J. Maling, "Heart rate variability and cardiac autonomic function in men with chronic alcohol dependence," *Br Heart J*, vol. 65, pp. 84–88, 1991.

[63] J. Hayano, M. Yamada, Y. Sakakibara, T. Fujinami, K. Yokoyama, Y. Watanabe, and K. Takata, "Short– and long–term effects of cigarette smoking on heart rate variability," *Am J Cardiol*, vol. 65, pp. 84–88, 1990.

[64] M. D. Rienzo, P. Castiglioni, and G. Parati, "Arterial blood pressure processing," *Wiley Encyclopedia of Biomedical Engineering*, 2006.

[65] N. Montano, T. Gnecchi-Ruscone, A. Porta, F. Lombardi, A. Malliani, and S. M. Barman, "Presence of vasomotor and respiratory rhythms in the discharge of single medullary neurons involved in the regulation of cardiovascular system," *J. Auton. Nerv. Syst.*, vol. 57, pp. 116–122, 1996.

[66] M. D. Rienzo, G. Bertinieri, G. Mancia, and A. Pedotti, "A new method for evaluating the baroreflex role by a joint pattern analysis of pulse interval and systolic blood pressure series," *Med. Biol. Eng. Comput.*, vol. 23(1), pp. 313–314, 1985.

[67] B. E. Westerhof, J. Gisolf, W. J. Stok, K. H. Wesseling, and J. M. Karemaker, "Time–domain cross–correlation baroreflex sensitivity: Performance on the EUROBAVAR data set," *J Hypertens.*, vol. 22, pp. 1371–1380, 2004.

[68] S. Gouveia, A. P. Rocha, P. Laguna, and P. Lago, "Time domain baroreflex sensitivity assessment by joint analysis of spontaneous SBP and RR series," *Biomedical Signal Processing and Control*, vol. 4, pp. 254–261, 2009.

[69] H. W. J. Robbe, L. J. M. Mulder, H. Ruddel, W. A. Langewitz, J. B. P. Veldman, and G. Mulder, "Assessment of baroreceptor reflex sensitivity by means of spectral analysis," *Hypertension*, vol. 10, pp. 538–543, 1987.

[70] D. J. Patton, J. K. Triedman, M. H. Perrott, A. A. Vidian, and J. P. Saul, "Baroreflex gain: Characterization using autoregressive moving average analysis," *Am. J. Physiol.*, vol. 270, pp. H1240–H1249, 1996.

[71] G. Nollo, A. Porta, L. Faes, G. M. Del, M. Disertori, and F. Ravelli, "Causal linear parametric model for baroreflex gain assessment in patients with recent myocardial infarction," *Am. J. Physiol. Heart Circ. Physiol.*, vol. 280, pp. H1830–H1839, 2001.

[72] K. Martinmäki, K. Häkkinen, J. Mikkola, and H. Rusko, "Effect of low–dose endurance training on heart rate variability at rest and during an incremental maximal exercise test," *Eur. J. Appl. Physiol.*, vol. 104(3), pp. 541–548, 2008.

[73] M. Buchheit, "Monitoring training status with HR measures: do all roads lead to Rome?," *Front Physiol*, vol. 5, p. 73, 2014.

[74] D. J. Plews, P. B. Laursen, A. E. Kilding, and M. Buchheit, "Training adaptation and heart rate variability in elite endurance athletes - opening the door to effective monitoring," *Sports Med*, vol. 43, pp. 773–781, 2013.

[75] M. Llamedo and JP. Martínez, "QRS detectors performance comparison in public databases," *XLI International Conference on Computing in Cardiology*, pp. 357–360, 2014.

[76] J. A. Drezner, P. Fischbach, V. Froelicher, J. Marek, A. Pelliccia, J. M. Prutkin, C. M. Schmied, S. Sharma, M. G. Wilson, M. J. Ackerman, J. Anderson, E. Ashley, C. A. Asplund, A. L. Baggish, M. Brjesson, B. C. Cannon, D. Corrado, J. P. DiFiori, K. G. Harmon, H. Heidbuchel, D. S. Owens, S. Paul, J. C. Salerno, R. Stein, and V. L. Vetter, "Normal electrocardiographic findings: recognising physiological adaptations in athletes," *Br J Sports Med*, vol. 47(3), pp. 125–136, 2013.

[77] L. Mainardi, "On the quantification of heart rate variability spectral parameters using time–frequency and time–varying methods," *Philosophical Transactions of the Royal Society of London A: Mathematical, Physical and Engineering Sciences*, vol. 367(1887), pp. 255–275, 2009.

[78] R. Bailón, P. Laguna, L. Mainardi, and L. Sörnmo, "Analysis of heart rate variability using time-varying frequency bands based on respiratory frequency," *29th Annual International Conference of the IEEE Engineering in Medicine and Biology Society (EMBC07)*, vol. 29, pp. 6674–6677, 2007.

[79] R. Bailón, L. Mainardi, M. Orini, L. Sörnmo, and P. Laguna, "Analysis of heart rate variability during exercise stress testing using respiratory information," *Biomedical Signal Processing and Control*, vol. 5, pp. 299–310, 2010.

[80] S. Sarmiento, J. García-Manso, J. Martín-González, D. Vaamonde, J. Calderón, and M. Da Silva-Grigoletto, "Heart rate variability during high–intensity exercise," *J Syst Sci Complex*, vol. 26, pp. 104–116, 2013.

[81] F. Cottin, C. Médigue, P. Leprêtre, Y. Papelier, J. Koralsztein, and V. Billat, "Heart rate variability during exercise performed below and above ventilatory threshold," *Med. Sci. Sports Exerc*, vol. 36(4), pp. 594–600, 2004.

[82] F. Cottin and Y. Papelier, "Regulation of cardiovascular system during dynamic exercise: Integrative approach," *Crit. Rev. Phys. Rehabil. Med*, vol. 14(1), pp. 53–81, 2002.

[83] F. Cottin and Y. Papelier, "Effect of heavy exercise on spectral baroreflex sensitivity, heart rate, and blood pressure variability in well–trained humans," *Amer. J. Physiol. Heart Circ. Physiol*, vol. 295, pp. H1150–H1155, 2008.

[84] G. Blain, O. Meste, A. Blain, and S. Bermon, "Time-frequency analysis of heart rate variability reveals cardiolocomotor coupling during dynamic cycling exercise in humans," *Amer. J. Physiol. Heart Circ. Physiol*, vol. 296, pp. 1651–1659, 2009.

[85] M. Javorka, I. Zila, T. Balhárek, and K. Javorka, "Heart rate recovery after exercise: relations to heart rate variability and complexity," *Braz J Med Biol Res*, vol. 35(8), pp. 991–1000, 2002.

[86] Y. Arai, J. P. Saul, P. Albrecht, L. H. Hartley, L. S. Lilly, R. J. Cohen, and W. S. Colucci, "Modulation of cardiac autonomic activity during and immediately after exercise," *Am J Physiol*, vol. 256, pp. H132–H141, 1989.

[87] L. Bernardi, F. Salvucci, R. Suardi, P. L. Soldá, A. Calciati, S. Perlini, C. Falcone, and L. Ricciardi, "Evidence for an intrinsic mechanism regulating heart rate variability in the transplanted and the intact heart during submaximal dynamic exercise?," *Cardiovasc Res*, vol. 24(12), pp. 969–981, 1990.

[88] J. P. Martínez, R. Almeida, S. Olmos, A. P. Rocha, and P. Laguna, "A wavelet-based ECG delineator: Evaluation on standard databases," *IEEE Trans Biomed Eng*, vol. 51(4), pp. 570–581, 2004.

[89] A. Dumont, A. Hernández, and G. Carrault, "Improving ECG beats delineation with an evolutionary optimization process," *IEEE Trans Biomed Eng*, vol. 57, no. 3, pp. 607–615, 2010.

[90] Z. Michalewicz, *Genetic Algorithms + Data Structures = Evolution Programs, 3rd ed.* Berlin/Heidelberg, Germany: Springer-Verlag, 1996.

[91] A. Hernández, G. Carrault, F. Mora, and A. Bardou, "Model–based interpretation of cardiac beats by evolutionary algorithms: Signal and model interaction," *Artif. Intell. Med.*, vol. 26, no. 3, pp. 211–235, 2002.

[92] R. E. West, E. D. Schutter, and G. Wilcox, *Using evolutionary algorithms to search for control parameters in a nonlinear partial differential equation.* Univ. Minnesota Supercomputer Inst. Res., Minneapolis UMSI 97/61, Tech. Rep. UMSI 97/61, 1998.

[93] G. B. Moody, W. E. Muldrow, and R. G. Mark, "A noise stress test for arrhythmia detectors," in *Computers in Cardiology 1984*, vol. 11, pp. 381–384, 1984.

[94] A. L. Goldberger, L. A. N. Amaral, L. Glass, J. M. Hausdorff, P. C. Ivanov, R. G. Mark, J. E. Mietus, G. B. Moody, C.-K. Peng, and H. E. Stanley, "PhysioBank, PhysioToolkit, and PhysioNet: Components of a new research resource for complex physiologic signals," *Circulation*, vol. 101, no. 23, pp. e215–e220, 2000.

[95] J. Pan and W. J. Tompkins, "A real-time QRS detection algorithm," *IEEE Trans Biomed Eng*, vol. 32, pp. 230–236, 1985.

[96] K. Wasserman, *Principles of Exercise Testing and Interpretation: Including Pathophysiology and Clinical Applications*. Lippincott Williams & Wilkins, 2011.

[97] L. Cohen, "Time–frequency distributions–a review," *Proceedings of the IEEE*, vol. 77(7), pp. 941–981, 1989.

[98] P. Flandrin, *Time–Frequency/Time–Scale Analysis*. New York: Academic Press, 1999.

[99] W. Martin and P. Flandrin, "Wigner–Ville spectral analysis of nonstationary processes," *IEEE Trans. Acoust. Speech Signal Process*, vol. 33, pp. 1461–1470, 1985.

[100] M. Orini, R. Bailón, R. Enk, S. Koelsch, L. Mainardi, and P. Laguna, "A method for continuously assessing the autonomic response to music-induced emotions through HRV analysis," *Med Biol Eng Comput*, vol. 48, pp. 423–433, 2010.

[101] D. Gabor, "Theory of communication," *J. IEE Part III*, vol. 93(26), pp. 429–441, 1946.

[102] P. Laguna, G. B. Moody, and R. Mark, "Power spectral density of unevenly sampled data by least-square analysis," *IEEE Trans Biomed Eng*, vol. 45(6), pp. 698–715, 1998.

[103] H. L. Chan, H. H. Huang, and J. L. Lin, "Time-Frequency analysis of heart rate variability during transient segments," *Annals of Biomedical Engineering*, vol. 29(11), pp. 983–996, 2001.

[104] O. Meste, B. Khaddoumi, G. Blain, and S. Bermon, "Time-varying analysis methods and models for the respiratory and cardiac system coupling in graded exercise," *IEEE Trans. Biomed. Eng*, vol. 52(11), pp. 1921–1930, 2005.

[105] J. Sacha and W. Pluta, "Which heart rate is more variable: a slow or a fast one? it depends on the method of heart rate variability analysis.," *Folia Cardiol*, vol. 12 (suppl. D), pp. 1–4, 2005.

[106] M. Orini, R. Bailón, L. Mainardi, and P. Laguna, "Synthesis of HRV signals characterized by predetermined time-frequency structure by means of time–varying ARMA models," *Biomedical Signal Processing and Control*, vol. 7, pp. 141–150, 2012.

[107] G. P. Millet, V. E. Vleck, and D. J. Bentley, "Physiological differences between cycling and running: lessons from triathletes," *Sports Med*, vol. 39(3), pp. 179–206, 2009.

[108] D. Nunan, G. Donovan, D. G. Jakovljevic, L. D. Hodges, G. R. Sandercock, and D. A. Brodie, "Validity and reliability of short-term heart-rate variability from the Polar S810," *Med Sci Sports Exerc*, vol. 41(1), pp. 243–250, 2009.

[109] M. Kumar, M. Weippert, R. Vilbrandt, S. Kreuzfeld, and R. Stoll, "Fuzzy evaluation of heart rate signals for mental stress assessment," *IEEE Trans Fuzzy Syst*, vol. 15, pp. 791–808, 2007.

[110] D. B. Kaber, C. M. Perry, N. Segall, and M. A. Sheik-Nainar, "Workload state classiffcation with automation during simulated air traffic control," *Int J Aviat Psychol*, vol. 17, pp. 371–390, 2007.

[111] S. E. Turner, P. R. Eastwood, N. M. Cecins, D. R. Hillman, and S. C. Jenkins, "Physiologic responses to incremental and self-paced exercise in COPD: a comparison of three tests," *Chest*, vol. 126, pp. 766–773, 2004.

[112] M. P. Rezende Barbosa, N. T. Silva, F. M. Azevedo, C. M. Pastre, and L. C. Vanderlei, "Comparison of Polar®RS800G3™ heart rate monitor with Polar®S810i™ and electrocardiogram to obtain the series of RR intervals and analysis of heart rate variability at rest," *Clin Physiol Funct Imaging*, 2014.

[113] F. X. Gamelin, G. Baquet, S. Berthoin, and L. Bosquet, "Validity of the polar S810 to measure R-R intervals in children," *Int J Sports Med*, vol. 29(2), pp. 134–138, 2008.

[114] D. Giles, N. Draper, and W. Neil, "Validity of the Polar V800 heart rate monitor to measure RR intervals at rest," *Eur J Appl Physiol*, vol. 116, pp. 563–571, 2016.

[115] A. Bouillod, J. Cassirame, J. M. Bousson, Y. Sagawa, and N. Tordi, "Accuracy of the Suunto system for heart rate variability analysis during a tilt-test," *Rev. Bras. Cineantropom. Desempenho*, vol. 17, pp. 410–417, 2015.

[116] M. B. Wallén, D. Hasson, T. Theorell, B. Canlon, and W. Osika, "Possibilities and limitations of the polar rs800 in measuring heart rate variability at rest," *Eur J Appl Physiol*, vol. 112(3), pp. 1153–1165, 2012.

[117] R. M. Marchant-Forde, D. J. Marlin, and J. N. Marchant-Forde, "Validation of a cardiac monitor for measuring heart rate variability in adult female pigs: accuracy, artefacts and editing," *Physiology & Behavior*, vol. 80, pp. 449–458, 2004.

[118] V. S. M. Jonckheer-Sheehy, C. M. Vinke, and A. Ortolani, "Validation of a polar human heart rate monitor for measuring heart rate and heart rate variability in adult dogs under stationary conditions," *Journal of Veterinary Behavior*, vol. 7, pp. 205–212, 2012.

[119] M. Weippert, M. Kumar, S. Kreuzfeld, D. Arndt, A. Rieger, and R. Stoll, "Comparison of three mobile devices for measuring R-R intervals and heart rate variability: Polar S810i, Suunto t6 and an ambulatory ECG system," *Eur J Appl Physiol*, vol. 109(4), pp. 779–786, 2010.

[120] J. M. Bland and D. Altman, "Statistical methods for assessing agreement between two methods of clinical measurement," *Lancet*, vol. 8, pp. 307–310, 1986.

[121] F. S. Acton, *Analysis of Straight-Line Data*. New York: Dover, 1966.

[122] L. I. Lin, "A concordance correlation coefficient to evaluate reproducibility," *Biometrics*, vol. 45, pp. 255–268, 1989.

[123] R. A. Fisher, *Statistical methods for research workers*. Edinburgh: Oliver & Boyd, 1925.

[124] C. Costa-Santos, L. Antunes, A. Souto, and J. Bernardes, "Assessment of disagreement: a new information-based approach," *Annals of epidemiology*, vol. 20(7), pp. 555–561, 2010.

[125] C. Costa-Santos, J. Bernardes, D. A. de Campos, A. Costa, and C. Costa, "The limits of agreement and the intraclass correlation coefficient may be inconsistent in the interpretation of agreement," *Journal of Clinical Epidemiology*, vol. 64(3), pp. 264–269, 2011.

[126] E. Burdock, J. L. Fleiss, and A. S. Hardesty, "A new view of interobserver agreement," *Person Psychol*, vol. 16, pp. 373–384, 1963.

[127] R. Hernaez, "Reliability and agreement studies: a guide for clinical investigators," *Gut*, vol. 64(7), pp. 1018–1027, 2015.

[128] D. Mozaffarian et. al., "Heart disease and stroke statistics-2016 Update: A report from the American Heart Association," *Circulation*, vol. 133(4), pp. e38–360, 2016.

[129] T. J. Ryan, E. M. Antman, N. H. Brooks, R. M. Califf, L. D. Hillis, L. F. Hiratzka, E. Rapaport, B. Riegel, R. O. Russell, E. E. Smith 3rd, W. D. Weaver, R. J. Gibbons, J. S. Alpert, K. A. Eagle, T. J. Gardner, A. Garson Jr, G. Gregoratos, T. J. Ryan, and S. C. Smith Jr, "1999 update: ACC/AHA guidelines for the management of patients with acute myocardial infarction. A report of the American College of Cardiology/American Heart Association Task Force on Practice Guidelines (Committee on Management of Acute Myocardial Infarction)," *J Am Coll Cardiol*, vol. 34(3), pp. 890–911, 1999.

[130] E. D. Grech, "Pathophysiology and investigation of coronary artery disease," *BMJ*, vol. 326(7397), pp. 1027–1030, 2003.

[131] K. Wattanakit, A. R. Folsom, L. E. Chambless, and F. J. Nieto, "Risk factors for cardiovascular event recurrence in the Atherosclerosis Risk in Communities (ARIC) study," *Am Heart J*, vol. 149(4), pp. 606–612, 2005.

[132] B. Wennerblom, L. Lurje, H. Tygesen, R. Vahisalo, and A. Hjalmarson, "Patients with uncomplicated coronary artery disease have reduced heart rate variability mainly affecting vagal tone," *Heart*, vol. 83(3), pp. 290–294, 2000.

[133] M. Virtanen, M. Kähönen, T. Nieminen, P. Karjalainen, M. Tarvainen, T. Lehtimäki, R. Lehtinen, K. Nikus, T. Kööbi, M. Niemi, K. Niemelä, V. Turjanmaa, J. Malmivuo, and J. Viik, "Heart rate variability derived from exercise ECG in the detection of coronary artery disease," *Physiol Meas*, vol. 28(10), pp. 1189–1200, 2007.

[134] T. Nieminen, R. Lehtinen, J. Viik, T. Lehtimäki, K. Niemelä, K. Nikus, M. Niemi, J. Kallio, T. Kööbi, V. Turjanmaa, and M. Kähönen, "The finnish cardiovascular study (FINCAVAS): characterising patients with high risk of cardiovascular morbidity and mortality," *BMC Cardiovasc Disord*, vol. 6, p. 9, 2006.

[135] E. Toledo, O. Gurevitz, H. Hod, M. Eldar, and S. Akselrod, "Wavelet analysis of instantaneous heart rate: a study of autonomic control during thrombolysis," *Am J Physiol Regul Integr Comp Physiol*, vol. 284(4), pp. R1079–R1091, 2003.

[136] B. M. Nes, I. Janszky, U. Wisløff, A. Støylen, and T. Karlsen, "Age-predicted maximal heart rate in healthy subjects: The HUNT Fitness Study," *Scand J Med Sci Sports*, vol. 23(6), pp. 697–704, 2012.

[137] J. A. Hirsch and B. Bishop, "Respiratory sinus arrhythmia in humans: how breathing pattern modulates heart rate," *Am J Physiol*, vol. 241(4), pp. H620–H629, 1981.

[138] J. Bigger Jr, J. Fleiss, R. Steinman, L. Rolnitzky, W. Schneider, and P. Stein, "RR variability in healthy, middle-aged persons compared with patients with chronic coronary heart disease or recent acute myocardial infarction," *Circulation*, vol. 91(7), pp. 1936–1943, 1995.

[139] F. Kardelen, G. Akçurin, H. Ertuğ, S. Akcurin, and I. Bircan, "Heart rate variability and circadian variations in type 1 diabetes mellitus," *Pediatr Diabetes*, vol. 7(1), pp. 45–50, 2006.

[140] H. Tanaka, K. D. Monahan, and D. R. Seals, "Age–predicted maximal heart rate revisited," *J Am Coll Cardiol*, vol. 37(1), pp. 153–156, 2001.

[141] R. L. Gellish, B. R. Goslin, R. E. Olson, A. McDonald, G. D. Russi, and V. K. Moudgil, "Longitudinal modeling of the relationship between age and maximal heart rate," *Med Sci Sports Exerc*, vol. 39(5), pp. 822–829, 2007.

[142] F. Javed, A. V. Savkin, G. S. H. Chan, J. D. Mackie, and N. H. Lovell, "Identification and control for automated regulation of hemodynamic variables during hemodialysis," *IEEE Trans Biomed Eng*, vol. 58, pp. 1686–1697, 2011.

[143] J. T. Daugirdas, "Dialysis hypotension: A hemodynamic analysis," *Kidney Int.*, vol. 39, pp. 233–246, 1991.

[144] L. Henderson, "Symptomatic hypotension during hemodialysis," *Kidney Int.*, vol. 17, pp. 571–576, 1980.

[145] T. Shoji, Y. Tsubakihara, M. Fujii, and E. Imai, "Hemodialysis–associated hypotension as an independent risk factor for two–year mortality in hemodialysis patients," *Kidney Int.*, vol. 66, pp. 1212–1220, 2004.

[146] A. Tislér, K. Akócsi, B. Borbás, L. Fazakas, S. Ferenczi, S. Görögh, I. Kulcsár, L. Nagy, J. Sámik, J. Szegedi, E. Tóth, G. Wágner, and I. Kiss, "The effect of frequent or occasional dialysis-associated hypotension on survival of patients on maintenance haemodialysis," *Nephrol Dial Transplant*, vol. 18(12), pp. 2601–2605, 2003.

[147] A. Davenport, "Can advances in hemodialysis machine technology prevent intradialytic hypotension?," *Semin. Dial.*, vol. 22, pp. 231–236, 2009.

[148] R. Sherman, J. Daugirdas, and T. Ing, *Handbook of Dialysis*. Williams & Wilkins, 2007.

[149] E. Mancini, L. Corazza, D. C. Cannarile, M. L. Soverini, S. Cavalcanti, S. Cavani, A. Fiorenzi, and A. Santoro, "Short term variability of oxygen saturation during hemodialysis is a warning parameter for hypotension appearance," in *2008 Computers in Cardiology*, pp. 881–884, 2008.

[150] L. Sörnmo, "Vectorcardiographic loop alignment and morphologic beat-to-beat variability," *IEEE Trans Biomed Eng*, vol. 45(12), pp. 1401–1413, 1998.

[151] J. Benesty, J. Chen, and Y. Huang, "A generalized mvdr spectrum," *Signal Processing Letters, IEEE*, vol. 12, pp. 827–830, 2005.

[152] J. Benesty, J. Chen, and Y. Huang, "Estimation of the coherence function with the mvdr approach," *Proc. IEEE Int. Conference on Acoustics, Speech and Signal Processing (ICASSP)*, vol. 3, 2006.

[153] M. N. Murthi and B. D. Rao, "Minimum variance distortionless response (MVDR) modeling of voiced speech," in *1997 IEEE International Conference on Acoustics, Speech, and Signal Processing*, vol. 3, pp. 1687–1690, 1997.

[154] L. Faes, G. D. Pinna, A. Porta, R. Maestri, and G. Nollo, "Surrogate data analysis for assessing the significance of the coherence function," *IEEE Transactions on Biomedical Engineering*, vol. 51, pp. 1156–1166, 2004.

[155] M. Orini, R. Bailón, L. Mainardi, and P. Laguna, "Characterization of dynamic interactions between cardiovascular signals by time–frequency coherence," *IEEE Trans Biomed Eng*, vol. 59(3), pp. 663–673, 2012.

[156] P. Pudil, J. Novovicova, and J. Kittler, "Floating search methods in feature selection," *Pattern Recognition Letters*, vol. 79, pp. 1119–1125, 1994.

[157] M. S. Srivastava and E. M. Carter, *Applied multivariate statistics*. North Holland, 1983.

[158] R. Kohavi, "A study of cross-validation and bootstrap for accuracy estimation and model selection," *Proceedings IJCAI-95*, pp. 1137–1143, 1995.

[159] S. Akselrod, D. Gordon, J. B. Madwed, N. C. Snidman, D. C. Shannon, and R. J. Cohen, "Hemodynamic regulation: investigation by spectral analysis," *Am J Physiol Heart Circ Physiol*, vol. 249, pp. 867–875, 1985.

[160] J. A. Taylor, D. L. Carr, and C. W. Myers, "Mechanisms underlying very low frequency rr–interval oscillations in humans," *Circulation*, vol. 98, pp. 547–555, 1997.

[161] I. Szollosi, H. Krum, D. Kaye, and M. T. Naughton, "Sleep apnea in heart failure increases heart rate variability and sympathetic dominance," *Sleep*, vol. 30, pp. 1509–1514, 2007.

[162] D. P. Francis, K. Willson, L. C. Davies, A. J. Coats, and M. Piepoli, "Quantitative general theory for periodic breathing in chronic heart failure and its clinical implications," *Circulation*, vol. 102, no. 18, pp. 2214–2221, 2000.

[163] D. Hernando, A. Alcaine, E. Pueyo, P. Laguna, A. Arcentales, B. Giraldo, A. Voss, A. Bayés-Genís, and R. Bailón, "Influence of respiration in the very low frequency modulation of QRS slopes and heart rate variablitiy in cardiomyopathy patients," in *Computers in Cardiology 2013*, pp. 117–120, 2013.

[164] D. Hernando, A. Alcaine, P. Laguna, E. Pueyo, and R. Bailón, "Very low frequency modulation in QRS slopes and its relation with respiration and heart rate variability during hemodialysis," in *35th Conf Proc IEEE Eng Med Biol Soc*, pp. 5365–5368, 2013.

[165] S. L. Marple, *Digital spectral analysis with applications*. New Jersey: Prentice Hall, 1987.

[166] E. Gil, M. Orini, R. Bailón, J. Vergara, L. Mainardi, and P. Laguna, "Photoplethysmography pulse rate as a surrogate measurement of heart rate variability during non-stationary conditions," *Physiol Meas*, vol. 31, pp. 1271–1290, 2010.

[167] R. Longadge, S. S. Dongre, and L. Malik, "Class imbalance problem in data mining: Review," *Int. J. of Computer Science and Network (IJCSN)*, vol. 2, 1, 2013.

[168] J. E. Skinner, M. Meyer, B. A. Nester, U. Geary, P. Taggart, A. Mangione, G. Ramalanjaona, C. Terregino, and W. C. Dalsey, "Comparison of linear-stochastic and nonlinear-deterministic algorithms in the analysis of 15-minute clinical ECGs to predict risk of arrhythmic death," *Therap and Clin Risk Manag*, vol. 5, pp. 671–682, 2009.

[169] Q. Maggiore, "Isothermic dialysis for hypotension-prone patients," *Seminars in Dialysis*, vol. 15, pp. 187–190, 2002.

[170] C. Barth, W. Boer, D. Garzoni, T. Kuenzi, W. Ries, R. Schaefer, D. Schneditz, T. Tsobanelis, F. van der Sande, R. Wojke, H. Schilling, and J. Passlick-Deetjen, "Characteristics of hypotension-prone haemodialysis patients: is there a critical relative blood volume?," *Nephrol Dial Transplant*, vol. 18, pp. 1353–1360, 2003.

[171] V. Abouei, H. Sharifian, F. Towhidkhah, V. Nafisi, and H. Abouie, "Using neural network in order to predict hypotension of hemodialysis patients," in *Electrical Engineering (ICEE), 2011 19th Iranian Conference on*, pp. 1–4, may 2011.

[172] E. Gil, P. Laguna, J. P. Martínez, O. Barquero-Pérez, A. García-Alberola, and L. Sörnmo, "Heart rate turbulence analysis based on photoplethysmography," *IEEE Trans Biomed Eng*, vol. 60(11), pp. 3149–3155, 2013.

[173] E. Grigonyte, E. Gil, P. Laguna, and L. Sörnmo, "Relative peripheral blood volume changes induced by premature ectopic beats and their role in hemodialysis," *Biomedical Signal Processing and Control*, vol. 31, pp. 524–528, 2017.

[174] D. Romero, M. Ringborn, P. Laguna, and E. Pueyo, "Depolarization changes during acute myocardial ischemia by evaluation of QRS slopes: standard lead and vectorial approach," *IEEE Trans Biomed Eng.*, vol. 58(1), pp. 110–120, 2011.

[175] A. Alcaine, R. Bailón, D. Romero, E. Pueyo, and P. Laguna, "Very low frequency modulation of QRS slopes in patients with angina pectoris," pp. 757–760, 2011.

[176] F. Sandberg, R. Bailón, D. Hernando, P. Laguna, J. P. Martinez, K. Solem, and L. Sörnmo, "Prediction of hypotension in hemodialysis patients," *Physiol Meas*, vol. 35, pp. 1885–1898, 2014.

[177] H. Schmidt, D. Hoyer, and et al., "The alteration of autonomic function in multiple organ dysfunction syndrome," *Crit Care Clin*, vol. 24, no. 1, pp. 149–163, ix, 2008.

[178] L. Wieske, D. R. Chan Pin Yin, and et al., "Autonomic dysfunction in ICU-acquired weakness: a prospective observational pilot study," *Intensive Care Med*, vol. 39, no. 9, pp. 1610–1617, 2013.

[179] M. L. Ryan, M. P. Ogilvie, B. M. Pereira, and et al., "Heart rate variability is an independent predictor of morbidity and mortality in hemodynamically stable trauma patients," *J Trauma*, vol. 70, no. 6, pp. 1371–1380, 2011.

[180] J. C. Jackson, R. P. Hart, S. M. Gordon, A. Shintani, B. Truman, L. May, and E. W. Ely, "Six-month neuropsychological outcome of medical intensive care unit patients," *Crit Care Med*, vol. 31, pp. 1226–1234, 2003.

[181] R. O. Hopkins, L. K. Weaver, D. Collingridge, R. B. Parkinson, K. J. Chan, and J. F. Orme Jr, "Two-year cognitive, emotional, and quality-of-life outcomes in acute respiratory distress syndrome," *Am J Respir Crit Care Med*, vol. 171, pp. 340–347, 2005.

[182] B. C. Norman, J. C. Jackson, J. A. Graves, T. D. Girard, P. P. Pandharipande, N. E. Brummel, L. Wang, J. L. Thompson, R. Chandrasekhar, and E. W. Ely, "Employment outcomes after critical illness: an analysis of the bringing to light the risk factors and incidence of neuropsychological dysfunction in ICU survivors cohort," *Crit Care Med*, vol. 44, pp. 2003–2009, 2016.

[183] J. López-Aguilar, M. E. Quilez, O. Martí-Sistac, C. García-Martín, G. Fuster, F. Puig, and et al., "Early physiological and biological features in three animal models of induced acute lung injury," *Intensive Care Med*, vol. 36, pp. 347–355, 2010.

[184] A. Reichenberg, R. Yirmiya, A. Schuld, T. Kraus, M. Haack, A. Morag, and T. Pollmacher, "Cytokine–associated emotional and cognitive disturbances in humans," *Arch Gen Psychiatry*, vol. 58, no. 5, pp. 445–452, 2001.

[185] R. J. Zitnik, "Treatment of chronic inflammatory diseases with implantable medical devices," *Cleve Clin J Med*, vol. 78 Suppl 1, pp. S30–34, 2011.

[186] J. M. Huston and J. C. Tracey, "The pulse of inflammation: heart rate variability, the cholinergic anti-inflammatory pathway and implications for therapy," *Journal of Internal Medicine*, vol. 269, p. 7, 2010.

[187] J. F. Thayer, S. S. Yamamoto, and et al., "The relationship of autonomic imbalance, heart rate variability and cardiovascular disease risk factors," *Int J Cardiol*, vol. 141, no. 2, pp. 122–131, 2010.

[188] A. L. Thorsen, K. Johansson, and et al., "Neurobiology of cognitive remediation therapy for schizophrenia: a systematic review," *Front Psychiatry*, vol. 5, p. 103, 2014.

[189] L. Blanch, B. Sales, J. Montanya, U. Lucangelo, O. Garcia-Esquirol, A. Villagra, E. Chacon, A. Estruga, M. Borelli, M. J. Burgueño, J. C. Oliva, R. Fernandez, J. Villar, R. Kacmarek, and G. Murias, "Validation of the better care® system to detect ineffective efforts during expiration in mechanically ventilated patients: a pilot study," *Intensive Care Med*, vol. 38, pp. 772–780, 2012.

[190] M. Piepoli, C. S. Garrard, D. A. Kontoyannis, and L. Bernardi, "Autonomic control of the heart and peripheral vessels in human septic shock," *Intensive Care Med*, vol. 21, pp. 112–119, 1995.

[191] A. H. Garde, B. Laursen, A. H. Jørgensen, and B. R. Jensen, "Effects of mental and physical demands on heart rate variability during computer work," *Eur J Appl Physiol*, vol. 87, no. 4–5, pp. 456–461, 2002.

[192] I. J. Zaal, A. W. van der Kooi, L. J. van Schelven, P. L. Oey, and A. J. Slooter, "Heart rate variability in intensive care unit patients with delirium," *J Neuropsychiatry Clin Neurosci*, vol. 27, no. 2, pp. e112–116, 2015.

[193] R. J. Myerburg and M. J. Junttila, "Sudden cardiac death caused by coronary heart disease," *Circulation*, vol. 125(8), pp. 1043–1052, 2012.

[194] L. Politano, A. Palladino, G. Nigro, M. Scutifero, and V. Cozza, "Usefulness of heart rate variability as a predictor of sudden cardiac death in muscular dystrophies," *Acta Myol*, vol. 27, pp. 114–122, 2008.

[195] H. Fujitaa, U. R. Acharyab, V. K. Sudarshanb, D. N. Ghistae, S. V. Sreef, L. W. J. Eugeneb, and J. E. W. Kohb, "Sudden cardiac death (SCD) prediction based on nonlinear heart rate variability features and SCD index," *Applied Soft Computing*, vol. 43, pp. 510–519, 2016.

[196] E. Ebrahimzadeh, M. Pooyan, and A. Bijar, "A novel approach to predict sudden cardiac death (SCD) using nonlinear and time-frequency analyses from hrv signals," *PLoS One*, vol. 9(2), p. e81896, 2014.

List of Publications

Journal Publications

- F. Sandberg, R. Bailón, **D. Hernando**, P. Laguna, J.P. Martínez, K. Solem, L. Sörnmo (2014). Prediction of hypotension in hemodialysis patients. *Physiological Measurement*. Vol. 35, pp. 1885-1898.

- **D. Hernando**, L. Sörnmo, F. Sandberg, P. Laguna, M. Llamedo, R. Bailón (2015). Identification of Hypotension Prone Patients During Hemodialysis based on the Analysis of Heart Rate Variability. *Medical & Enginering & Physics*. Vol. 37, n.12, pp. 1156-1161.

- **D. Hernando**, N. Garatachea, R. Almeida, J. A. Casajús, R. Bailón (2017). Validation of heart rate monitor Polar RS800 for heart rate variability analysis during exercise. *Journal of Strength and Conditioning Research*. DOI: 10.1519/JSC.0000000000001662.

Submitted Publications

- **D. Hernando**, A. Hernando, J.A. Casajús, P. Laguna, N. Garatachea, R. Bailón. Methodological Framework for Heart Rate Variability Analysis During Exercise: Application to Running and Cycling Stress Testing. Submitted to *Medical & Biological Engineering & Computing*. Accepted with minor revisions.

- M. Turon, S. Fernandez-Gonzalo, M. Jodar, G. Gomà, J. Montanyà, **D. Hernando**, R. Bailón, C. de Haro, V. Gomez-Simon, J. López-Aguilar, R. Magrans, M. Martinez-Perez, J.C. Oliva, L. Blanch. Feasibility and safety of virtual-reality-based early neurocognitive stimulation in critically ill patients. Submitted to *Annals of Intensive Care*. Under review.

Conference Publications

- **D. Hernando**, R. Bailón, P. Laguna, L. Sörnmo (2011). Heart Rate Variability Analysis during Hemodialysis and its Relation with Hypotension. *XXXVIII International Conference on Computing in Cardiology*. Hangzhou, China, pp. 189-192.

- **D. Hernando**, A. Alcaine, P. Laguna, E. Pueyo and R. Bailón (2013). Very low frequency modulation in QRS slopes and its relation with respiration and heart rate variability during hemodialysis. *35nd Annual International Conference of the IEEE EMBS*. Osaka, Japan, pp. 5365-5368.

- **D. Hernando**, A. Alcaine, E. Pueyo, P. Laguna, M. Orini, A. Arcentales, B. Giraldo, A. Voss, A. Bayés-Genís, R. Bailón (2013). Influence of Respiration in the Very Low Frequency Modulation of QRS slopes and Heart Rate Variability in Cardiomyopathy Patients. *XL International Conference on Computing in Cardiology*. Zaragoza, Spain, pp. 117-120.

- F. Sandberg, R. Bailón, **D. Hernando**, P. Laguna, J.P. Martínez, K. Solem, L. Sörnmo (2013). Prediction of Intradialytic Hypotension using PPG and ECG. *XL International Conference on Computing in Cardiology*. Zaragoza, Spain, pp. 1227-1230.

- **D. Hernando**, R. Bailón, R. Almeida, A. Hernández (2014). QRS Detection Optimization in Stress Test Recordings using Evolutionary Algorithms. *XLI International Conference on Computing in Cardiology*. Cambridge, USA, pp. 737-740.

- A. Hernando, **D. Hernando**, N. Garatachea, J.A. Casajús, R. Bailón (2015). Attenuation of the Influence of Cardiolocomotor Coupling in Heart Rate Variability Interpretation During Exercise Test. *37nd Annual International Conference of the IEEE EMBS*. Milan, Italy, pp. 1508-1511.

- **D. Hernando**, M. Turon, R. Bailón, S. Fernandez-Gonzalo, J. Lázaro, G. Gomà, E. Gil, J. Montanyà, J. López-Aguilar, C. de Haro, P. Laguna, L. Blanch (2015). Autonomic Nervous System Assessment in Critically Ill Patients Undergoing a Cognitive Rehabilitation Therapy. *XLII International Conference on Computing in Cardiology*. Nice, France, pp. 785-788.

- M. Turon, **D. Hernando**, S. Fernandez-Gonzalo, R. Bailón, G. Gomà, J. Lázaro, J. Montanyà, E. Gil, M. Martinez-Perez, C. de Haro, J. López-Aguilar, A. Martinez-Rubio, M. Jodar, P. Laguna, L. Blanch (2015). Effect of an early neurocognitive rehabilitation on autonomic nervous system in critically ill patients. *Intensive Care Medicine Experimental*, 3(Suppl 1):A989.

- M. Turon, **D. Hernando**, S. Fernandez-Gonzalo, R. Bailón, G. Gomà, J. Lázaro, J. Montanyà, E. Gil, C. de Haro, M. Martinez-Perez, J. López-Aguilar, A.

Martinez-Rubio, M. Jodar, P. Laguna, L. Blanch (2016). Differential effect of early neurocognitive rehabilitation on autonomic nervous system in critically ill patients with and without delirium. *American Thoracic Society (ATS) International Conference*. San Francisco.

- **D. Hernando**, M. Kähönen, J. Lázaro, R. Lehtinen, T. Nieminen, K. Nikus, T. Lehtimäki, R. Bailón, J. Viik. Coronary artery disease diagnosis by means of heart rate variability analysis using respiratory information. Submitted to *EMBEC 2017 conference*.

- **D. Hernando**, N. Garatachea, J. A. Casajús, R. Bailón. Comparison of HRV assessment during exercise from Polar RS800 and ECG. Submitted to *Computing in Cardiology 2017 conference*.